ECO SUPPORT

SMHI

OCEANOGRAFI Nr 108, 2011

Transient scenario simulations for the Baltic Sea Region during the 21st century

H.E.M. Meier[1,2], H. Andersson[1], C. Dieterich[1], K. Eilola[1], B. Gustafsson[3], A. Höglund[1], R. Hordoir[1] and S. Schimanke[1]

[1] Swedish Meteorological and Hydrological Institute, Department of Research and Development, Norrköping, Sweden

[2] Department of Meteorology, Stockholm University, Stockholm, Sweden

[3] Stockholm Resilience Centre/Baltic Nest Institute, Stockholm University, Stockholm, Sweden

Front: Bråviken – a Baltic Sea fjord. Photo: Silke Malz.

ISSN 0283-7714

OCEANOGRAFI Nr 108, 2011

Transient scenario simulations for the Baltic Sea Region during the 21st century

H.E.M. Meier[1,2], H. Andersson[1], C. Dieterich[1], K. Eilola[1], B. Gustafsson[3], A. Höglund[1], R. Hordoir[1] and S. Schimanke[1]

[1] Swedish Meteorological and Hydrological Institute, Department of Research and Development, Norrköping, Sweden

[2] Department of Meteorology, Stockholm University, Stockholm, Sweden

[3] Stockholm Resilience Centre/Baltic Nest Institute, Stockholm University, Stockholm, Sweden

Summary

The combined future impacts of climate change and industrial and agricultural practices in the Baltic Sea catchment on the Baltic Sea ecosystem were assessed. For this purpose 16 transient simulations for 1961-2099 using a coupled physical-biogeochemical model of the Baltic Sea have been performed. Four climate scenarios were combined with four nutrient load scenarios ranging from a pessimistic business-as-usual to a more optimistic case following the Baltic Sea Action Plan (BSAP). In this study we focussed on annual and seasonal mean changes of ecological quality indicators describing the environmental status of the Baltic Sea. In correspondence with earlier studies we found that the impact of changing climate on the Baltic biogeochemistry might be significant. Assuming reference loadings the water quality in all climate scenarios is reduced at the end of the century. The impact of nutrient load reductions according to the BSAP will be less effective in future climate compared to present climate. However, the results of the pessimistic business-as-usual scenario suggest that policy makers should act to avoid much worse environmental conditions than today.

Sammanfattning

Den kombinerade framtida inverkan på Östersjöns ekosystem från klimatförändring, jordbruk och industri i Östersjöns avrinningsområde har analyserats. För detta syfte har 16 transienta simuleringar utförts för perioden 1961-2099 med en kopplad fysisk-biogeokemisk modell för Östersjön. Fyra klimatscenarier kombinerades med fyra scenarier för olika tillförslar av näringsämnen. Dessa varierade från ett pessimistiskt scenario där verksamhet i jordbruk och industri fortsätter att utvecklas utan sammanfallande reningsåtgärder, till ett mer optimistiskt scenario där reduceringar enligt Aktionsplanen för Östersjön (BSAP) genomförs. I denna studie har vi fokuserad på förändringar av års- och säsongsmedelvärden av ekologiska kvalitetsindikatorer som beskrivning av Östersjöns miljöstatus. I enighet med tidigare studier fanns att effekten på Östersjöns biogeokemi från en klimatförändring är signifikant. Vid antagande om samma näringstillförsel i framtiden som idag fanns att vattenkvaliteten vid slutet av århundradet var försämrad i alla klimatscenarierna. Inverkan av åtgärder enligt BSAP kommer att vara mindre effektiva i ett framtida klimat jämfört med dagens klimat. Resultaten från det mer pessimistiska sceneriet indikerar dock betydelsen av åtgärder med näringsreduceringar för att inte förvärra dagens miljöstatus i Östersjön.

1. Introduction

Regional climate modeling results suggest that global warming may cause increased water temperatures and reduced sea ice cover combined with eventually increased wind speeds and eventually increased river runoff. The projected hydrographic changes could therefore have significant impacts on the marine ecosystem. To estimate these effects and to calculate the impact of nutrient load reductions in future climate an ensemble of model simulations for the period 1961-2099 were carried out. Ensemble simulations are necessary to quantify uncertainties that might limit the predictability. Uncertainties are caused by biases of global climate and regional coupled climate-environmental models of the Baltic Sea and by unknown socio-economic future developments with impact on greenhouse gas emissions and nutrient loadings from land. In this study, agreement and disagreement of the simulated changes were assessed from the statistics of the ensemble of 16 scenario simulations.

Regionalized data from four scenario simulations driven by two General Circulation Models (GCMs) and two greenhouse gas emission scenarios (A1B, A2) were used to force a state-of-the-art coupled physical-biogeochemical model of the Baltic Sea, the Swedish Coastal and Ocean Biogeochemical model coupled to the Rossby Centre Ocean circulation model (RCO-SCOBI). These four climate scenarios were combined with four nutrient load scenarios: a reference scenario assuming present-day nutrient concentrations in the rivers, a pessimistic business-as-usual scenario assuming an exponential growth in agriculture in all Baltic Sea countries, a scenario of riverine nutrient loads and atmospheric deposition according to current legislations and the more optimistic case following the Baltic Sea Action Plan (BSAP).

The results of this study will contribute to the Ecosystem Approach to Management (EAM) tool to be developed within the ECOSUPPORT project (Advanced modeling tool for scenarios of the Baltic Sea ECOsystem to SUPPORT decision making, http://www.baltex-research.eu/ecosupport). ECOSUPPORT addresses the urgent need for policy-relevant information on the combined future impacts of climate change and industrial and agricultural practices in the Baltic Sea catchment on the marine ecosystem. The main aim is to provide a multi-model system tool to support decisison makers.

In the next section the method of the dynamical downscaling approach and the models are briefly introduced. In the third section results of annual and seasonal mean changes of atmospheric, hydrological and oceanographic key parameters including ecological quality indicators are presented and discussed. Finally, some conclusions of the study are highlighted.

2. Methods

2.1. Model overview

We have used the three-dimensional circulation model RCO, the Rossby Centre Ocean model. RCO is a Bryan-Cox-Semtner primitive equation circulation model with a free surface and open boundary conditions in the northern Kattegat. In case of inflow prognostic variables like temperature, salinity and nutrients are nudged towards climatologically annual mean profiles calculated from observations of present climate and are not adjusted to future climate. In case of outflow a Orlanski radiation condition is used. RCO is coupled to a Hibler-type sea ice model with elastic-viscous-plastic rheology. Subgrid-scale vertical mixing is parameterized using a turbulence closure scheme of the k-ε type. In the present study, RCO was used with a horizontal resolution of 3.7 km (2 nautical miles) and with 83 vertical levels with layer thicknesses of 3 m. A flux-corrected, monotonicity preserving transport (FCT) scheme is embedded and no explicit horizontal diffusion is applied. For further details of the RCO model the reader is refered to *Meier* [2001], *Meier et al.* [2003] and *Meier* [2007].

The Swedish Coastal and Ocean Biogeochemical model (SCOBI) is coupled to the physical model RCO. SCOBI describes the dynamics of nitrate, ammonium, phosphate, phytoplankton, zooplankton, detritus, and oxygen. Here, phytoplankton consists of three algal groups representing diatoms, flagellates and others, and cyano–bacteria. Besides the possibility to assimilate inorganic nutrients the modelled cyanobacteria also has the ability to fix molecular nitrogen which may constitute an external nitrogen source for the model system. The sediment contains nutrients in the form of benthic nitrogen and benthic phosphorus including aggregated process descriptions for oxygen dependent nutrient regeneration, denitrification and adsorption of ammonium to sediment particles, as well as permanent burial of organic matter. For further details of the SCOBI model description the reader is refered to *Eilola et al.* [2009] and *Almroth-Rosell et al.* [2011].

Four climate change scenario simulations have been performed. The forcing was calculated applying a dynamical downscaling approach using a regional climate model (RCM) with lateral boundary data from two General Circulation Models (GCMs). The two GCMs used were HadCM3 from the Hadley Centre in the U.K. and ECHAM5/MPI-OM from the Max Planck Institute for Meteorology in Germany. For each of these two driving global models scenario simulations forced with either the A1B or the A2 emission scenario were

conducted.

Future projections refer to a period at the end of this century (2070-2099). Annual and seasonal mean changes were calculated from the differences between the periods 2070-2099 and 1969-1998. For further details of the downscaling method and the quality of the atmospheric forcing the reader is refered to *Meier et al.* [2011b]. In contrast to the earlier studies by *Meier* [2006] and *Meier et al.* [2011a] no bias correction of the atmospheric forcing was applied. An exception is the wind speed. Following *Höglund et al.* [2009] wind speed is modified using simulated gustiness to improve wind speed extremes [*Meier et al.*, 2011b].

For the scenario simulations runoff and the sea surface height (SSH) at the open boundary of the regional RCO domain were estimated from atmospheric surface parameters. The method used in order to compute the SSH at the Kattegat boundary is very close to the method suggested by *Gustafsson and Andersson* [2001], except that the locations used to calculate the atmospheric pressure gradient are changed to provide a better fit with the SSH observed in Kattegat during the period for which measurements are available.

Runoff is computed based on precipitation and evaporation over the Baltic Sea drainage basin in the regional climate model, and a simple statistical correlation is used.

2.2. SSH at the open boundaries

SSH in Kattegat is estimated from a meridional atmospheric pressure gradient ΔP, taken as the difference of atmospheric pressure between two grid points located in the Netherlands and Norway. ΔP is computed on daily average basis. Thus, ΔP_n and ΔP_{n+1} are defined as the meridional pressure gradients at day n and day $n+1$, respectively. The SSH η at day n is calculated from

$$\eta(n) = \alpha \Delta P(n) + \beta \Delta P(n-1)\,. \tag{1}$$

The coefficients α and β are computed using a simple optimisation method in order to get the best possible fit to sea level observations in Smögen located at the Swedish west coast. For the optimisation procedure atmospheric pressure data from the Rossby Centre Atmosphere model (RCA) driven with ERA40 re-analysis data at the lateral boundaries [*Samuelsson et al.*, 2011] are used. This approach provides a good correlation of calculated and observed SSHs, but the calculated standard deviations are too small compared to observations. The probability density function shows that positive extremes of SSH are underestimated (Fig. 1). These extremes are essential for salt water inflows into the Baltic Sea. On the other hand, the method overestimates small positive SSH values.

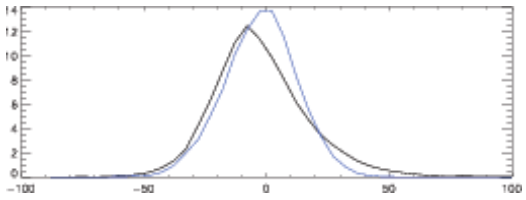

Figure 1. Probability density function of the sea surface height (in cm) in Kattegat: observations from Smögen (black line) and calculated values (blue line).

If the calculated SSH is used as forcing for the Baltic Sea model, the overall salinity of the Baltic Sea will decrease to too small values on a short time scale. We suspect that this shortcoming of the estimated SSH is related to underestimated atmospheric depressions in RCA causing an underestimation of the meridional pressure gradient variability.

In order to overcome this problem, estimated SSH data are bias corrected using statistical information from the observations. $\eta_{sim}(n)$ and $\eta_{obs}(n)$ are descrete values of simulated and observed SSH for a given period of time containing N time steps ($1 \leq n \leq N$). Further, $O(\eta_{sim}(n))$ and $O(\eta_{obs}(n))$ are defined as the sorted discrete functions corresponding to $\eta_{sim}(n)$ and $\eta_{obs}(n)$, respectively. A third function F is defined by the relation

$$O(\eta_{obs}(n)) = F\left[O(\eta_{sim}(n))\right] \tag{2}$$

F is unknown, but can be calculated from the relation of $O(\eta_{sim}(n))$ and $O(\eta_{obs}(n))$ using a polynomial function as approximation. We chose a 3^{rd} order polynomial function with coefficients estimated from a simple optimisation method. Figure 2 shows $O(\eta_{sim}(n))$ against $O(\eta_{obs}(n))$ when F is used or not used demonstrating the improvement from a statistical perspective.

Once F is estimated, the bias corrected $\eta_{sim}(n)$ is given as

$$\eta_{sim-corr}(n) = F\left[\eta_{sim}(n)\right]\,. \tag{3}$$

The variability of $\eta_{sim-corr}(n)$ is much closer to that of $\eta_{obs}(n)$ and the correlation between estimated and observed SSH is slightly larger. Using $\eta_{sim-corr}(n)$ instead of $\eta_{sim}(n)$ as forcing at the lateral boundary in Kattegat improves the simulated Baltic Sea salinity during present climate. Figure 3 shows that the agreement between the probability density functions of the reconstructed and corrected SSH and the observations is very good.

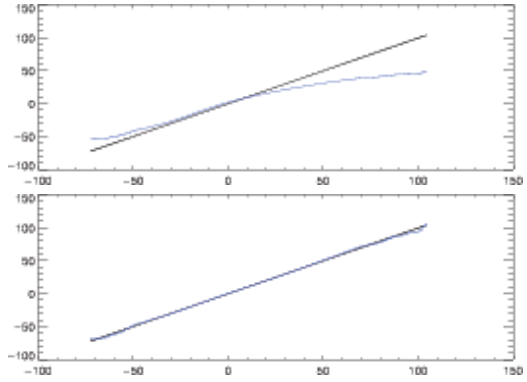

Figure 2. Reconstructed sorted sea surface height against observed sorted sea surface height (in cm). The upper and lower panels show the relationship between the two sea surface heights when F is not used and when it is used, respectively.

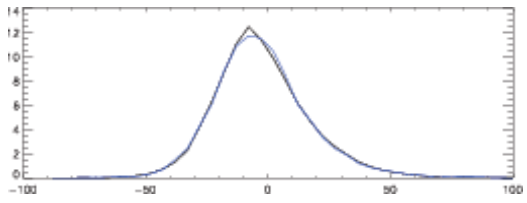

Figure 3. Probability density functions of the reconstructed and statistically corrected sea surface height (blue line) and of the observations (black line) (in cm).

In the transient simulations we applied the statistically correction both in past and future climates assuming that the statistical relationship will not change with time.

2.3. Runoff

In the transient simulations the runoff is estimated from the net water budget (precipitation minus evaporation) over the Baltic drainage area simulated with RCA using a statistical method. Thus, we assume that the net water budget in the scenario simulations is realistically simulated. Indeed, only the variability of annual mean runoff anomalies is calculated allowing a bias correction of the annual mean runoff. We do not consider changes of the seasonal cycle of the runoff.

Our method assumes that the annual mean runoff from a given drainage area p during the year n is correlated with the net water budget anomaly (in %) over this given water area during the given year and the one before:

$$R_{p,n} = b_p B_{p,n-1} + a_p B_{p,n} \tag{4}$$

in which $R_{p,n}$ is the runoff for the year n and for the drainage area p. $B_{p,n}$ is the net water budget (precipitation minus evaporation) anomaly for year n and area p. Finally, b_p and a_p are two coefficients. The statistical model is constrained for present climate when observations of the annual mean runoff anomaly are available. b_p and a_p are determined using an optimisation method.

Five different sub-basins are considered, i.e. Bothnian Bay, Bothnian Sea, Gulf of Finland, Baltic proper and Kattegat. For each of the sub-basins the interannual variability of the runoff is computed based on the above mentioned method. A climatological mean seasonal cycle is calculated for each sub-basin which does not change in future climate. This assumptions is very likely not true but changes of the seasonal cycle have only a small impact on the large-scale salinity distribution in the Baltic Sea.

The correlation coefficients are determined during 1980-2006. Thus, the statistical model is validated during 1960-1979 when both runoff observations and simulation results from RCA driven by ERA40 are available. Figure 4 shows the results of the statistical model for 1960-2006. The results are satisfactory except for the Gulf of Finland and the Gulf of Riga. The annual variability is fairly well reproduced for the entire Baltic Sea although it is obvious that the standard deviation of the re-constructed runoff is smaller than the standard deviation of the observations.

Depending on the scenario simulation this method suggests an increase of the total runoff between 17 and 23% at the end of the century (see Section 3). It is

assumed that the statistical relationship between runoff and precipitation minus evaporation does not change in time. However, biases of precipitation and evaporation may affect the estimated runoff changes.

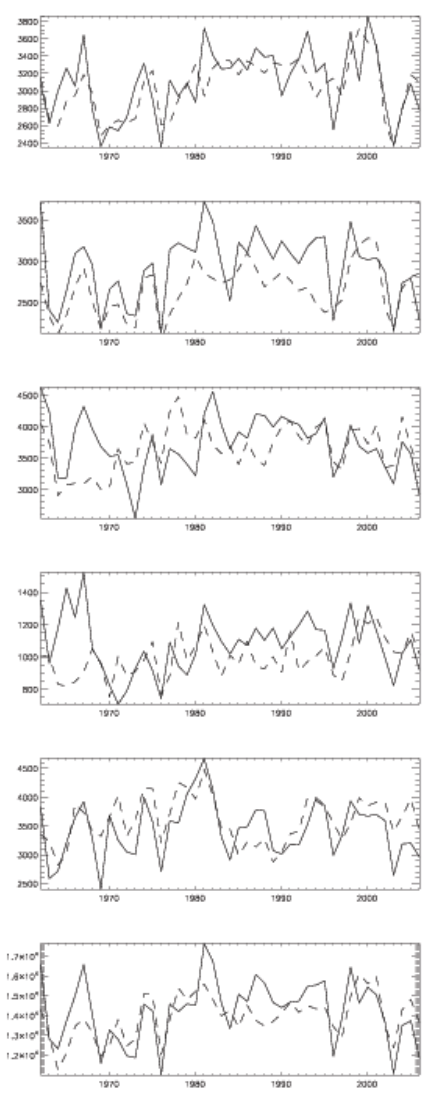

Figure 4. Interannual variability of observed (solid line) and reconstructed (dashed line) annual mean runoff (in $m^3\ s^{-1}$) in different sub-basins of the Baltic Sea and correlation coefficients (BB = Bothnian Bay, BS = Bothnian Sea, GF = Gulf of Finland, GR = Gulf of Riga, BP = Baltic proper, Total = Baltic Sea with Kattegat).

2.4. Nutrient loads scenarios

Nutrient loads from rivers are calculated from the product of the nutrient concentration and the volume flow following *Eilola et al.* [2009] and *Meier et al.* [2011a]. The volume flow changes in the scenarios simulations as outlined in the previous Section 2.3. For the nutrient concentrations four scenarios are considered:

- REFerence (REF): current loads from rivers and current atmospheric deposition (see *Eilola et al.* [2009]),
- Current LEGislation (CLEG): loads from rivers according to legislation on sewage water treatment (EU wastwater directive) and 25% reduction of atmospheric nitrogen,
- Baltic Sea Action Plan (BSAP): reduced river loads following *HELCOM* [2007] and 50% reduced atmospheric deposition,
- Business As Usual (BAU): business as usual for loads from rivers assuming an exponential growth of agriculture in all Baltic Sea countries following *HELCOM* [2007] and current atmospheric deposition.

A summary of the nutrient load scenarios can be found in *HELCOM* [2007] based upon *Wulff et al.* [2007] and *Humborg et al.* [2007].

These scenarios are combined with the future IPCC scenarios A1B and A2 using two regionalizations driven by HadCM3 (reference version) and ECHAM5/MPI-OM (henceforth short ECHAM5) each. Thus, the atmosperic and hydrological forcing for RCO-SCOBI is calculated from RCAO-HadCM3-A1B, RCAO-ECHAM5-A1B_3, RCAO-ECHAM5-A1B_1 and RCAO-ECHAM5-A2. For ECHAM5-A1B two realizations of the emission scenario A1B (ECHAM5-A1B_1 and RCAO-ECHAM5-A1B_3) with differing initial conditions in year 2000 are used.

For the transient scenario simulations the future nutrient input into the Baltic Sea is represented by piecewise linear ramp functions. We run RCO-SCOBI until the end of 2007, ramp to the end of 2020 and then use constant nutrient concentrations in river runoff according to BSAP, CLEG and BAU (for REF the nutrient concentrations are constant with time). Coastal point sources are lumped into the river loads. The same functional form will be used for the atmospheric deposition of nutrients.

The averaging period for the reference river load concentration is 1995 - 2002. This excludes some abnormal years in the early 2000s. Load changes are applied on the total loads (not only on bioavailable fractions). Table 1 shows the nutrient load changes beyond the year 2020 calculated with the coupled physical-biogeochemical model BALTSEM from the Baltic Nest Institute.

In all scenario simulations lateral boundary conditions in the Skagerrak are unchanged.

Table 1. Scenarios of nutrient load changes in % per sub-basin (KT = Kattegat, DS = Danish Straits, BP = Baltic proper, BS = Bothnian Sea, BB = Bothnian Bay, GR = Gulf of Riga, GF = Gulf of Finland). Coastal point sources are included in the riiver loads.

	KT	DS	BP	BS	BB	GR	GF	Sum
BSAP N	-30.0	-32.7	-25.6	0.0	0.0	0.0	-5.6	-17.5
BSAP P	0.0	0.0	-56.9	0.0	0.0	-17.9	-23.0	-35.1
CLEG N	-0.1	-0.3	-4.4	0.0	0.0	0.0	-5.3	-2.9
CLEG P	0.0	0.0	-20.1	0.0	0.0	-15.3	-15.1	-14.7
BAU N	0.0	0.0	62.6	0.0	0.0	62.6	62.6	44.1
BAU P	0.0	0.0	46.1	0.0	0.0	46.1	46.1	37.0

2.5. Analysis parameters

In this study we focus on annual and seasonal mean changes of some physical parameters and ecological quality indicators describing the environmental status of the Baltic Sea like sea surface temperature (SST), sea surface salinity (SSS), bottom salinity, sea surface height (SSH), bottom oxygen concentration, surface layer phosphate concentration, surface layer nitrate concentration, surface layer diatom concentration, surface layer concentration of flagellates and others, surface layer cyanobacteria concentration, surface layer phytoplankton concentration, and Secchi depth. Phosphate, nitrate, diatom, flagellates and others, cyanobacteria and phytoplankton concentrations are vertically averaged for the upper 10 m.

The Secchi depth (Sd) is calculated from $Sd = 1.7/kd(m)$ where kd is the mean vertical attenuation in the depth range 0-Sd. Factors controlling light attenuation in the Baltic Sea model are the concentrations of yellow substances, phytoplankton and detritus. In the scenario simulations changes of the Secchi depth are given by changing phytoplankton and detritus concentrations because yellow substances are assumed to remain unchanged. The total phytoplankton concentration is the sum of all three phytoplankton groups and vertically averaged for the upper 10 m (in mg Chl m^{-3}). We assume the following carbon to chlorophyll ratio $C : Chl = 50 : 1\,(mgC : mgChl)$.

In addition integrated pools of nutrients in the water column and in the sediments, the ratio between nitrogen and phosphorus, hypoxic area and cod reproductive volumes are analyzed.

From the atmosphere model we analyzed the following variables: 2 m air temperature, sea level pressure (SLP), precipitation, total cloud cover, mean 10 m wind speed and maximum estimated gust wind. RCA3 provides two different output parameters for wind extremes: the maximum 10 m wind speed and the maximum of estimated gust wind. The maximum 10 m wind speed is calculated following the Monin-Obukhov theorie and is interpolated from the lowest atmospheric level (90 m) down to 10 m. The maximum estimated gust wind is calculated from the turbulent kinetic energy (TKE) equation. Here the gust winds can propagate down to the surface from all boundary layer levels if the mixing is strong enough.

For both parameters the absolute maximum over the output interval (3h) is stored while the internal time step is 15 minutes for 25 km resolution (Samuelsson et al. 2011). In general the estimated gust wind should be stronger than the maximum 10 m wind speed.

We calculated the ensemble mean of all four climate scenario simulations because the emission scenarios A2 and A1B do not differ substantially in ECHAM5 scenario simulations. To characterize the ensemble spread we calculated the difference between the maximum and minimum values within the ensemble.

3. Results and discussion

3.1. Atmospheric forcing

3.1.1. Biases of atmospheric variables Biases were calculated from the differences between the GCM driven RCAO simulations during the control period (December 1968 to November 1998) and the hindcast simulation using RCA3 forced with ERA40. During autumn and winter the 2 m air temperatures in all three ECHAM5 driven simulations are too high (with up to more than 2.5 °C) and too low in summer whereas the biases in HadCM3 driven simulations are relatively smaller except during spring when differences in the northern Baltic Sea are larger than -3.5 °C (Fig. 5). In all experiments the seasonal cycle over the northern part of the Baltic Sea is too weak.

The corresponding SLP fields in ECHAM5 driven simulations show a positive anomaly over northern Scandinavia during all seasons except in summer (Fig. 6). This pattern is only regional. According to *Kjellström et al.* [2011], in winter all investigated regional climate simulations are too zonal in parts of the North Atlantic and European region. As a result of this SLP bias too much mild and moist air is advected from the North Atlantic in over Europe causing the overestimated 2 m air temperatures in particular in ECHAM5 driven simulations.

Precipitation during summer is too low in all sim-

ulations in particular over the Norwegian mountains (Fig. 7). Precipitation in HadCM3 driven simulations is reasonably close to the ERA40 driven hindcast experiment.

In all experiments and during all seasons (except in HadCM3 driven simulations in summer) cloud cover is slightly overestimated (Fig. 8).

In all experiments the mean wind speed over the sea in winter is underestimated whereas the wind fields over land are relatively well simulated (Fig. 9). To the contrary, the largest differences of the maximum 10 m wind speed appear along the coasts in most seasons with overestimations of more than 1 m/s (Fig. 10). Similar results are found for the maximum of the estimated gust wind fields (Fig. 11).

3.1.2. Projected changes of atmospheric variables The largest increases of the 2 m air temperature are found in the northern Baltic Sea in particular during winter and spring (Fig. 12). Surprisingly the largest increase occur in the HadCM3 driven simulation with the A1B greenhouse gas emission scenario and not in the ECHAM5 driven simulation with the A2 emission scenario. *Meier et al.* [2011b] showed that the warmer control climate in ECHAM5 driven simulations reduces the ice-albedo feedback causing a smaller signal in changing climate.

Despite of regional details and overall magnitude in all experiments the SLP will get more zonal at the end of the century. In high and low latitudes over the Baltic Sea the SLP will decrease and increase, respectively (Fig. 13)

The largest changes of precipitation occur over the mountain areas (Fig. 14). We found similar patterns of changing precipitation in HadCM3 and ECHAM5 driven simulations.

Cloud cover changes are small (Fig. 15). During spring the cloudiness will slightly increase in ECHAM5 driven simulations. In the other seasons the cloudiness will slightly decrease over the Baltic Sea which is a common signal in all scenario simulations.

Also the changes of the 10 m wind speed are small (Fig. 16). Significantly increased wind speeds of about 1 m s^{-1} are found in RCAO-ECHAM5-A1B_1 and RCAO-ECHAM5-A2 during winter and autumn. In all simulations the maximum 10 m wind speed and the maximum estimated gust wind increase with up to 1 m s^{-1} in the Bothnian Bay and Gulf of Finland during winter and spring (Figs. 17 and 18).

3.2. Hydrological forcing

Table 2 summarizes the total volume flows in present and future climates calculated with the statistical model (Section 2.3). For comparison the corresponding figures from the hydrological model HYPE [*Lindström et al.*, 2010] are listed in Table 3. These figures are not used in our simulations. In Figure 19 the absolute and relative changes per sub-basin are shown. We found changes of the total volume flows into the Baltic Sea between 4 and 22 % approximately. In the Baltic proper all changes are positive except for the HYPE results driven by RCAO-HadCM3-A1B. The changes are larger in the northern sub-basins than in the southern sub-basins. Although the changes of the statistical model (15 to 22 %) are larger than in HYPE (4 to 13 %), the ratios between the individual simulations are rather consistent within the two approaches.

3.3. Biases and changes of ecological quality indicators

3.3.1. Biases of the GCM driven simulations Biases of the 12 selected parameters characterizing the hydrographical and environmental status of the Baltic Sea are shown in Figures 20 to 31. In the presented analysis we focus on climatological mean differences between control and hindcast simulations. These biases are induced by the shortcomings of the GCMs on the regional scales.

Seasonal mean SST biases are smaller than 2°C in all regions (Fig. 20). Bias patterns are similar for all ECHAM5 driven similations but differ substantially between the two models, ECHAM5 and HadCM3. The latter result is illustrated by the large standard deviation (not shown) and range of the ensemble spread which locally exceeds 2°C. In HadCM3 driven simulations the SST biases are largest during summer with too low and too high SSTs in the Bothnian Bay and western Gotland Basin, respectively. In the annual mean SST biases are in most regions smaller than 0.5°C. The area averaged annual mean SST bias is close to zero. To the contray, ECHAM5 driven simulations are systematically too warm, especially during winter. In large parts of the model domain SST biases are larger than 1°C. A common bias in all GCM driven simulations is the too high SST in the Gulf of Finland during autumn. This bias is clearly visible in the ensemble mean.

In general, both SSS and bottom salinity biases are positive in HadCM3 driven simulations and negative in ECHAM5 driven simulations (Figs. 21 and 22). Especially in the southern Baltic proper SSS is too low in ECHAM5 driven simulations. These deficiencies are explained mainly by shortcomings of the sea level in Kattegat calculated from the RCM results (Section 2). A common bias in all simulations is the overestimated SSS in the Gulf of Finland. The ensemble spread is largest in Kattegat and in the southern Baltic proper.

Similar results are found for bottom salinity biases (Fig. 22). The uncertainty is largest in narrow bands along the slopes. These areas correspond to the depth interval of the halocline in the Gotland Basin and in the Gulf of Finland in various control simulations. Biases of the saltwater transport into the Baltic cause biases

Table 2. Total volume flow (in m^3 s^{-1}) into the Baltic Sea (without Kattegat) in present and future climates calculated with the statistical model (Section 2.3). For comparison, the observed total volume flow (without Kattegat) for the period 1957-1990 amounts to 14,400 m^3 s^{-1} [*Bergström and Carlsson*, 1994]. The latter figure is used to calculate the biases.

Period	HadCM3 A1B	ECHAM5 A1B_3	ECHAM5 A1B_1	ECHAM5 A2
Mean 1957-1990	13,600	13,900	14,200	14,400
Mean 1971-2000	14,200	14,300	14,300	14,600
Mean 2070-2098	17,300	16,400	17,900	17,600
Bias 1957-1990	-800	-400	-200	50
Change 2070-2098	3,100	2,100	2,800	3,000
Change in %	22	15	20	20

Table 3. As Table 2 but for results of the hydrological model HYPE [*Lindström et al.*, 2010].

Period	HadCM3 A1B	ECHAM5 A1B_3	ECHAM5 A1B_1	ECHAM5 A2
Mean 1957-1990	13,300	13,200	13,700	13,800
Mean 1971-2000	12,700	12,600	13,000	13,300
Mean 2070-2098	14,100	13,100	14,700	15,000
Bias 1957-1990	-1,100	-1,200	-700	-500
Change 2070-2098	1,300	500	1,700	1,700
Change in %	10	4	13	13

of the depth of the permanent halocline.

In all scenario simulations the west wind during autumn and winter is underestimated causing large negative SSH biases especially in the eastern Baltic Sea (Fig. 23). The ensemble spread is largest during summer.

Bottom oxygen concentration biases are explained by biases of the vertical stratification. In HadCM3 driven simulations the permanent halocline is shallower compared to the location in the hindcast simulation causing lower oxygen concentrations at the depth of the halocline (Fig. 24). In ECHAM5 driven simulations the bottom oxygen concentrations in areas along the western slopes of the Northwestern Gotland Basin and along the northern slopes of the Gulf of Finland are higher than in the hindcast simulation because the halocline is deeper located. Interestingly, bottom oxygen concentrations along the slopes of the eastern Gotland Basin and along the Bay of Gdansk are lower than in the hindcast simulation although the concentration biases are not as large as in the HadCM3 driven simulation. Although in ECHAM5 driven simulations the halocline in the eastern parts of the Gotland Basin is deeper than in the hindcast simulation the bottom oxygen concentrations are still lower than in the hindcast simulation. We found in all climate simulations a slightly positive bottom oxygen concentration bias in the Gotland Deep area. The ensemble spread is largest in regions along the slopes and in the Gulf of Finland. Despite of the discussed shortcomings the biases are in all regions and during all seasons generally smaller than 1 ml l^{-1}.

In the HadCM3 driven simulation we found a pronounced positive bias of surface phosphate concentration in the entire Gulf of Finland (Fig. 25). In ECHAM5 driven simulations positive biases are found in the eastern Gotland Basin, in the Gulf of Riga and in the eastern part of the Gulf of Finland. The spread of the biases is largest in the Gulf of Riga, in the southern Gotland Basin and in the Gulf of Finland.

In all climate simulations we found a pronounced negative bias of surface nitrate concentration in the Gulf of Riga and in the eastern Gotland Basin along the coasts (Fig. 26). The differences between the biases are largest in the Gulf of Riga and in the coastal regions of the Baltic proper where the mouths of important rivers are located. Perhaps shortcomings of the calculated volume flow from land explain the negative biases in surface nitrate concentrations. Note that the runoff variability in the Gulf of Riga calculated with the statistical model has low quality.

Biases of surface concentrations of diatoms, flagellate and others, and cyanobacteria are in the range of $\pm$ 0.5 mg Chl m^{-3} (Figs. 27 to 29). Bias patterns of phytoplankton concentrations are similar compared to the corresponding patterns of the concentrations of flagellates and others. Thus, in the biogeochemical model the response of the various algal groups to forcing biases are dominated by flagellates and others which are most sensitive to temperature changes.

In all simulations the biases of the climate simulations cause increased cyanobacteria blooms during autumn with maxima along the coasts of the eastern Gotland Basin and in the Gulf of Finland (Fig. 29). However, in these regions the uncertainties of the biases within the ensemble are largest as well.

We found a positive ensemble mean bias of Secchi

depth in the central Baltic proper and negative biases along the coasts in the Gotland Basin and in the Kattegat (Fig. 31). Typical values of ensemble mean biases of Secchi depth amount to ± 0.5 m. The differences between biases are largest in the coastal zone along the Baltic proper and amount to ± 1 m at maximum.

3.3.2. Changes of nutrient pools, hypoxic areas and cod reproductive volumes In all scenario simulations the volume averaged water temperature increases with time as a response of the increased air temperature and the volume averaged salinity decreases as a response of the increased runoff during the 21st century (Fig. 32). During the control period volume averaged salinities in the ECHAM5 driven scenario simulations are too low compared to observations indicating too low salt water inflows (Fig. 22). To the contrary, in the HadCM3 driven scenario simulation the volume averaged salinity is too high indicating an overstimation of salt water inflows.

After the spinup of about 10 years DIN is constant during the control period. After 2007 DIN increases in the scenario simulations REF and BAU and decreases in BSAP (about constant in CLEG) (Fig. 32). In all nutrient load scenarios DIP increases during the control period which is consistent with the hindcast simulation (not shown). After 2007 DIP increases in REF and BAU and decreases in BSAP (about constant in CLEG).

Interestingly, the sediment pools of nitrogen and phosphorus decrease in all nutrient load and climate scenarios towards the end of the century (Fig. 32).

In all scenarios there is a tendency of increased DIN to DIP ratio in the water column (Fig. 33). Especially in the BSAP scenario driven by ECHAM5 A2 and ECHAM5 A1B_1 (the scenario simulations with an increase of the wind speed over the Baltic proper) the overall DIN to DIP ratios increase with about 7 and 5 at maximum, respectively.

In all scenario simulations the hypoxic areas increase and the cod reproductive volumes decrease (Fig. 33). An exception is the BSAP nutrient load scenario with constant or slightly reduced hypoxic areas after 2020.

3.3.3. Projected changes for the nutrient load scenario REF In Figures 34 to 69 changes between the periods 2070-2099 and 1969-1998 are depicted. We considered four nutrient load scenarios REF, BSAP, CLEG and BAU and four climate scenarios driven by HadCM3-A1B, ECHAM5-A1B_3, ECHAM5-A1B_1 and ECHAM5-A2 (see Section 2). In this sub-section we focus on REF.

In all scenario simulations are SST changes between 2070-2099 and 1969-1998 largest in the Bothnian Bay and Bothnian Sea during summer (Fig. 34). This pattern is a robust feature of our mini-ensemble although the amount of the warming differs substantially between HadCM3 and ECHAM5 driven simulations such that the ensemble spread is also largest in the Bothnian Bay and Bothnian Sea during summer. However, the climate change signal is much larger than the uncertainty caused by the GCMs as indicated both by the standard deviation of the ensemble mean (not shown) and the range of the ensemble. We found largest SST increases of more than 6°C in the southern Bothnian Bay in the HadCM3 driven scenario simulation. In ECHAM5 driven simulations the largest SST increase is located in the central Bothnian Bay and does not exceed 4°C approximately. Further, in all scenario simulations the SST increase during winter and spring is largest in the Gulf of Finland. Perhaps this increase may affect changing surface nutrient concentrations in the Gulf of Finland due to increased decomposition of organic matter in the sediments as discussed below.

Also spatial patterns of the SSS projections show an overall agreement with largest decreases in the Baltic proper of about 1.5-2 g kg^{-1} (Fig. 35). Salinity is reduced because in all scenario simulations runoff is significantly increased. Changes of the wind speed are of minor importance for SSS changes. Largest discrepancies between scenario simulations are found for the SSS projections in Kattegat.

The changes of the bottom salinity concentrations follow the SSS changes (Fig. 36). As the deepwater salinity at the open boundary in Kattegat does not change by definition, bottom salinity changes are smallest in the entire Kattegat and in the Belt Sea area. As in the ECHAM5 A1B_1 and A_2 driven simulations the mean wind speed increases over the Baltic proper during winter and autumn by about 1 m s^{-1}, in future climate wind induced mixing is larger and the permanent halocline is deeper located. Consequently, we found largest bottom salinity changes along the slopes of the Baltic proper and Gulf of Finland at depths of the halocline changes. As the wind changes occur only in two scenario simulations of our mini-ensemble, the largest uncertainty of projected bottom salinity is related to the unknown depth of the halocline.

As already mentioned, in all scenario simulations projected mean wind speed changes are small except in ECHAM5-A1B_1 and A_2 driven simulations. In these projections the mean west wind will increase causing a rise of the mean SSH in the Gulf of Finland and Gulf of Riga of about 12-16 cm during autumn (Fig. 37). The impact on mixing was discussed already.

The bottom oxygen concentrations decrease in all scenario simulations in almost all regions (Fig. 38). Exceptions are the deep water in the Gulf of Finland and regions along the slopes of the Gotland Basin where the stratification will decrease due to a deeper halocline caused by increased runoff in future climate. In addition, in the ECHAM5-A1B_1 driven simulation increased wind induced mixing will cause improved bottom oxygen concentrations. However, in most regions

the bottom oxygen concentration will decrease. As the oxygen saturation concentration is lower in warmer water the surface oxygen concentrations will decrease slightly in future climate. In the coastal zone with only a weak vertical stratification the bottom oxygen concentration will decrease as well. The decrease is larger in regions with larger water depth and with a permanent halocline because inflowing water is mixed with surface water which will have lower oxygen concentrations and because the inflow of oxygen rich salt water will decrease. We found the largest decrease of bottom oxygen concentrations in the HADCM3 driven simulation in the central area of the deep Bornholm Basin, Gotland Basin and Bothnian Sea. The uncertainty is largest in regions that are affected by the unknown position of the halocline.

As the phosphorus release capacity of the sediments is oxygen dependent, the generally decreased bottom oxygen concentration will cause an increase of the phosphate concentrations in the surface waters (Fig. 39). We found the largest phosphate concentration increase in the HadCM3 driven simulation in the Baltic proper and Gulf of Finland. In the ensemble mean the largest increase of surface phosphate concentrations occurs in the southern Baltic proper (Arkona Basin, Bornholm Basin and southern Gotland Basin) during winter. This signal is a common pattern in all scenario simulations. The surface phosphate concentration changes in the Gulf of Finland during spring have the largest spread within our ensemble.

In all scenario simulations the surface nitrate concentration remains unchanged or increases (Fig. 40). The patterns of changing nitrate concentration are similar in the various simulations. Especially during winter and especially in the eastern Gulf of Finland, Gulf of Riga and along the eastern coasts of the Gotland Basin nitrate concentrations will increase in future climate. The increased supply of nitrogen from the rivers and the increased oxygen concentrations in the Gulf of Finland might be the reason for the increased nitrate concentrations particularly in the coastal zone close to the river mouths of the large rivers.

The increased concentrations of both nitrate and phosphate during winter will impact the spring and summer blooms. During spring particularly the concentrations of flagellates and others will increase in the eastern Baltic proper, Gulf of Riga and Gulf of Finland (Fig. 42) whereas the concentration changes of diatoms are much smaller (Fig. 41). During summer and autumn the concentration of cyanobacteria will increase in the southern Baltic proper (Arkona Basin, Bornholm Basin and southern Gotland Basin) in all simulations (Fig. 43). In the HadCM3 driven simulation the cyanobacteria blooms in the Gulf of Finland will also be more intensive.

Both changes of the group of flagellates and others during spring and of the cyanobacteria during summer dominate the seasonal changes of the phytoplankton concentration (Fig. 44). The uncertainty is largest during summer due to the differences of the cyanobacteria changes in HadCM3 and ECHAM5 driven simulations. As a consequence the Secchi depths particularly during summer and autumn in the southern Baltic proper (Arkona Basin, Bornholm Basin and southern Gotland Basin) will decrease (Fig. 45). In the ensemble mean the largest decrease of Secchi depth amounts to about 1.2 - 1.4 m.

3.3.4. Projected changes for the nutrient load scenario BSAP As the oxygen bottom concentration will decrease significantly in the HadCM3 driven simulation assuming present day nutrient loads, in this scenario the improvements of the Baltic Sea Action Plan (BSAP) will be counteracted by the effect of changing climate at the end of the century (Fig. 46). As a consequence bottom oxygen concentration changes are small in BSAP. However, we found increased bottom oxygen concentrations in the ECHAM5 driven simulations in the Gulf of Finland and in the Gotland Basin when we applied the nutrient load scenario BSAP. In the ECHAM5-A1B_1 and A_2 driven simulations we found the largest increases of the oxygen bottom concentration along the slopes of the Gotland Basin and in the Gulf of Finland due to the deeping of the halocline and the corresponding decreased stratification in that depth interval. Thus, depending on the climate scenario the Baltic Sea Action Plan does not necessarily improve the environmental status of the Baltic Sea.

While in the HadCM3 driven simulation surface phosphate and nitrate concentration changes are small, we found in ECHAM5 driven simulations in the Gulf of Finland reduced surface phosphate and increased surface nitrate concentrations (Figs. 47 and 48). Thus, the response of surface nutrient concentrations seems to be modified by changing bottom oxygen concentrations and changing water temperature changes (affecting the decomposition of organic matter in the sediments)

Surface concentration changes of diatoms, flagellates and others and cyanobacteria are diverse (Figs. 49 to 51). During spring in all scenario simulations surface diatom concentrations decrease especially along the southern and eastern coasts of the Baltic proper and in the Gulf of Finland. To the contrary, we found slight increases of the surface concentrations of flagellate and others mainly in the Gulf of Finland. Cyanobacteria concentrations increase in the southern Baltic proper (mainly in the Bornholm Basin) in the HadCM3 driven simulation and remain basically unchanged in ECHAM5 driven simulations. During spring surface phytoplankton concentrations in the ECHAM5 driven simulations decrease following diatom concentration changes (Fig. 52). During summer we found slight surface phytoplankton concentration increases in

the southern Baltic proper in the HadCM3 driven simulation following cyanobacteria concentration changes. Corresponding increases of the Secchi depth during spring amount to about 1 m at maximum (Fig. 53). During summer the Secchi depth in the HadCM3 driven simulation decreases by about 0.5 m in maximum.

3.3.5. Projected changes for the nutrient load scenario CLEG In CLEG bottom oxygen concentrations will decrease almost everywhere in the HadCM3 driven simulation at the end of the century (Fig. 54). In the ECHAM5 driven scenarios the bottom oxygen concentrations especially in the Gulf of Finland will increase. In the two scenarios with increased wind induced mixing in the Baltic proper (ECHAM5-A1B_1 and ECHAM5-A2) the bottom oxygen concentrations along the slopes will increase as well because of deeper locations of the halocline.

As a consequence of the bottom oxygen concentration changes surface phosphate concentrations increase in HadCM3 driven scenario simulations (Fig. 55). Nitrate concentration changes are largest in the Gulf of Finland and in the Gulf of Riga in ECHAM5-A1B_1 and ECHAM5-A2 driven simulations (Fig. 56).

Concentration changes of diatoms, flagellates and others, cyanobacteria and phytoplankton are relatively small (Figs. 57 to 60). As the projected phytoplankton concentrations in the ensemble mean slightly increases at the end of the 21st century, Secchi depths decreases (Fig. 61). Largest changes of about 1 m are found in the Bornholm Basin in the HadCM3 driven scenario simulation.

3.3.6. Projected changes for the nutrient load scenario BAU In the BAU scenario the impact of increased nutrient loads and the impact of changing climate seem to amplify each other with large consequences for the marine environment. Large reductions of bottom oxygen concentrations (Fig. 62), large increases of surface phosphate (Fig. 63) and nitrate concentrations (Fig. 64) and large increases of both the spring and summer blooms characterize the BAU scenario (Figs. 65 to 68). In this scenario Secchi depths will in the south-western Baltic be more than 2 m smaller at the end of the century compared to present conditions (Fig. 69).

4. Conclusions

In this study we focussed on annual and seasonal mean changes of ecological quality indicators describing the environmental status of the Baltic Sea. Agreement and disagreement of the simulated changes were assessed from the statistics of the ensemble of 16 scenario simulations. Projected changes at the end of the 21^{st} century are usually larger than biases induced by the deficiencies of GCMs at the regional scale. Especially ensemble mean biases are smaller than ensemble mean changes stressing the added value of ensemble modelling.

According to our mini-ensemble at the end of the 21^{st} century water temperatures will increase, runoff will increase, salinity will decrease, vertical stratification will decrease and changes of the wind speed and of gustiness over the Baltic proper will be diverse. In correspondence with earlier studies we found that the impact of changing climate on the Baltic biogeochemistry might be significant. The model simulations suggest that in addition to eutrophication projected changing climate is an important stressor for the Baltic ecosystem. According to our scenario simulations with reference loads water quality will be reduced in future climate. Reduced inflow of oxygen rich salt water will cause increased hypoxic bottom areas and increased surface nutrient and phytoplankton concentrations. Secchi depths in the Baltic proper will be reduced. In summer the ensemble mean of the Secchi depth will decrease in the southern Baltic proper by about 1.5 m at maximum.

According to our results nutrient load reductions included under current legislation will not be sufficient to improve the water quality at the end of the century. The climate effect is larger than the impact of nutrient load reductions and Secchi depth will decrease especially in the southern Baltic proper. The larger nutrient load reductions of the BSAP will improve the water quality at the end of the century. However for the same targets larger reductions will be necessary as in present climate. In summer the ensemble mean of the Secchi depth will increase in the southern Baltic proper by about 1 m in maximum. In case of an exponential growth of agriculture following a pessimistic business-as-usual scenario bottom oxygen concentrations will decrease, surface nutrient concentrations will increase and Secchi depth will decrease significantly. During the warmer seasons (spring to autumn) the ensemble mean of the Secchi depth in the southern Baltic proper will decrease by more than 2 m in some some regions.

Acknowledgments. The work presented in this study was jointly funded by the Swedish Environmental Protection Agency (SEPA, ref. no. 08/381) and the European Community's Seventh Framework Programme (FP/2007-2013) under grant agreement no. 217246 made with the joint Baltic Sea research and development programme BONUS (http://www.bonusportal.org) within the ECOSUPPORT project (Advanced modeling tool for scenarios of the Baltic Sea ECOsystem to SUPPORT decision making, http://www.baltex-research.eu/ecosupport). The RCO model simulations were partly performed on the climate computing resources 'Ekman' and 'Vagn' jointly operated by the Centre for High Performance Computing (PDC) at the Royal Institute of Technology (KTH) in Stockholm and the National Supercomputer Centre (NSC) at Linköping University. 'Ekman' and 'Vagn' are funded by a grant from the Knut and Alice Wallenberg foundation.

References

Almroth-Rosell, E., K. Eilola, R. Hordoir, H. E. M. Meier, and P. O. J. Hall, Transport of fresh and resuspended particulate organic material in the Baltic Sea - a model study, *J. Marine Systems*, 2011, doi:10.1016/j.jmarsys.2011.02.005.

Bergström, S., and B. Carlsson, River runoff to the Baltic Sea: 1950-1990, *Ambio*, *23*, 280–287, 1994.

Eilola, K., H. E. M. Meier, and E. Almroth, On the dynamics of oxygen, phosphorus and cyanobacteria in the Baltic Sea; a model study., *J. Marine Systems*, *75*, 163–184, 2009.

Gustafsson, B. G., and H. C. Andersson, Modeling the exchange of the Baltic Sea from the meridional atmospheric pressure difference across the North Sea, *J. Geophys. Res.*, *106*, 19,731–19,744, 2001.

HELCOM, Toward a Baltic Sea unaffected by eutrophication. Background document to Helcom Ministerial Meeting, Krakow, Poland, *Tech. rep.*, Helsinki Commission, Helsinki, Finland, 2007.

Höglund, A., H. E. M. Meier, B. Broman, and E. Kriezi, Validation and correction of regionalised ERA-40 wind fields over the Baltic Sea using the Rossby Centre Atmosphere model RCA3.0, *Tech. Rep. No.97*, Rapport Oceanografi, 2009, 29 pp.

Humborg, C., C. Mörth, M. Sundbom, and F. Wulff, Riverine transport of biogenic elements to the Baltic Sea - past and possible future perspectives, *Hydrology and Earth System Sciences*, *11(5)*, 1593–1607, 2007.

Kjellström, E., G. Nikulin, U. Hansson, G. Strandberg, and A. Ullerstig, 21st century changes in the european climate: uncertainties derived from an ensemble of regional climate model simulations, *Tellus*, *63A*, 24–40, 2011.

Lindström, G., C. Pers, J. Rosberg, J. Strömqvist, and B. Arheimer, Development and testing of the HYPE (HYdrological Predictions for the Environment) water quality model for different spatial scales, *Hydrology research*, *41*, 295–319, 2010.

Meier, H. E. M., On the parameterization of mixing in three-dimensional Baltic Sea models, *J. Geophys. Res.*, *106*, 30,997–31,016, 2001.

Meier, H. E. M., Baltic Sea climate in the late twenty-first century: a dynamical downscaling approach using two global models and two emission scenarios, *Clim. Dyn.*, 2006, published online 11 Apr 2006, doi:10.1007/s00382-006-0124-x.

Meier, H. E. M., Modeling the pathways and ages of inflowing salt- and freshwater in the Baltic Sea, *Estuarine, Coastal and Shelf Science*, *74*, 717–734, 2007.

Meier, H. E. M., R. Döscher, and T. Faxén, A multiprocessor coupled ice-ocean model for the Baltic Sea: Application to salt inflow, *J. Geophys. Res.*, *108(C8)*, 3273, doi:10.1029/2000JC000,521, 2003.

Meier, H. E. M., K. Eilola, and E. Almroth, Climate-related changes in marine ecosystems simulated with a three-dimensional coupled biogeochemical-physical model of the Baltic Sea, *Clim. Res.*, 2011a, in press.

Meier, H. E. M., A. Höglund, R. Döscher, H. Andersson, U. Löptien, and E. Kjellström, Quality assessment of atmospheric surface fields over the Baltic Sea of an ensemble of regional climate model simulations with respect to ocean dynamics, *Oceanologia*, 2011b, in press.

Samuelsson, P., et al., The Rossby Centre Regional Climate model RCA3: model description and performance, *Tellus*, *63A*, 4–23, 2011.

Wulff, F., O. P. Savchuk, A. Sokolov, and C. Humborg, Management options and effects on a marine ecosystem: assessing the future of the Baltic, *AMBIO*, *36*, 243–249, 2007.

This preprint was prepared with AGU's LaTeX macros v5.01, with the extension package 'AGU^{++}' by P. W. Daly, version 1.6b from 1999/08/19.

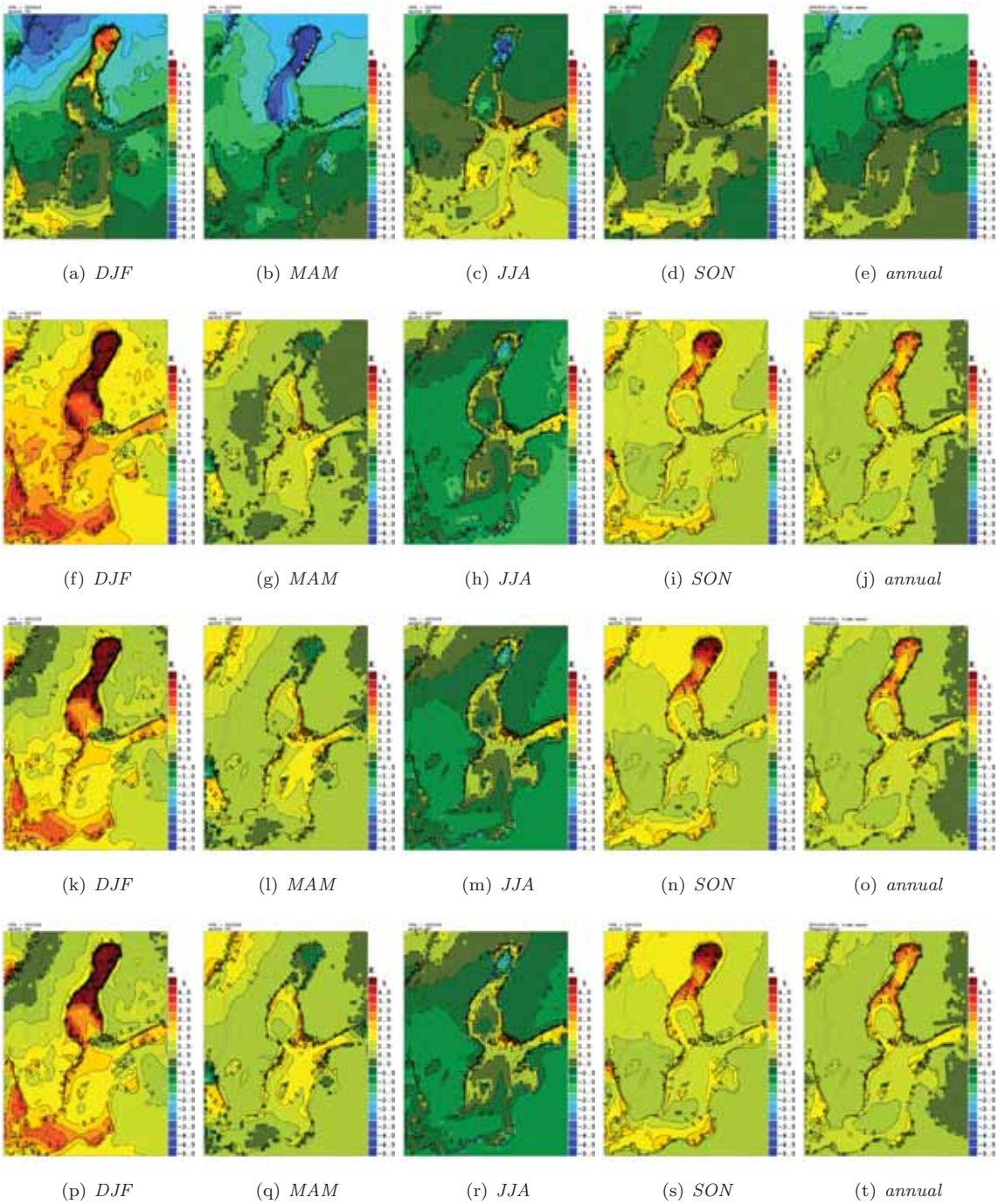

(a) *DJF* (b) *MAM* (c) *JJA* (d) *SON* (e) *annual*

(f) *DJF* (g) *MAM* (h) *JJA* (i) *SON* (j) *annual*

(k) *DJF* (l) *MAM* (m) *JJA* (n) *SON* (o) *annual*

(p) *DJF* (q) *MAM* (r) *JJA* (s) *SON* (t) *annual*

Figure 5. 2 m air temperature differences (in °C) between the GCM driven RCAO simulations during the control period (December 1968 to November 1998) and the hindcast simulation using RCA3 forced with ERA40. From left to right differences for the four seasons (DJF, MAM, JJA and SON) and for the annual mean are shown. The rows correspond to the RCAO simulation forced with HadCM3-A1B (first row)), ECHAM5-A1B_3 (second row), ECHAM5-A1B_1 (third row) and ECHAM5-A2 (fourth row).

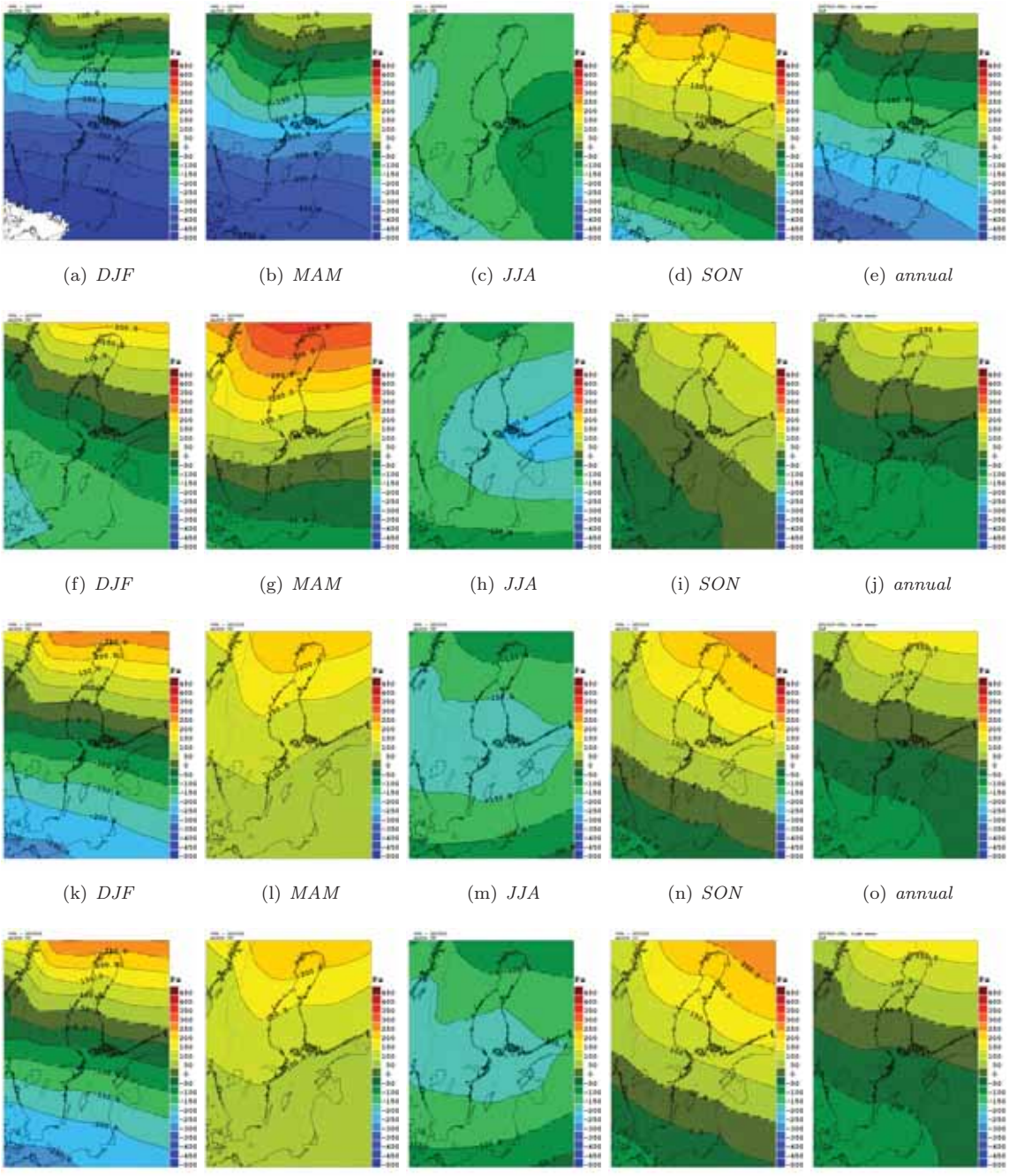

(a) *DJF* (b) *MAM* (c) *JJA* (d) *SON* (e) *annual*

(f) *DJF* (g) *MAM* (h) *JJA* (i) *SON* (j) *annual*

(k) *DJF* (l) *MAM* (m) *JJA* (n) *SON* (o) *annual*

(p) *DJF* (q) *MAM* (r) *JJA* (s) *SON* (t) *annual*

Figure 6. Same as Figure 5 but for sea level pressure (in Pa).

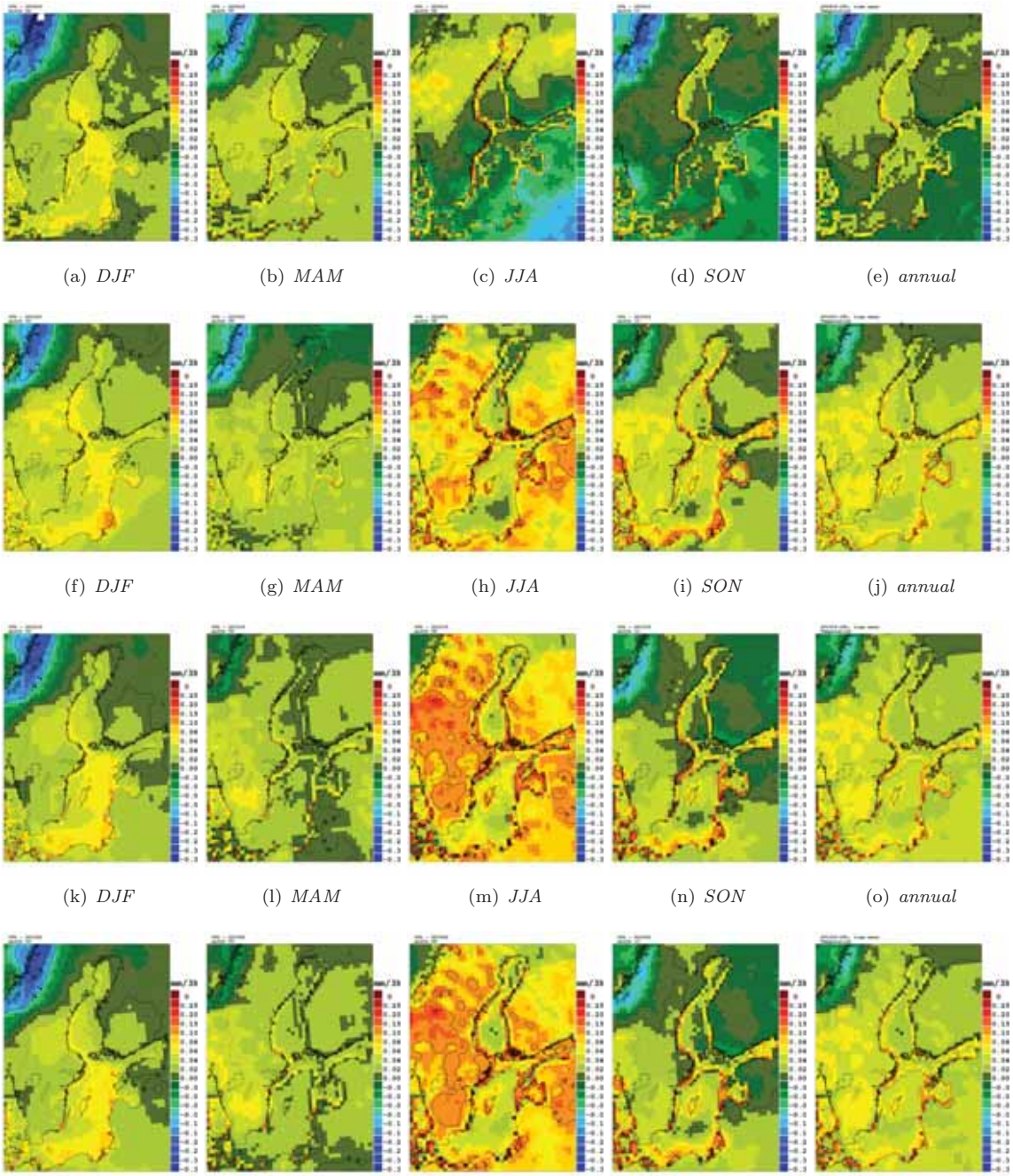

(a) *DJF* (b) *MAM* (c) *JJA* (d) *SON* (e) *annual*

(f) *DJF* (g) *MAM* (h) *JJA* (i) *SON* (j) *annual*

(k) *DJF* (l) *MAM* (m) *JJA* (n) *SON* (o) *annual*

(p) *DJF* (q) *MAM* (r) *JJA* (s) *SON* (t) *annual*

Figure 7. Same as Figure 5 but for precipitation (in mm/3h).

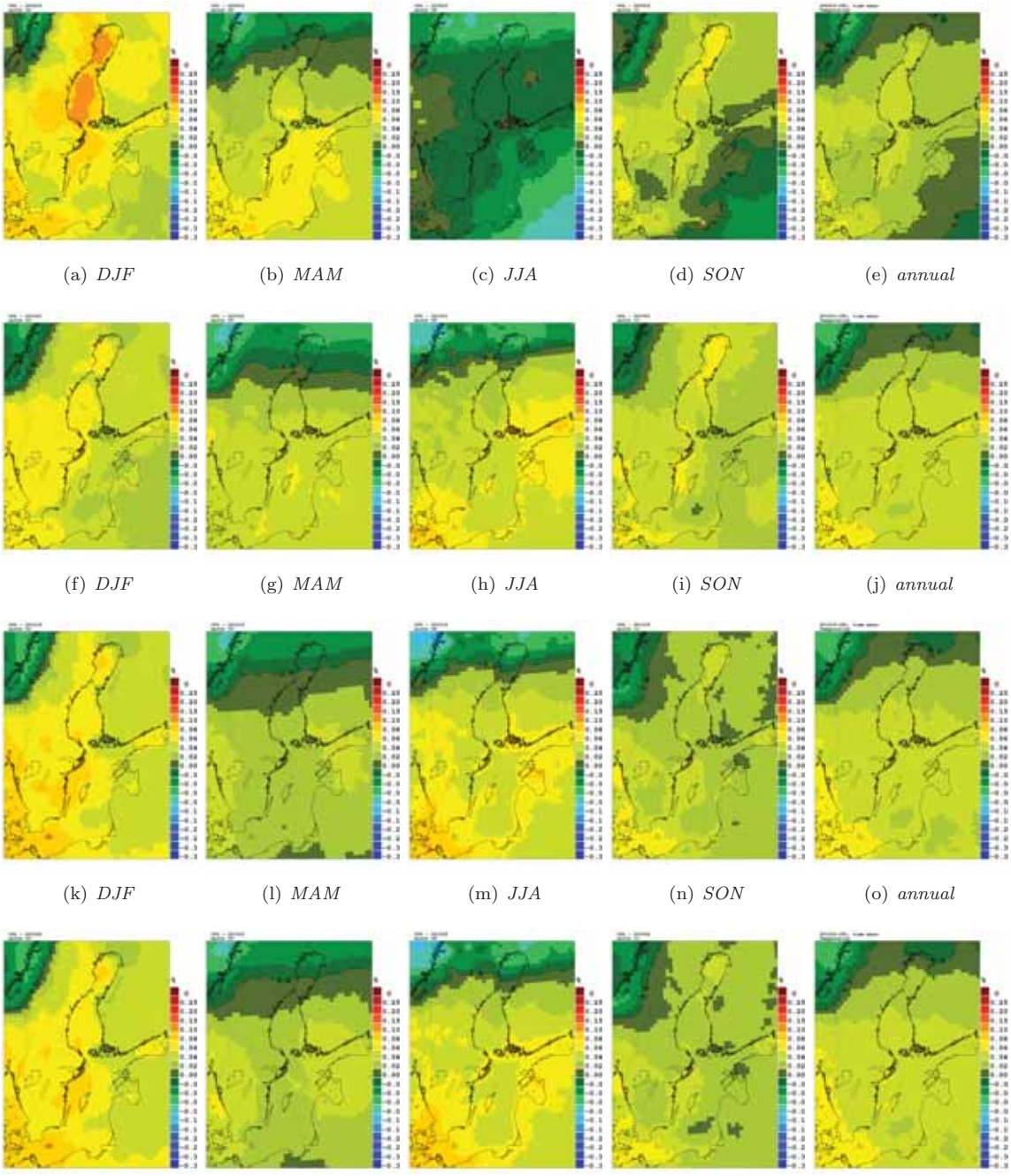

(a) *DJF* (b) *MAM* (c) *JJA* (d) *SON* (e) *annual*

(f) *DJF* (g) *MAM* (h) *JJA* (i) *SON* (j) *annual*

(k) *DJF* (l) *MAM* (m) *JJA* (n) *SON* (o) *annual*

(p) *DJF* (q) *MAM* (r) *JJA* (s) *SON* (t) *annual*

Figure 8. Same as Figure 5 but for cloud cover.

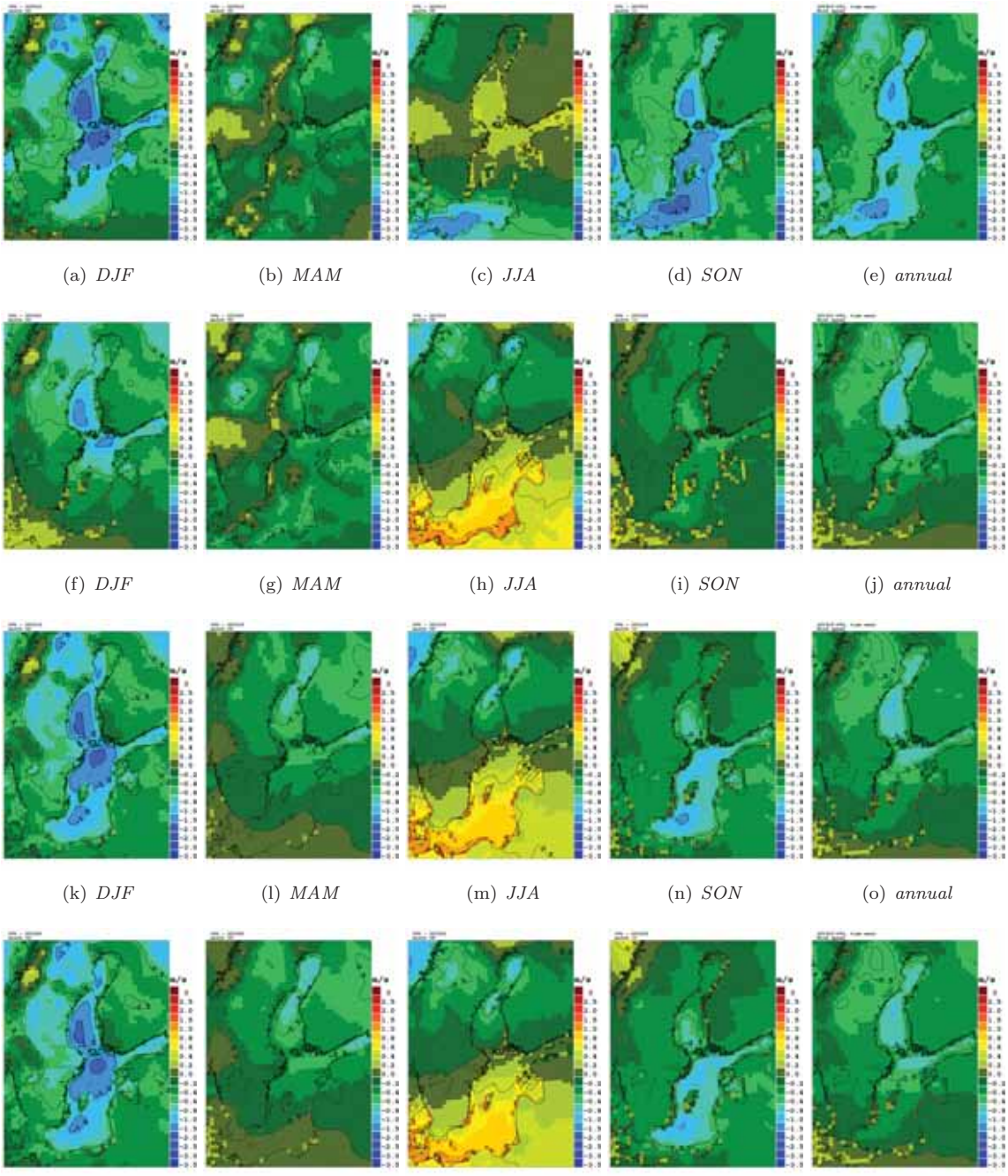

(a) *DJF* (b) *MAM* (c) *JJA* (d) *SON* (e) *annual*

(f) *DJF* (g) *MAM* (h) *JJA* (i) *SON* (j) *annual*

(k) *DJF* (l) *MAM* (m) *JJA* (n) *SON* (o) *annual*

(p) *DJF* (q) *MAM* (r) *JJA* (s) *SON* (t) *annual*

Figure 9. Same as Figure 5 but for the mean 10 m wind speed (in m/s).

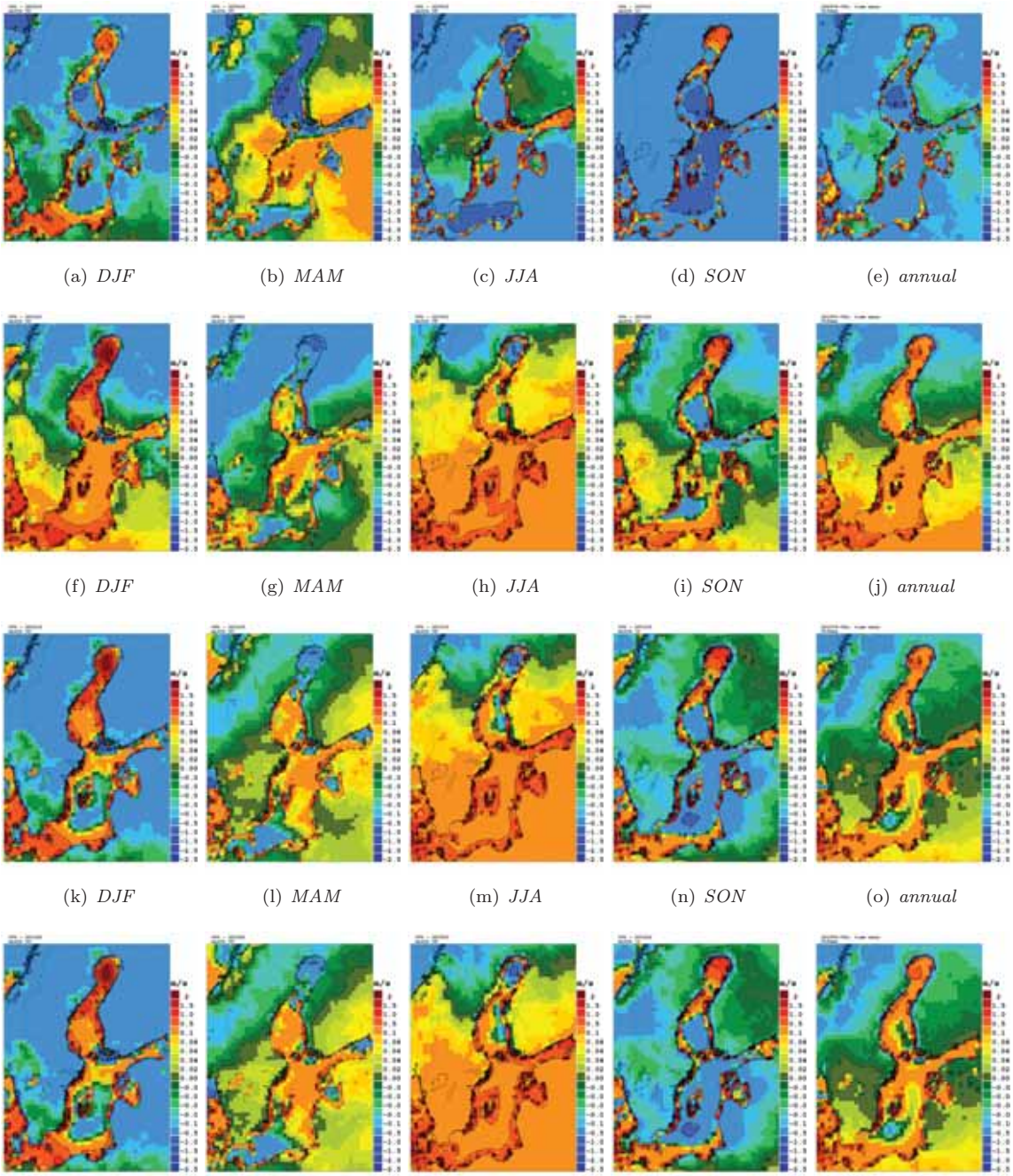

(a) *DJF* (b) *MAM* (c) *JJA* (d) *SON* (e) *annual*

(f) *DJF* (g) *MAM* (h) *JJA* (i) *SON* (j) *annual*

(k) *DJF* (l) *MAM* (m) *JJA* (n) *SON* (o) *annual*

(p) *DJF* (q) *MAM* (r) *JJA* (s) *SON* (t) *annual*

Figure 10. Same as Figure 5 but for the maximum 10 m wind speed (in m/s).

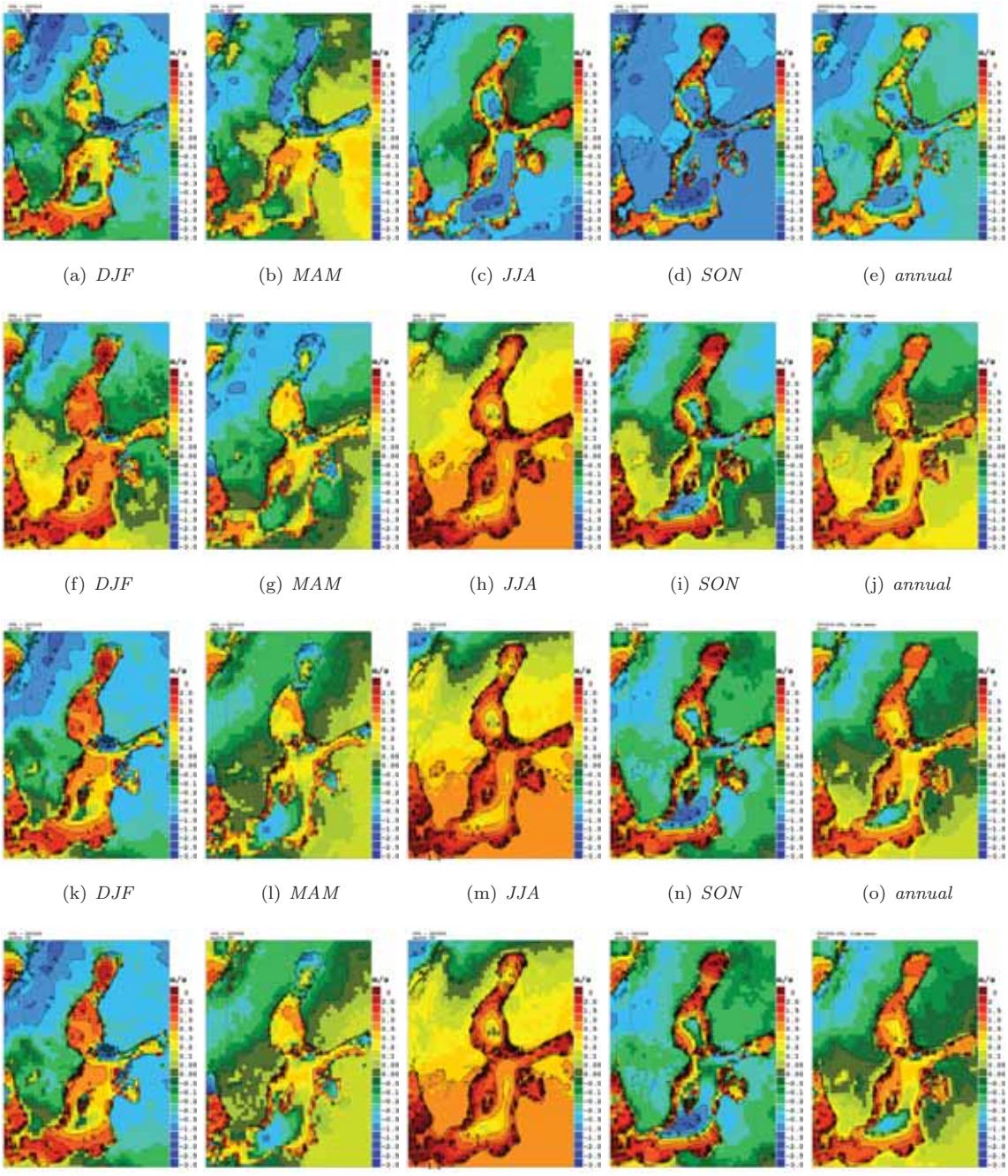

(a) *DJF* (b) *MAM* (c) *JJA* (d) *SON* (e) *annual*

(f) *DJF* (g) *MAM* (h) *JJA* (i) *SON* (j) *annual*

(k) *DJF* (l) *MAM* (m) *JJA* (n) *SON* (o) *annual*

(p) *DJF* (q) *MAM* (r) *JJA* (s) *SON* (t) *annual*

Figure 11. Same as Figure 5 but for the maximum estimated gust wind (in m/s).

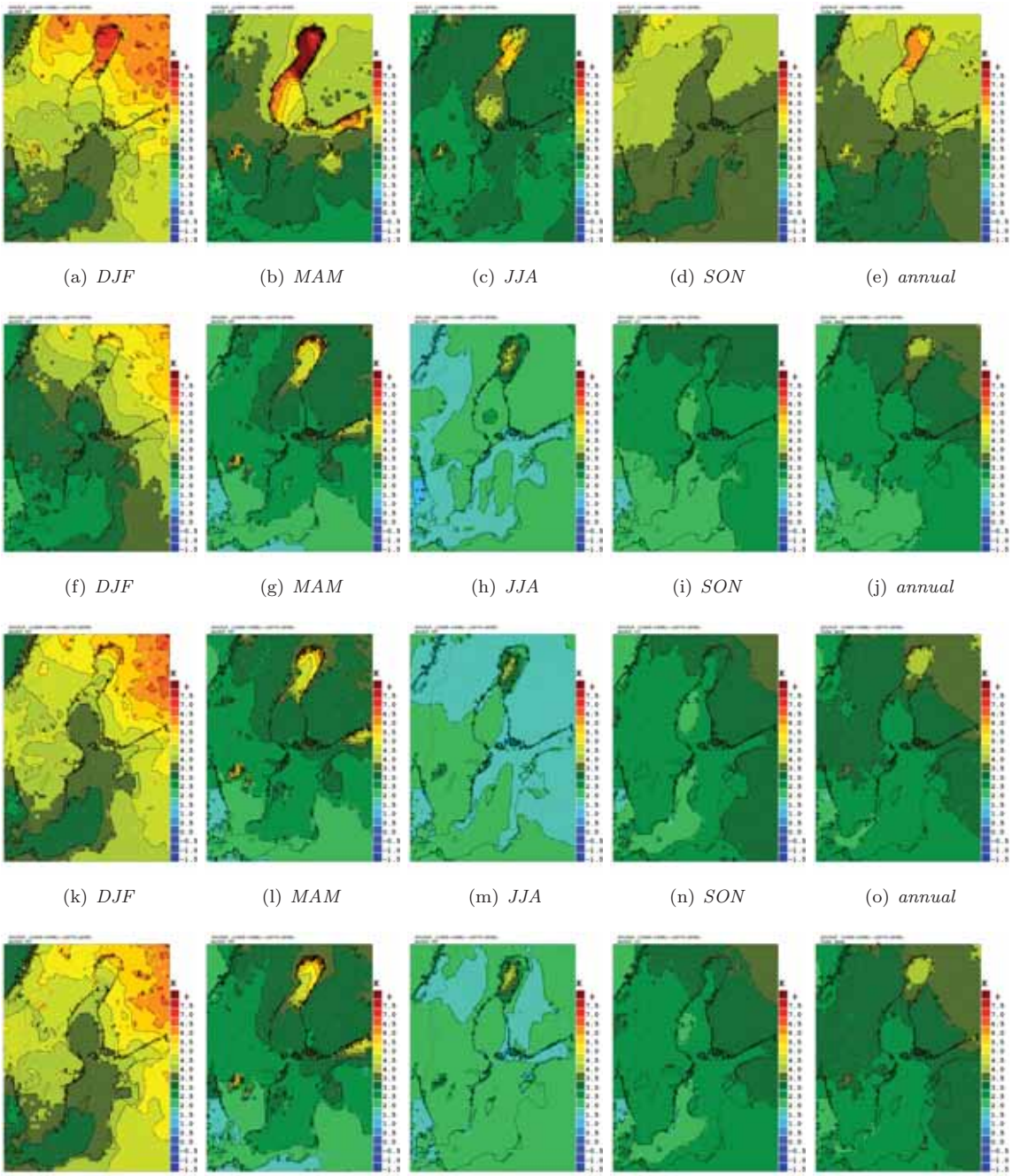

(a) *DJF* (b) *MAM* (c) *JJA* (d) *SON* (e) *annual*

(f) *DJF* (g) *MAM* (h) *JJA* (i) *SON* (j) *annual*

(k) *DJF* (l) *MAM* (m) *JJA* (n) *SON* (o) *annual*

(p) *DJF* (q) *MAM* (r) *JJA* (s) *SON* (t) *annual*

Figure 12. 2 m air temperature differences (in °C) between the projected changes at the end of the 21st century (November 2069 until December 2099) and the control period (December 1969 until November 1998). From left to right differences for the four seasons (DJF, MAM, JJA and SON) and for the annual mean are shown. The rows correspond to the RCAO simulations forced with HadCM3-A1B (first row), ECHAM5-A1B_3 (second row), ECHAM5-A1B_1 (third row) and ECHAM5-A2 (fourth row).

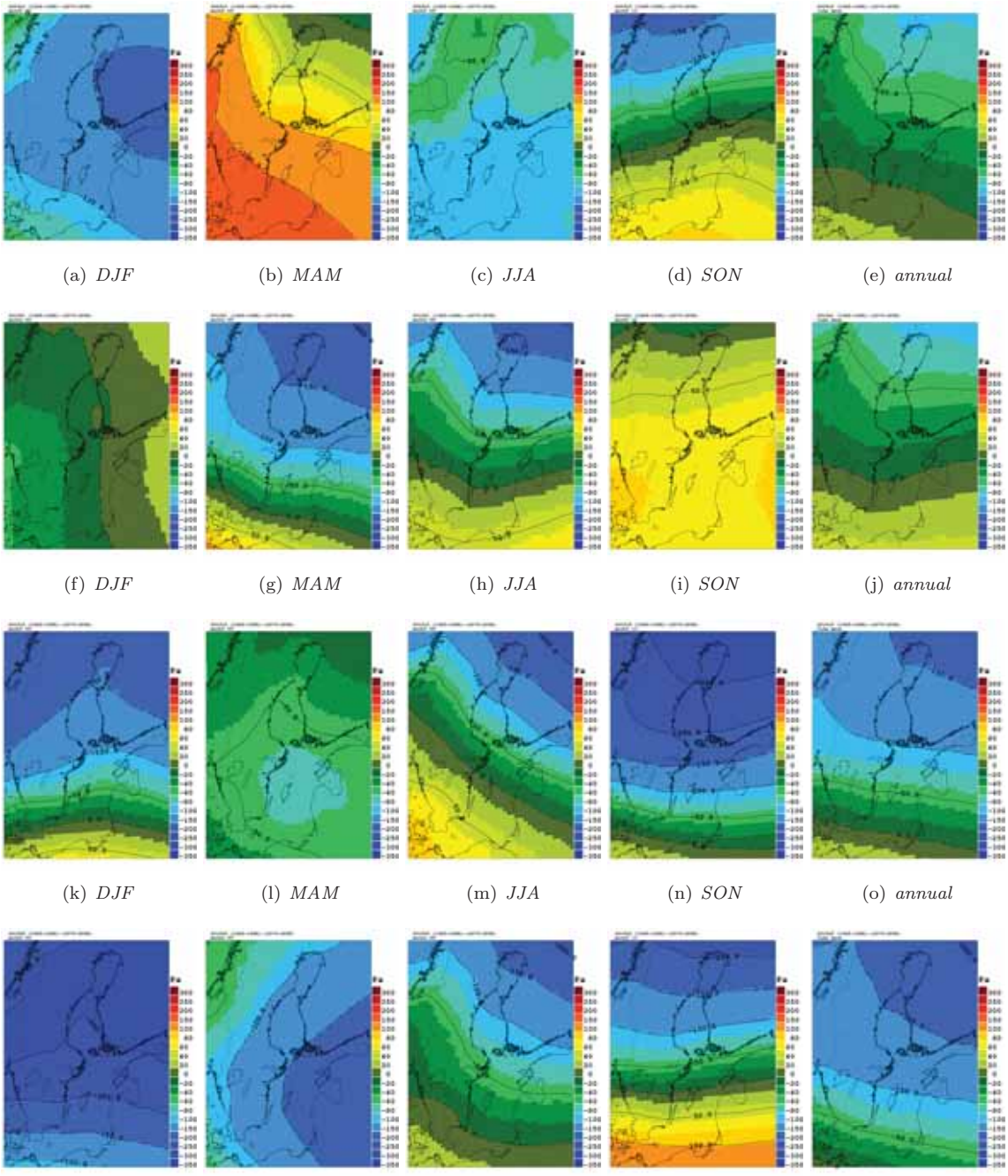

(a) *DJF* (b) *MAM* (c) *JJA* (d) *SON* (e) *annual*

(f) *DJF* (g) *MAM* (h) *JJA* (i) *SON* (j) *annual*

(k) *DJF* (l) *MAM* (m) *JJA* (n) *SON* (o) *annual*

(p) *DJF* (q) *MAM* (r) *JJA* (s) *SON* (t) *annual*

Figure 13. Same as Figure 12 but for sea level pressure (in Pa).

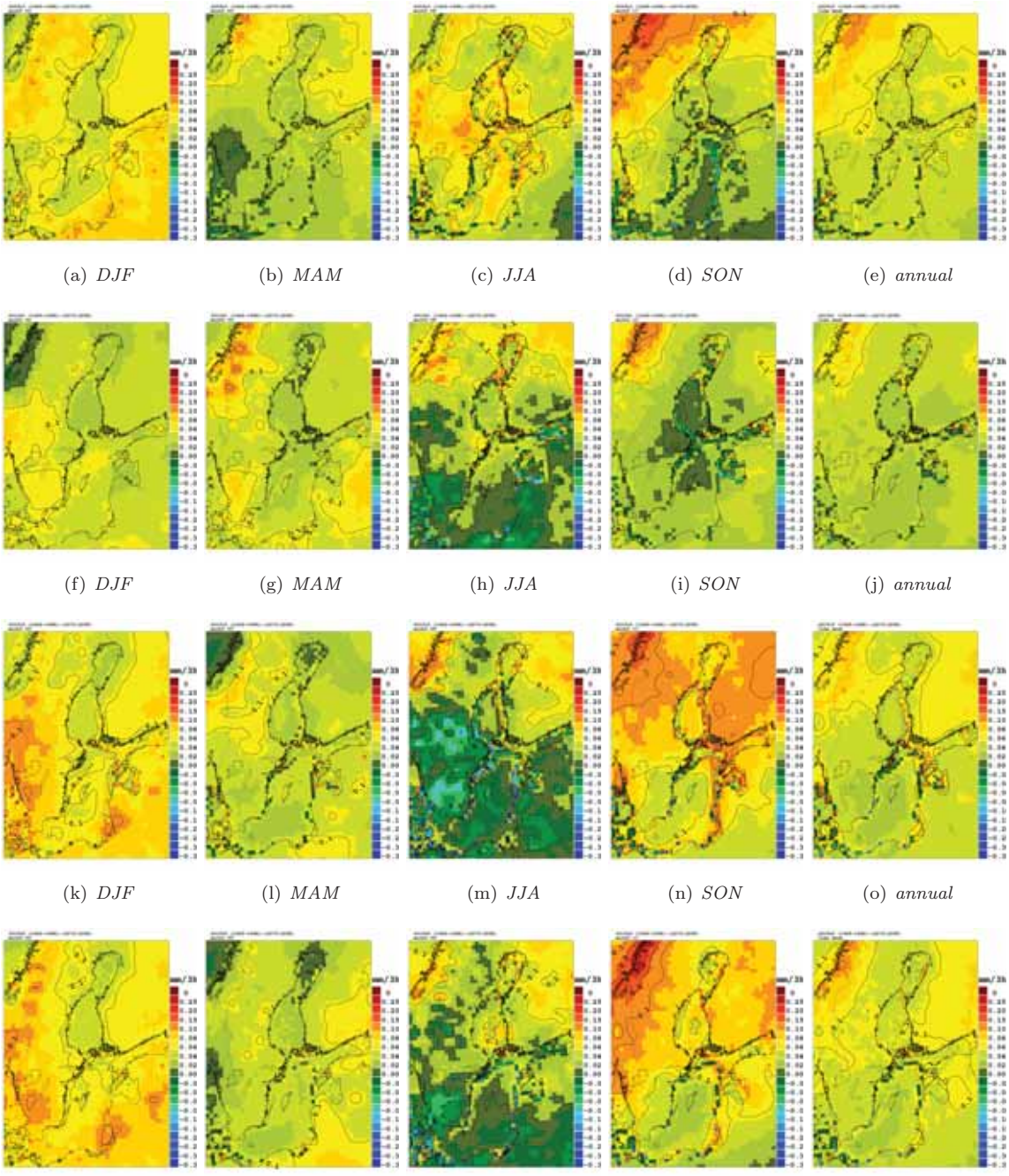

(a) *DJF* (b) *MAM* (c) *JJA* (d) *SON* (e) *annual*

(f) *DJF* (g) *MAM* (h) *JJA* (i) *SON* (j) *annual*

(k) *DJF* (l) *MAM* (m) *JJA* (n) *SON* (o) *annual*

(p) *DJF* (q) *MAM* (r) *JJA* (s) *SON* (t) *annual*

Figure 14. Same as Figure 12 but for precipitation (in mm/3h).

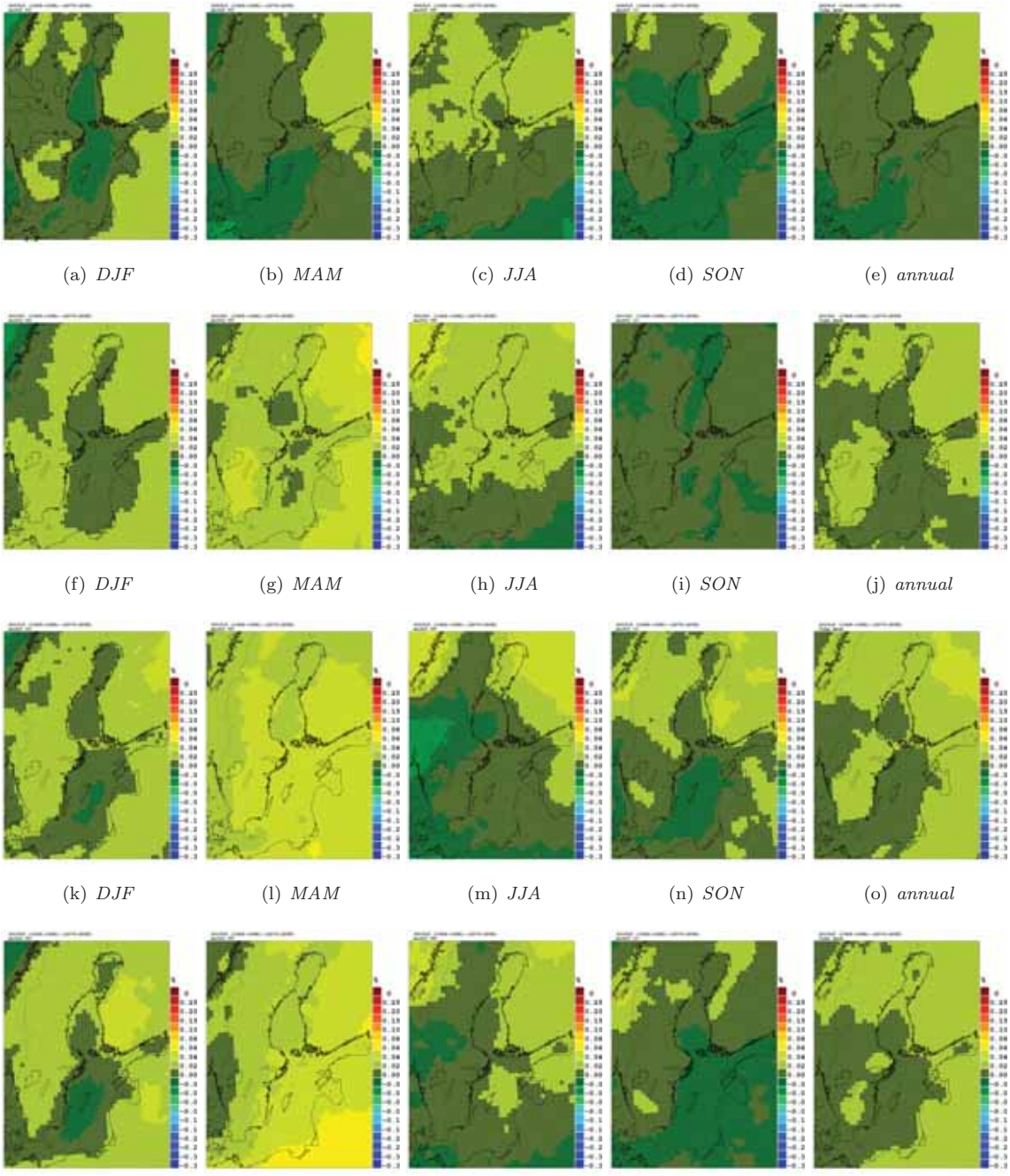

(a) *DJF* (b) *MAM* (c) *JJA* (d) *SON* (e) *annual*

(f) *DJF* (g) *MAM* (h) *JJA* (i) *SON* (j) *annual*

(k) *DJF* (l) *MAM* (m) *JJA* (n) *SON* (o) *annual*

(p) *DJF* (q) *MAM* (r) *JJA* (s) *SON* (t) *annual*

Figure 15. Same as Figure 12 but for cloud cover.

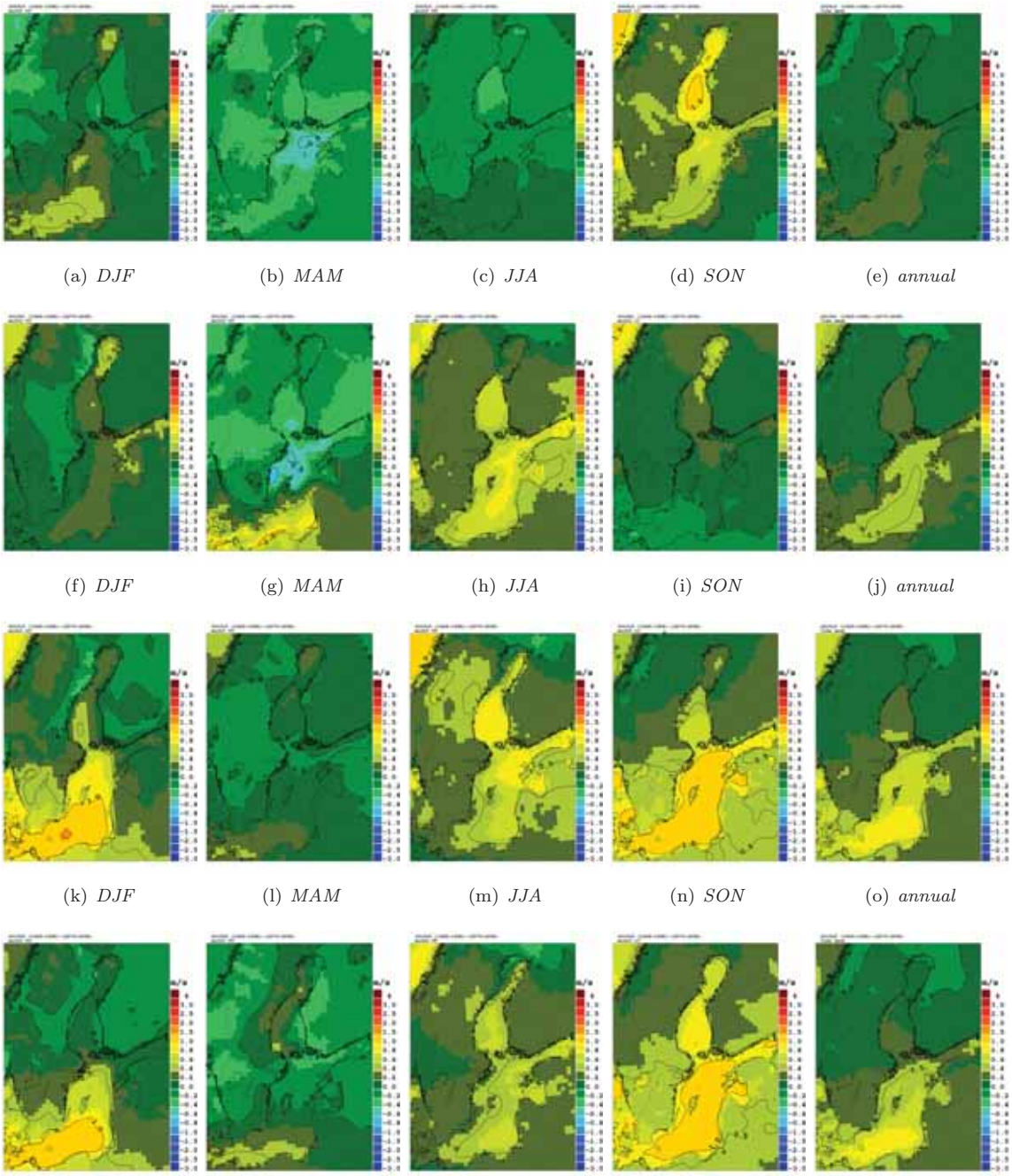

(a) *DJF* (b) *MAM* (c) *JJA* (d) *SON* (e) *annual*

(f) *DJF* (g) *MAM* (h) *JJA* (i) *SON* (j) *annual*

(k) *DJF* (l) *MAM* (m) *JJA* (n) *SON* (o) *annual*

(p) *DJF* (q) *MAM* (r) *JJA* (s) *SON* (t) *annual*

Figure 16. Same as Figure 12 but for 10 m wind speed (in m/s).

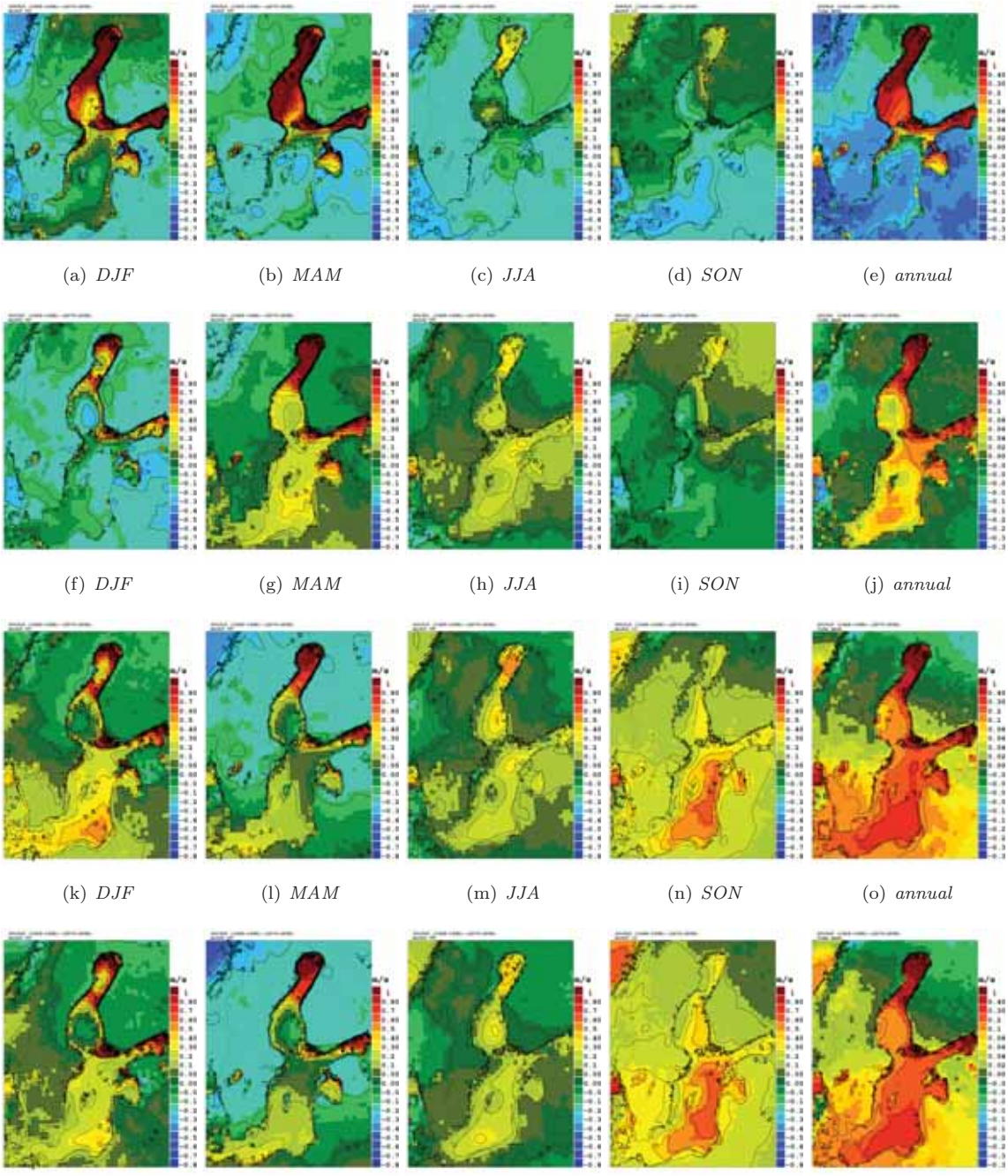

(a) *DJF* (b) *MAM* (c) *JJA* (d) *SON* (e) *annual*

(f) *DJF* (g) *MAM* (h) *JJA* (i) *SON* (j) *annual*

(k) *DJF* (l) *MAM* (m) *JJA* (n) *SON* (o) *annual*

(p) *DJF* (q) *MAM* (r) *JJA* (s) *SON* (t) *annual*

Figure 17. Same as Figure 12 but for the maximum 10 m wind speed (in m/s).

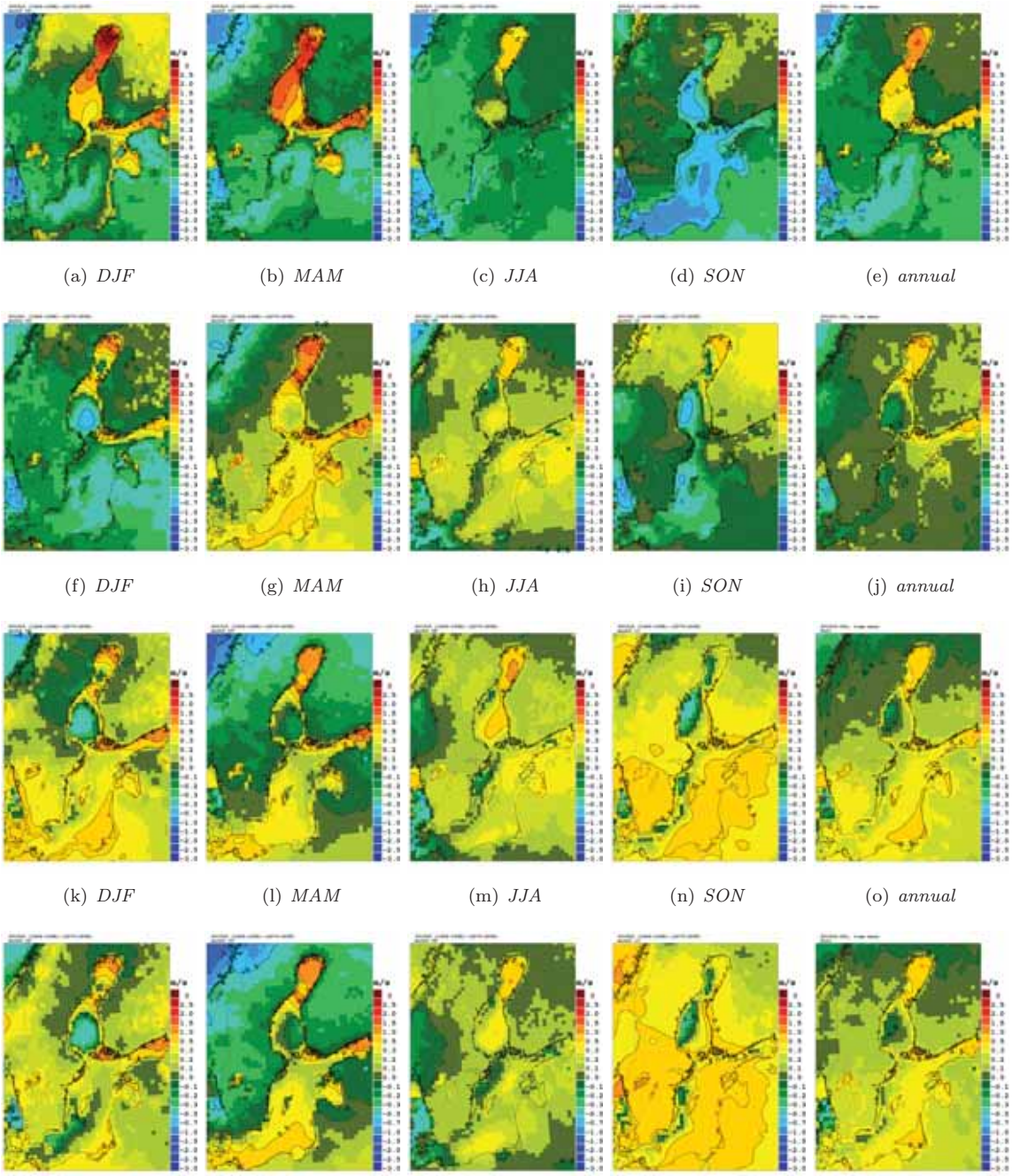

(a) *DJF* (b) *MAM* (c) *JJA* (d) *SON* (e) *annual*

(f) *DJF* (g) *MAM* (h) *JJA* (i) *SON* (j) *annual*

(k) *DJF* (l) *MAM* (m) *JJA* (n) *SON* (o) *annual*

(p) *DJF* (q) *MAM* (r) *JJA* (s) *SON* (t) *annual*

Figure 18. Same as Figure 12 but for the maximum estimated gust wind (in m/s).

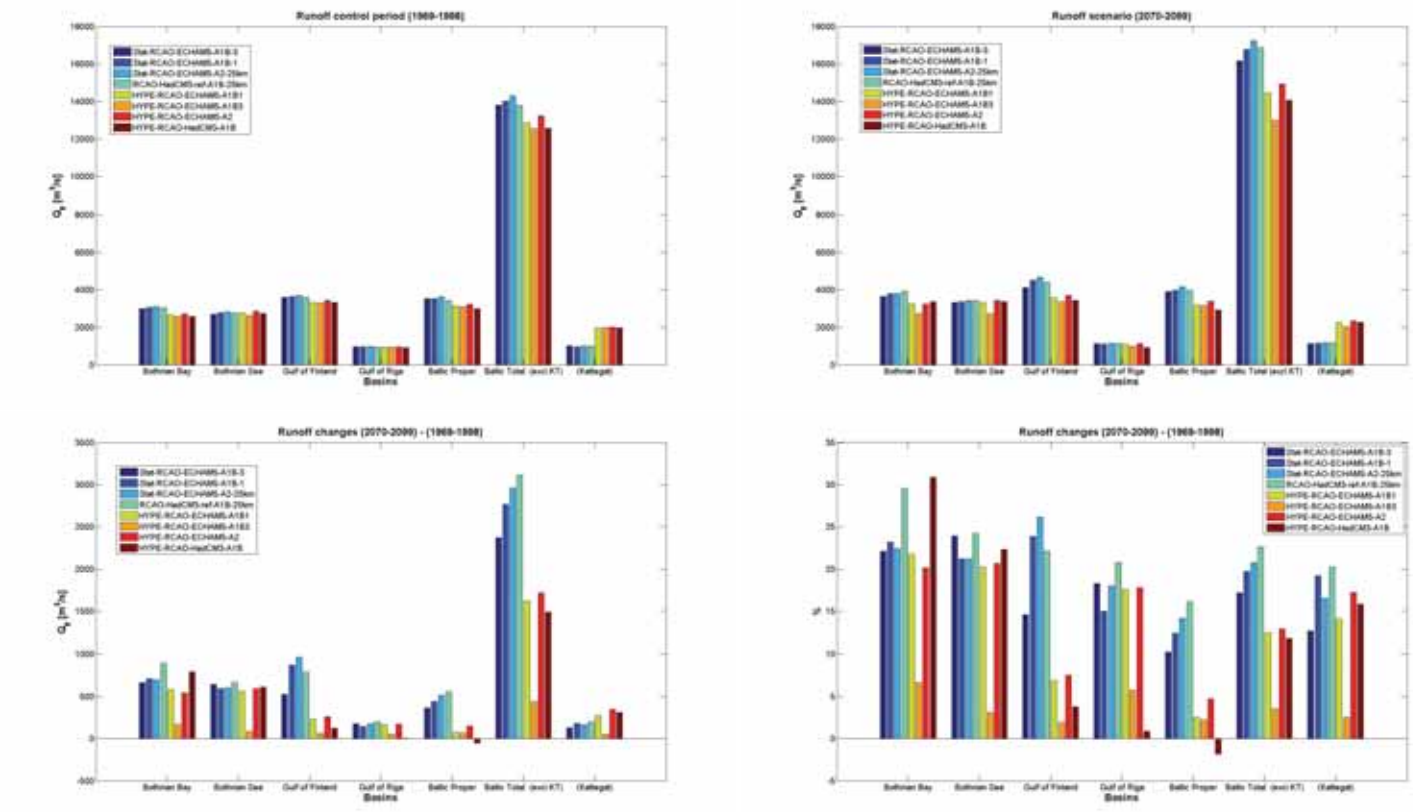

Figure 19. Volume flows (in $m^3\ s^{-1}$) in present and future climates calculated with the statistical model (Section 2.3) and with HYPE [*Lindström et al.*, 2010] during the control period 1969-1998 (upper left panel), at the end of the 21st century 2070-2099 (upper right panel) and changes between the periods 2070-2099 and 1969-1998 in absolute (lower left panel) and relative (lower right panel) values. The volume flows into the Bothnian Bay, Bothnian Sea, Gulf of Finland, Gulf of Riga, Baltic proper, total Baltic (without Kattegat) and Kattegat are depicted.

Figure 20. Annual and seasonal mean sea surface temperature (SST) biases (°C) during 1969-1998 in RCO-SCOBI simulations driven by regionalized GCM results. From left to right results for winter (December through February), spring (March through May), summer (June through August), autumn (September through November) and the annual mean are shown. From top to bottom the results of the following scenario simulations and analysis results are shown: RCAO-HadCM3-A1B-REF, RCAO-ECHAM5-A1B-3-REF, RCAO-ECHAM5-A1B-1-REF, RCAO-ECHAM5-A2-1-REF, ensemble mean, and range.

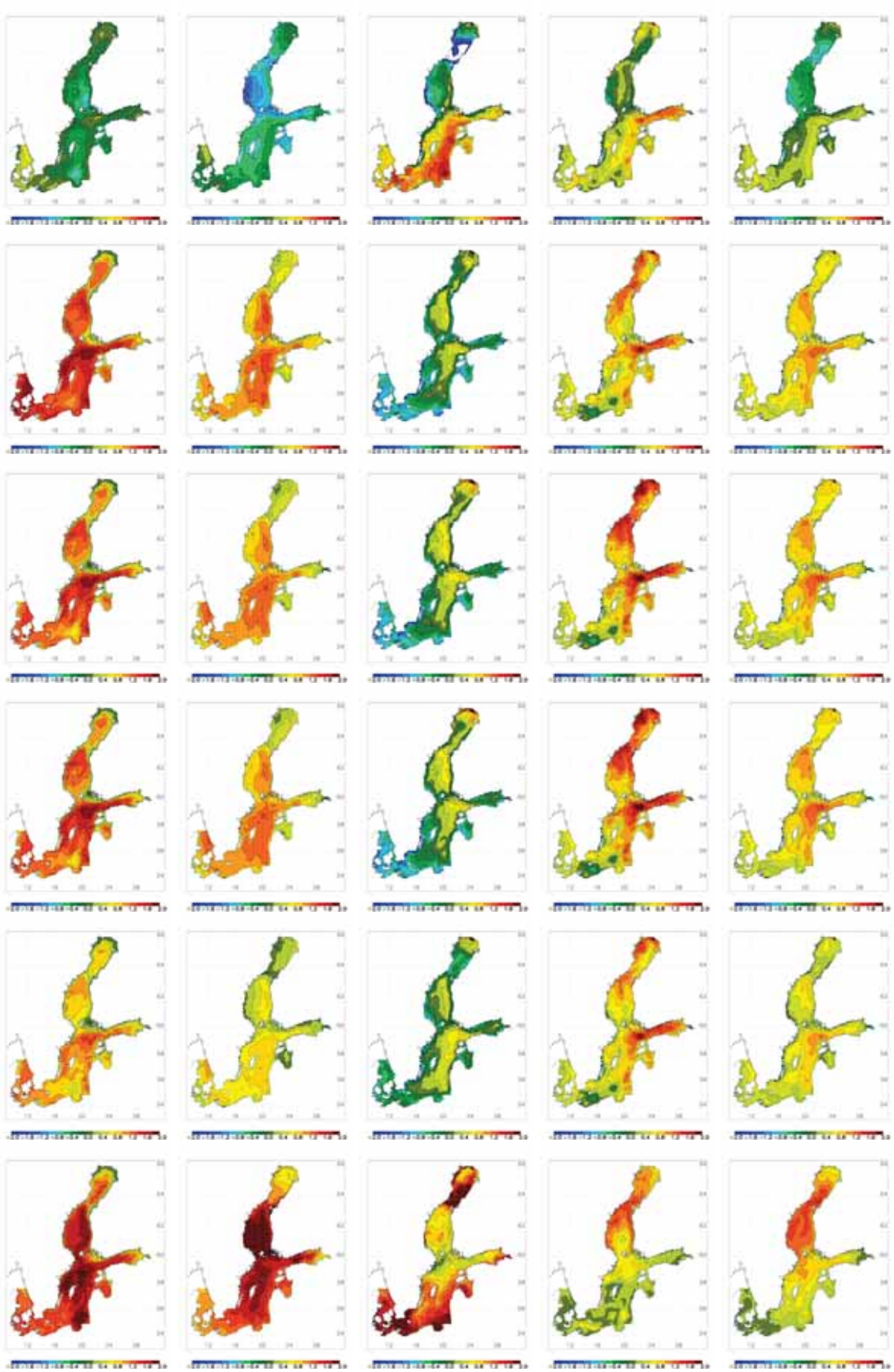

Figure 20. Continued.

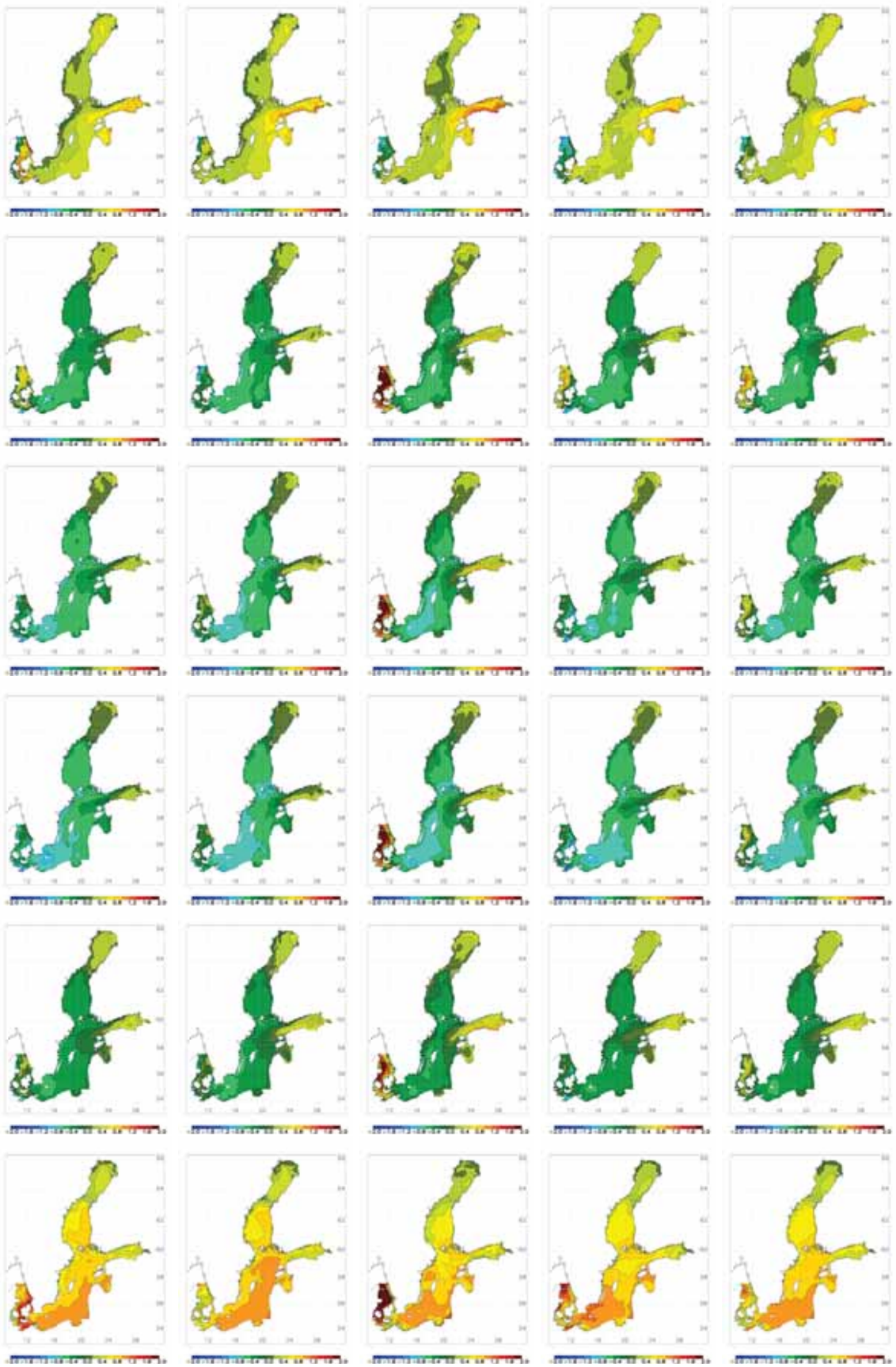

Figure 21. As Fig. 20 but for sea surface salinity (SSS) biases (in g kg^{-1}).

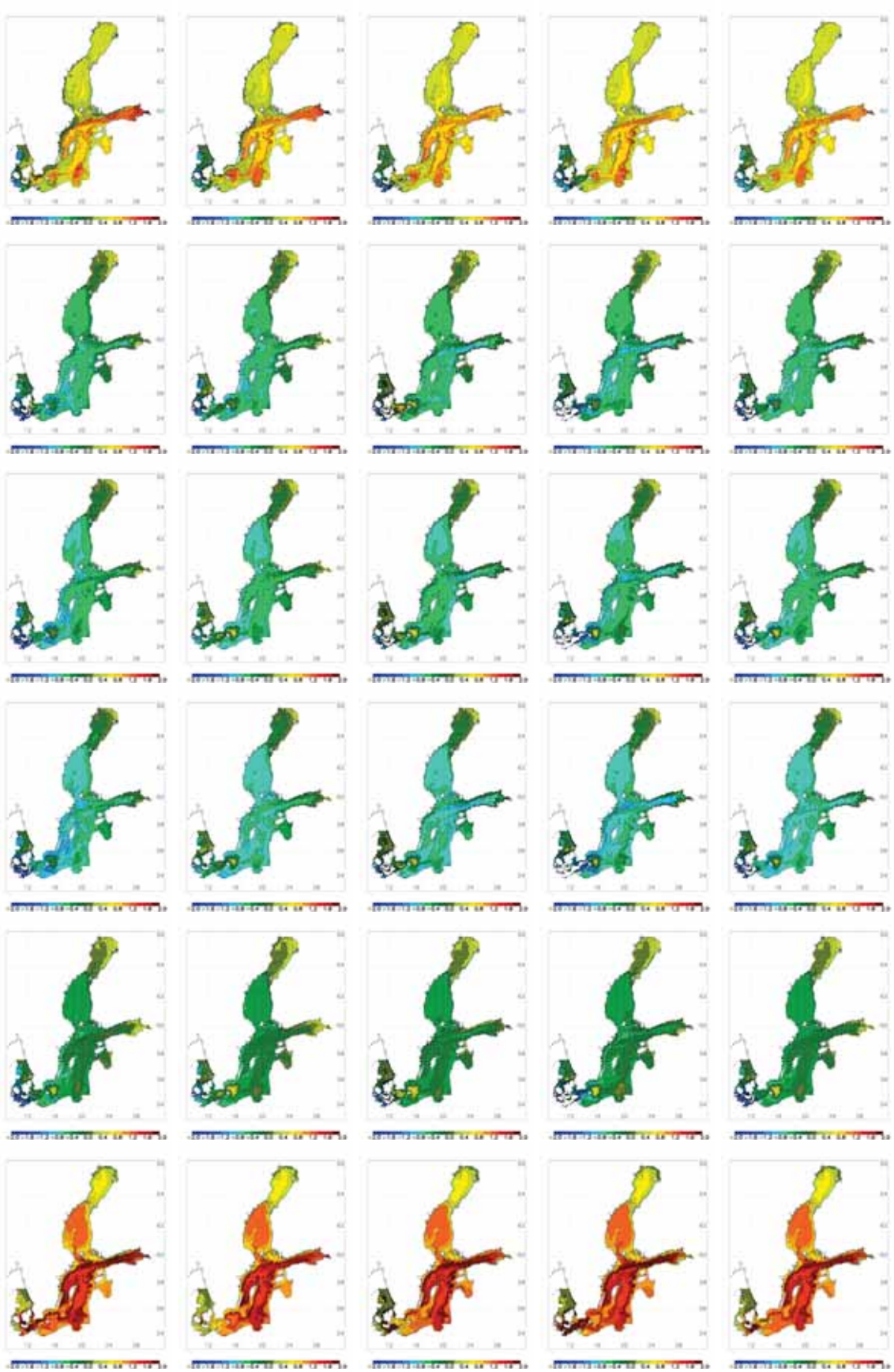

Figure 22. As Fig. 20 but for bottom salinity biases (in g kg^{-1}).

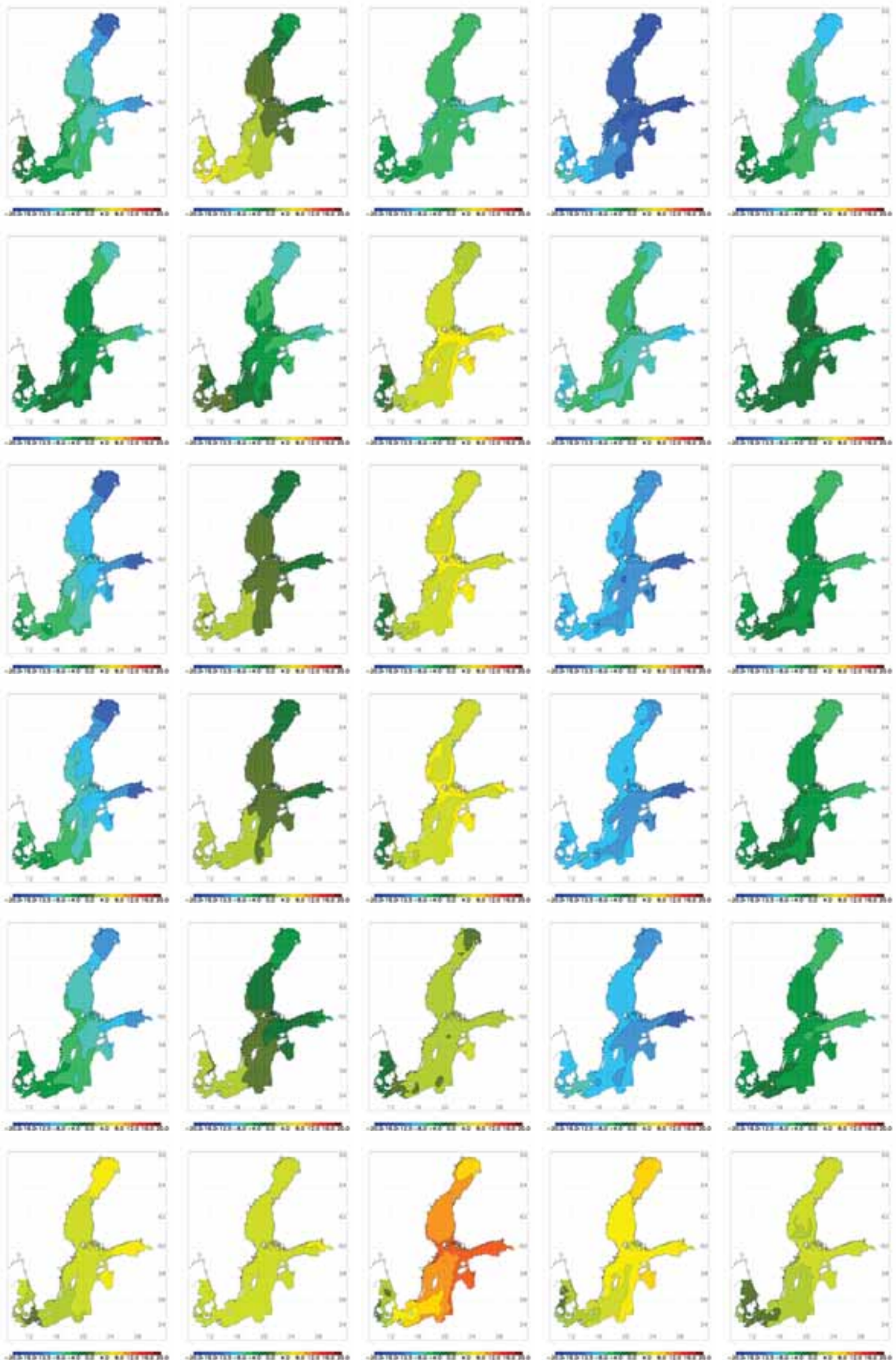

Figure 23. As Fig. 20 but for sea surface height (SSH) biases (cm).

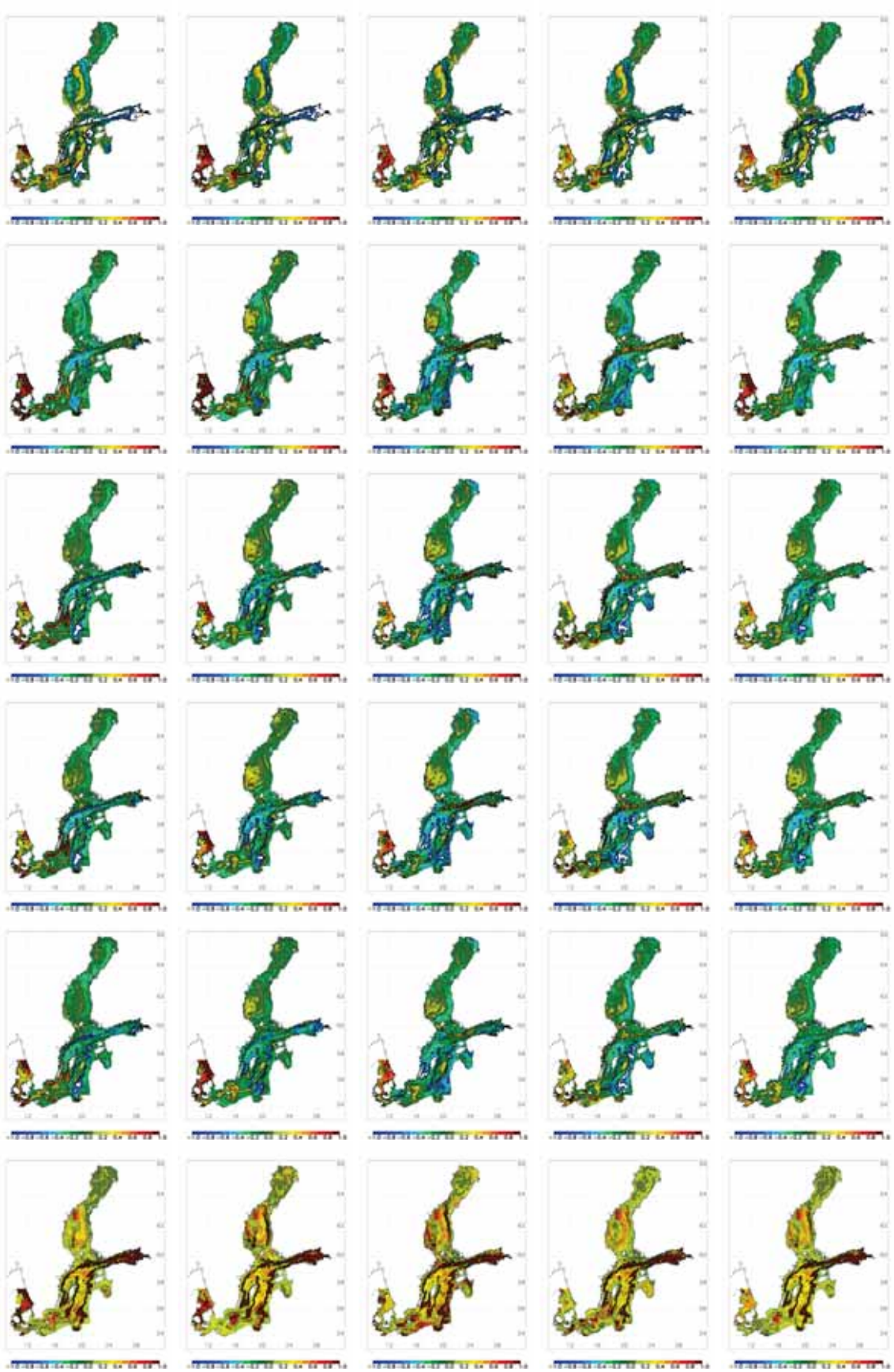

Figure 24. As Fig. 20 but for bottom oxygen concentration biases (ml l^{-1}).

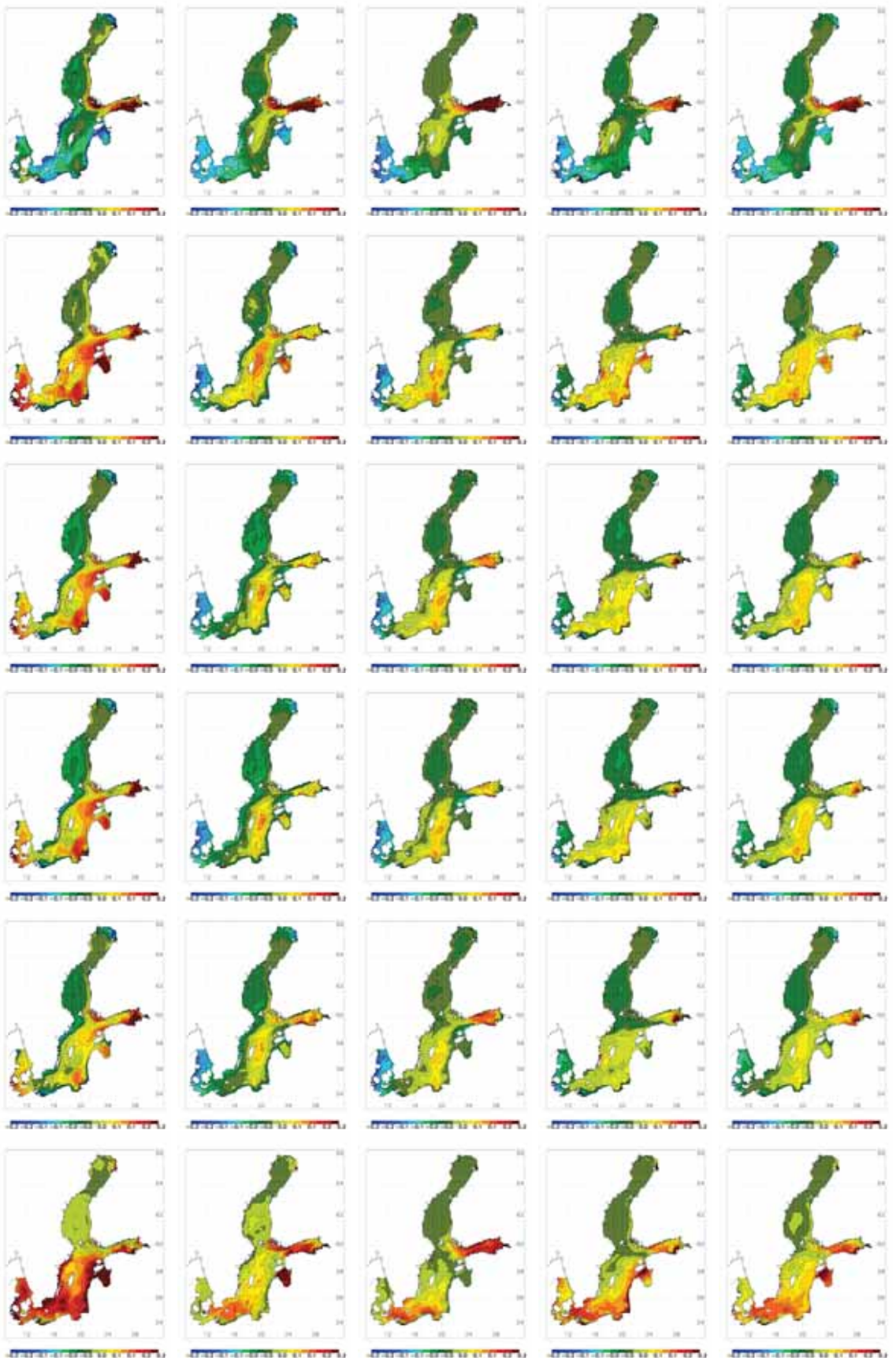

Figure 25. As Fig. 20 but for phosphate concentration biases (mmolP m^{-3}).

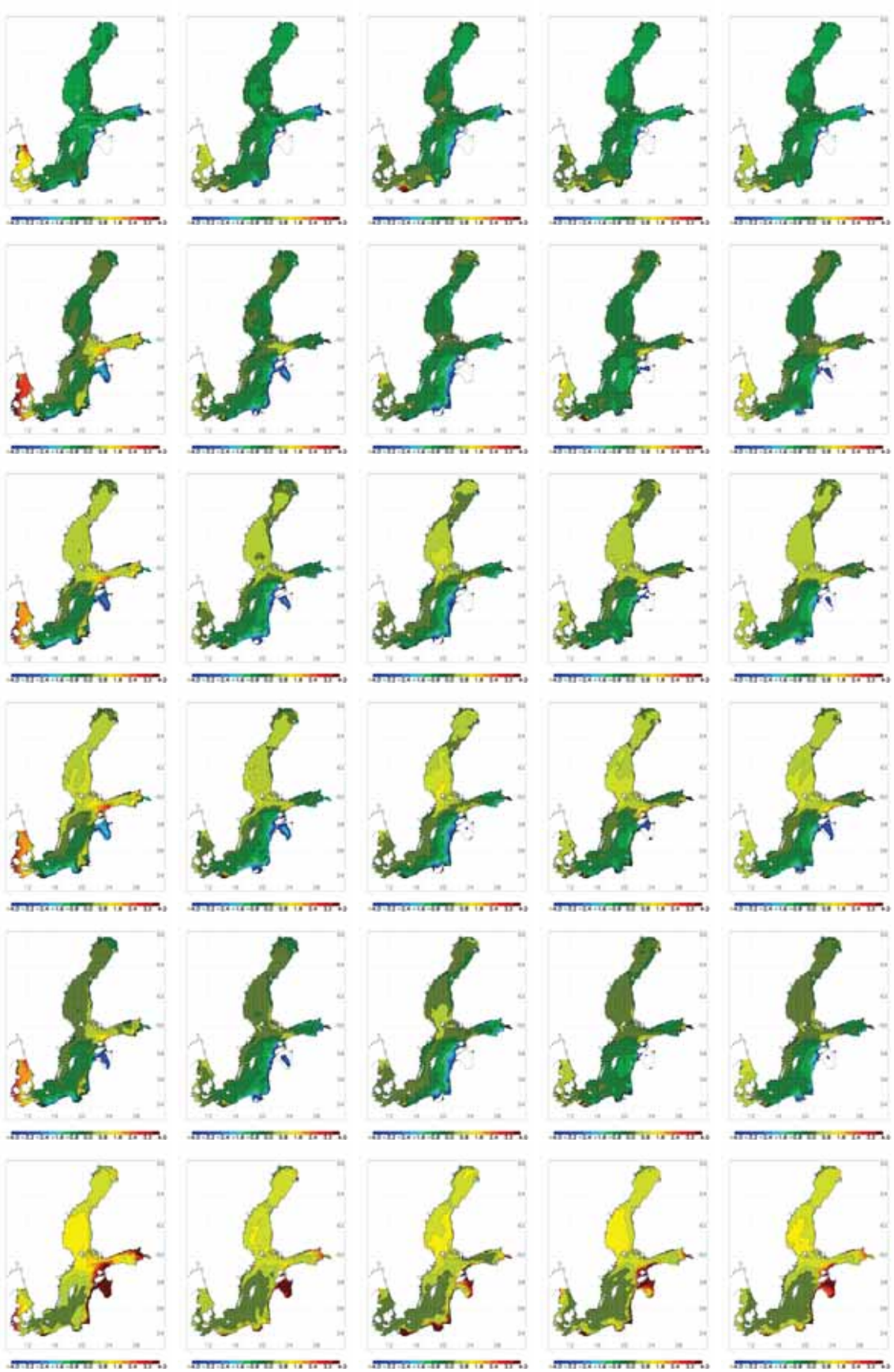

Figure 26. As Fig. 20 but for nitrate concentration biases (mmolN m^{-3}).

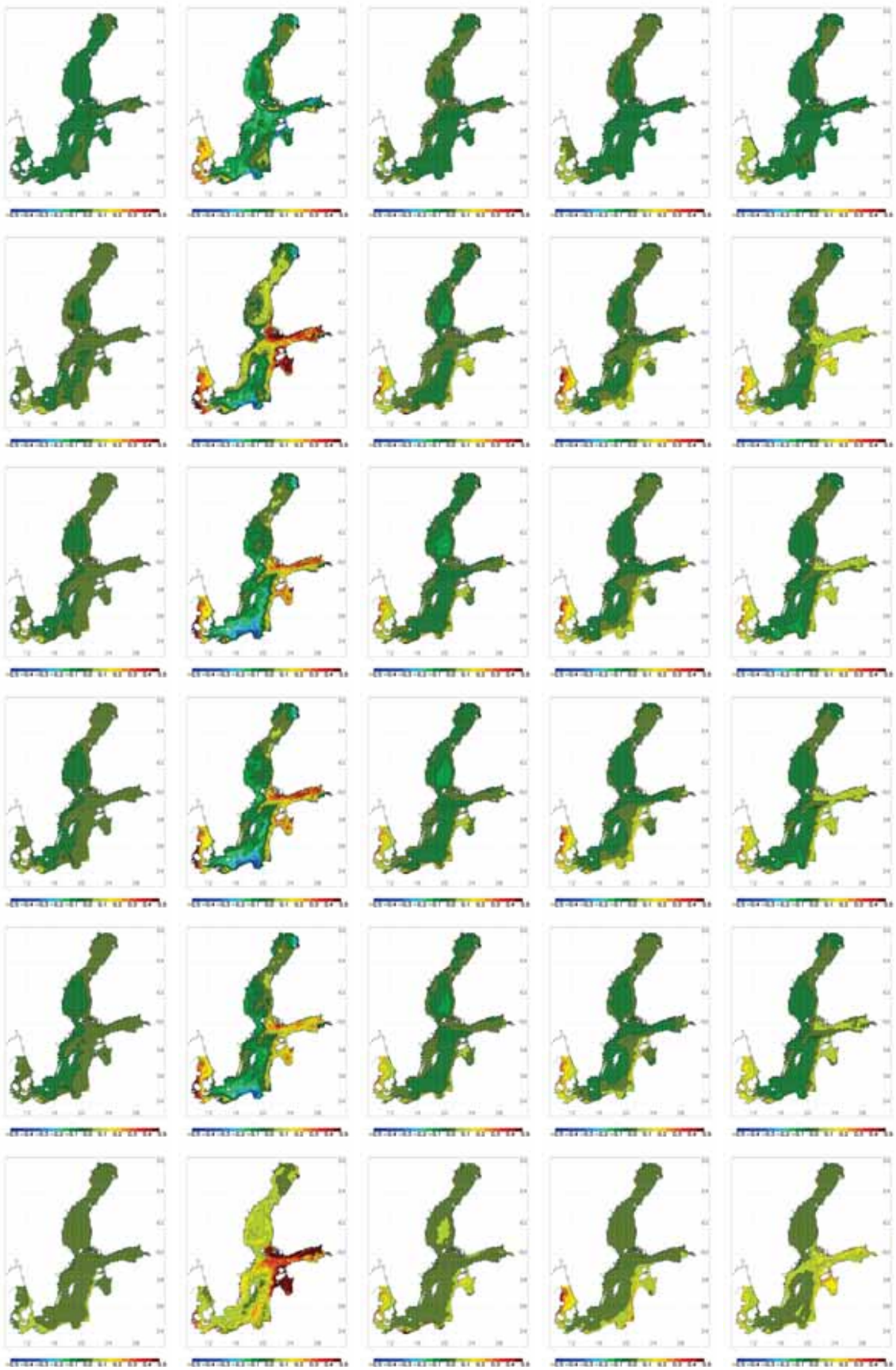

Figure 27. As Fig. 20 but for diatom concentration biases (mgChl m^{-3}).

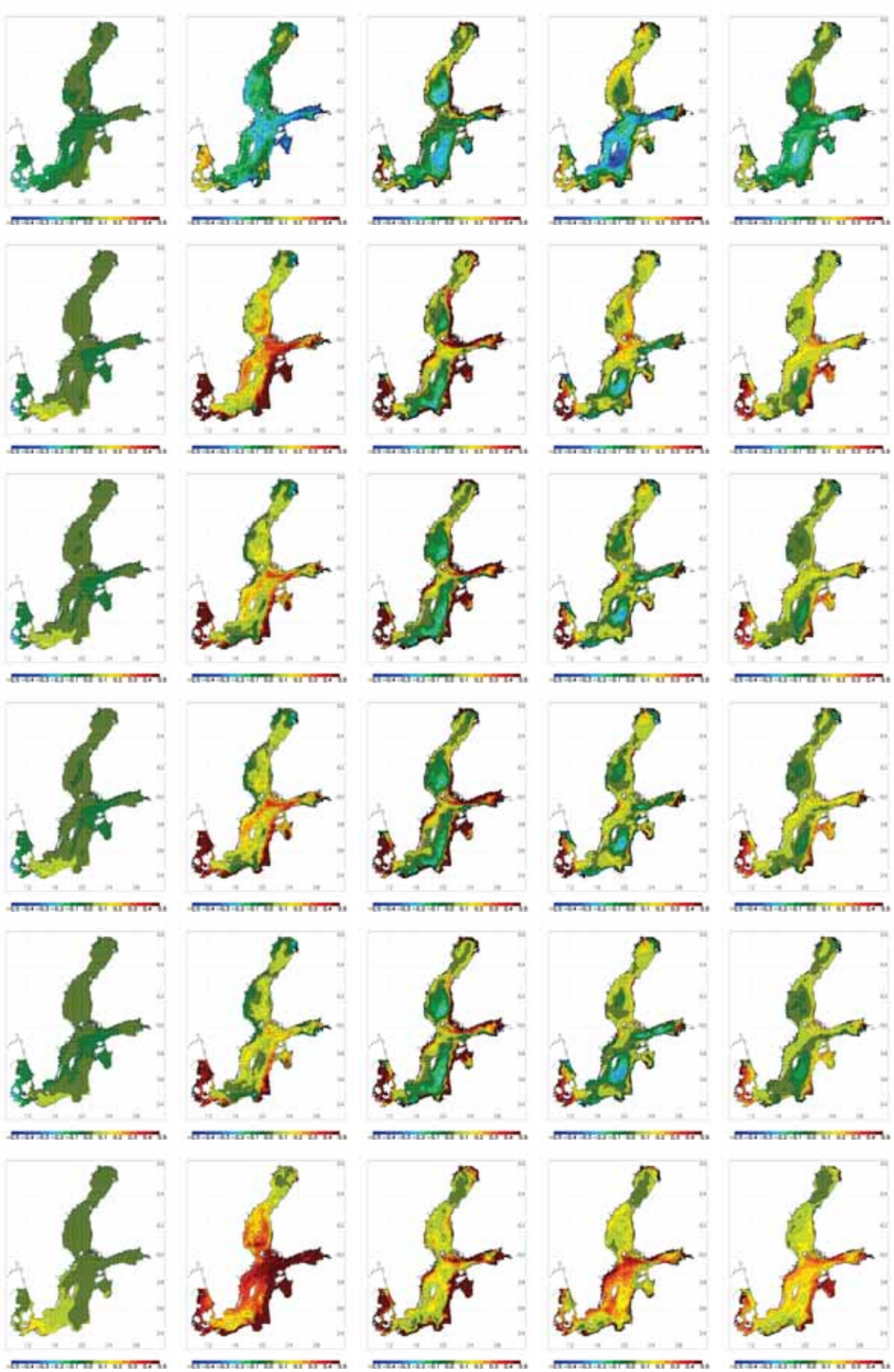

Figure 28. As Fig. 20 but for concentration biases of flagellates and others (mgChl m^{-3}).

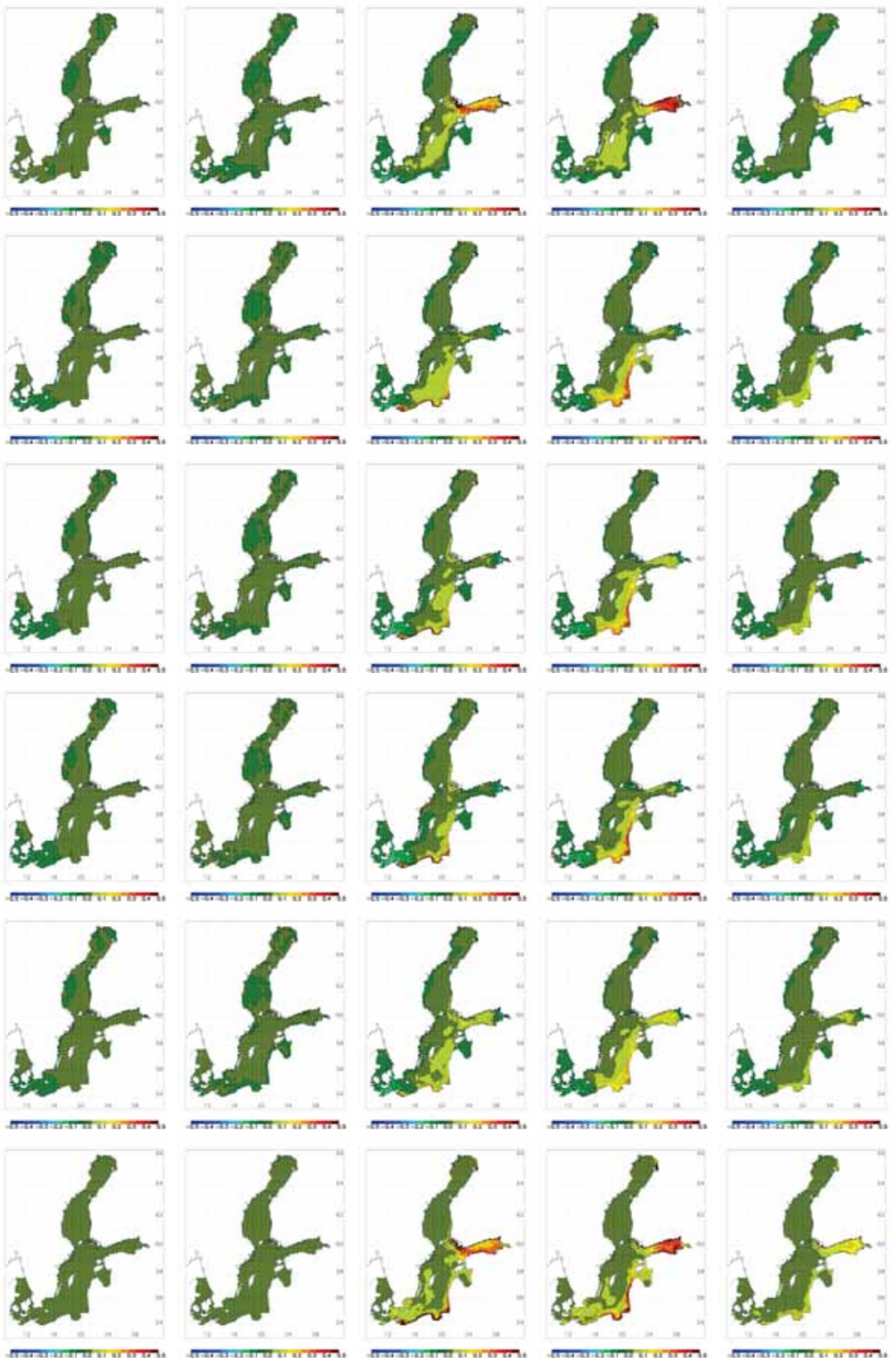

Figure 29. As Fig. 20 but for cyanobacteria concentration biases (mgChl m^{-3}).

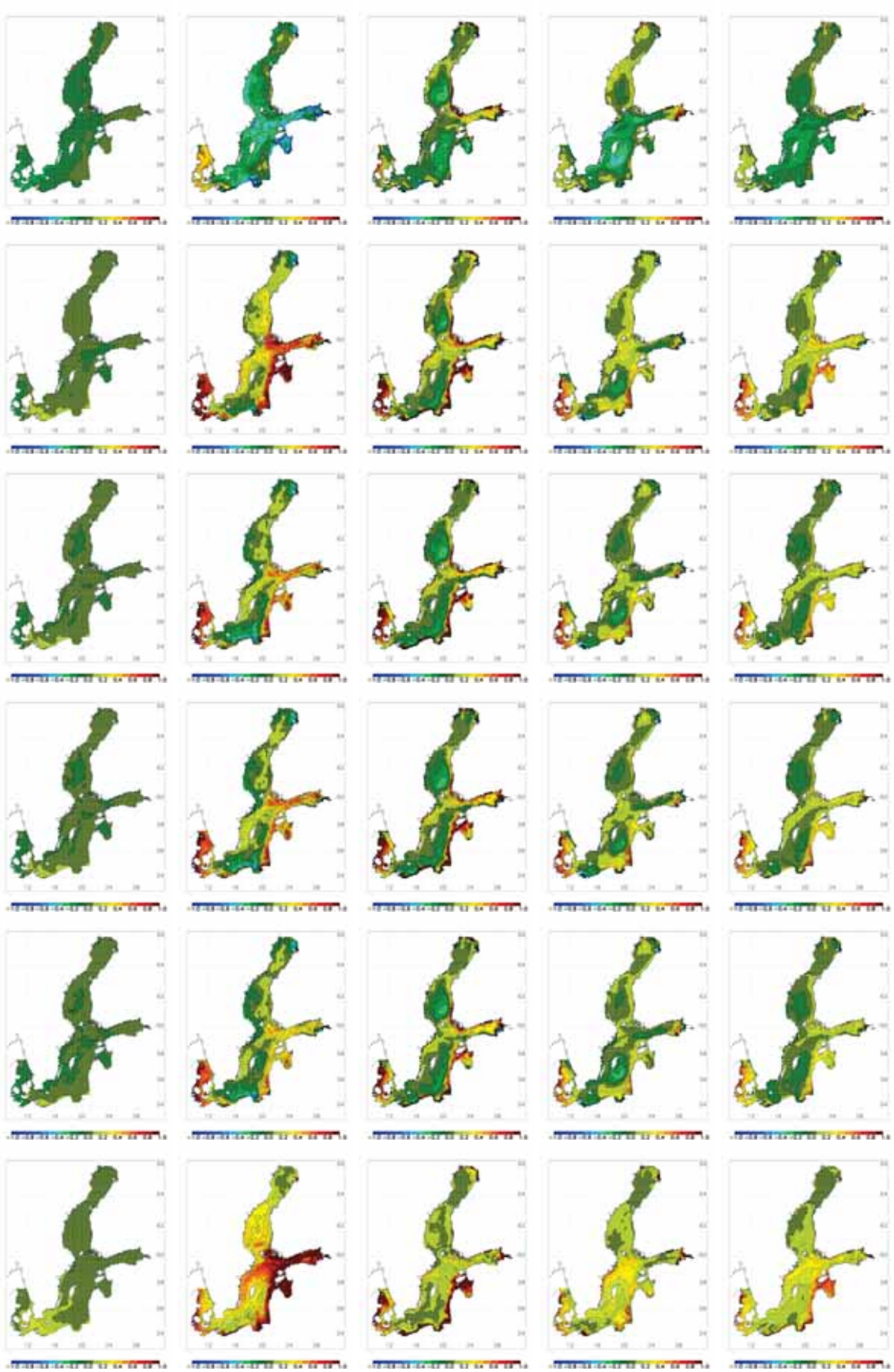

Figure 30. As Fig. 20 but for phytoplankton concentration biases (mgChl m^{-3}).

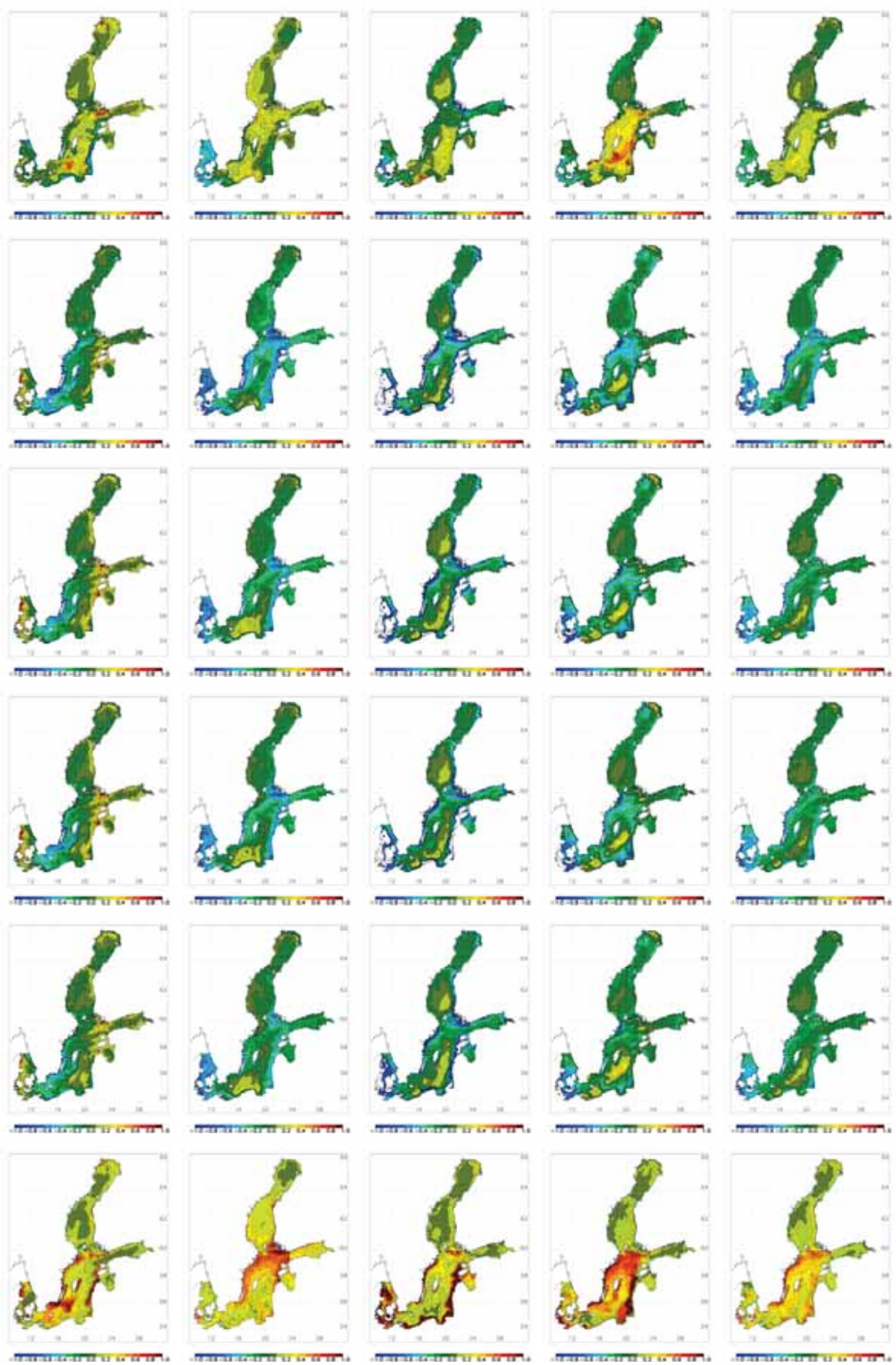

Figure 31. As Fig. 20 but for Secchi depth biases (m).

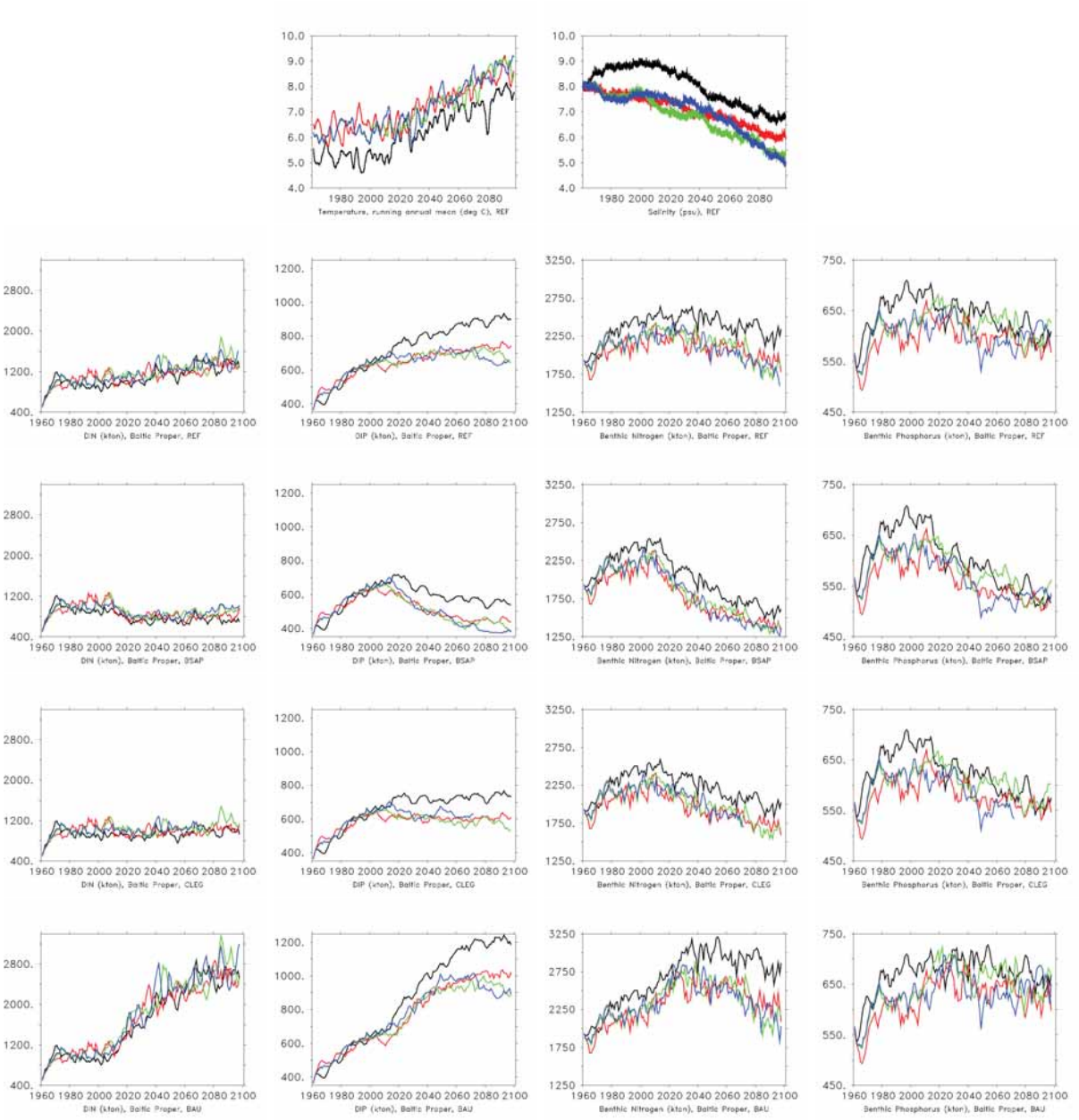

Figure 32. Volume averaged temperature (in $^{\circ}C$) and salinity (in g kg^{-1}) for 1961-2099 (upper panels). Further, volume integrated dissolved inorganic nitrogen (DIN, in kton, first column) and dissolved inorganic phosphorus (DIP, in kton, second column) in the water column, and benthic nitrogen (in kton, third column) and benthic phosphorus (in kton, fourth column) in the sediments are shown. The second to fifth rows show the results of the four nutrient load scenarios REF, BSAP, CLEG and BAU (see Section 2.4). The various curves show the scenario simulation results driven by HadCM3-A1B (black line), ECHAM5-A1B-3 (red line), ECHAM5-A1B-1 (green line) and ECHAM5-A2 (blue line).

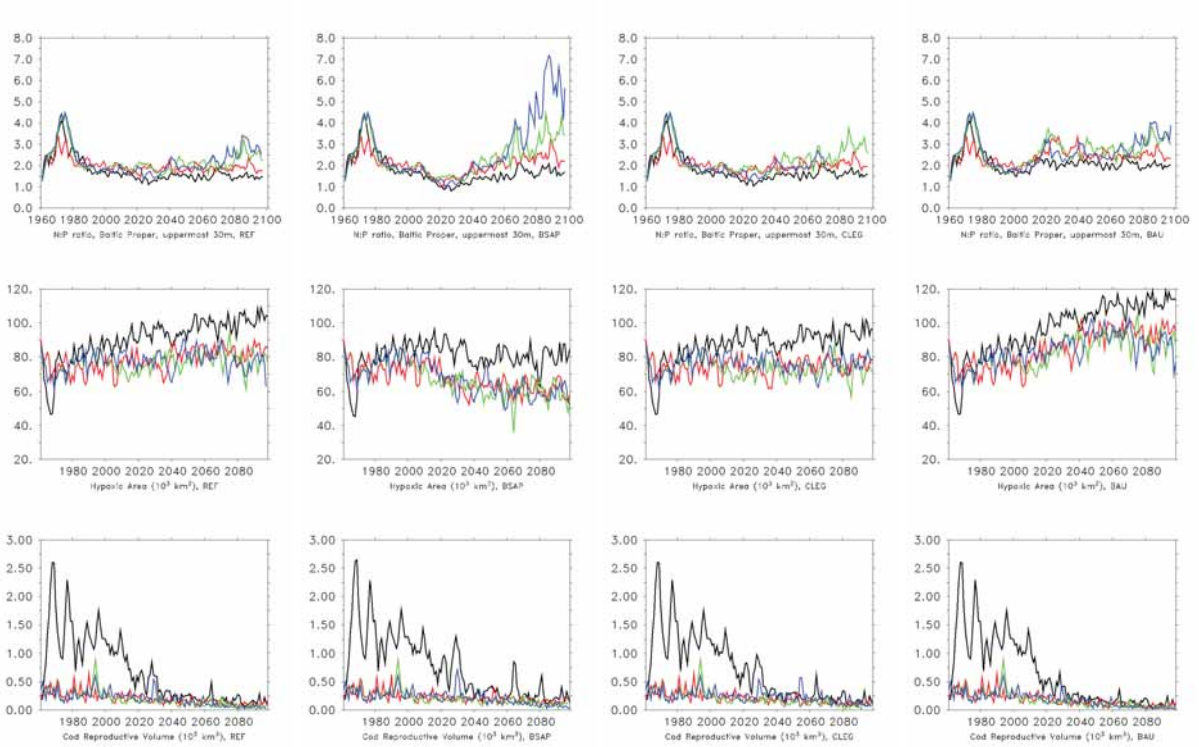

Figure 33. As Figure 32 but for the N:P ratio in the Baltic proper (first row), hypoxic area (in 10^3 km^2) (second row) and cod reproductive volume (in 10^3 km^3) (third row). The first to fourth columns contain results from the nutrient load scenarios REF, BSAP, CLEG and BAU, respectively.

Figure 34. Annual and seasonal mean sea surface temperature (SST) changes (°C) between 2070-2099 and 1969-1998 in RCO-SCOBI simulations driven by regionalized GCM results. From left to right results for winter (December through February), spring (March through May), summer (June through August), autumn (September through November) and the annual mean are shown. From top to bottom the results of the following scenario simulations and analysis results are shown: RCAO-HadCM3-A1B-REF, RCAO-ECHAM5-A1B-3-REF, RCAO-ECHAM5-A1B-1-REF, RCAO-ECHAM5-A2-1-REF, ensemble mean, and range.

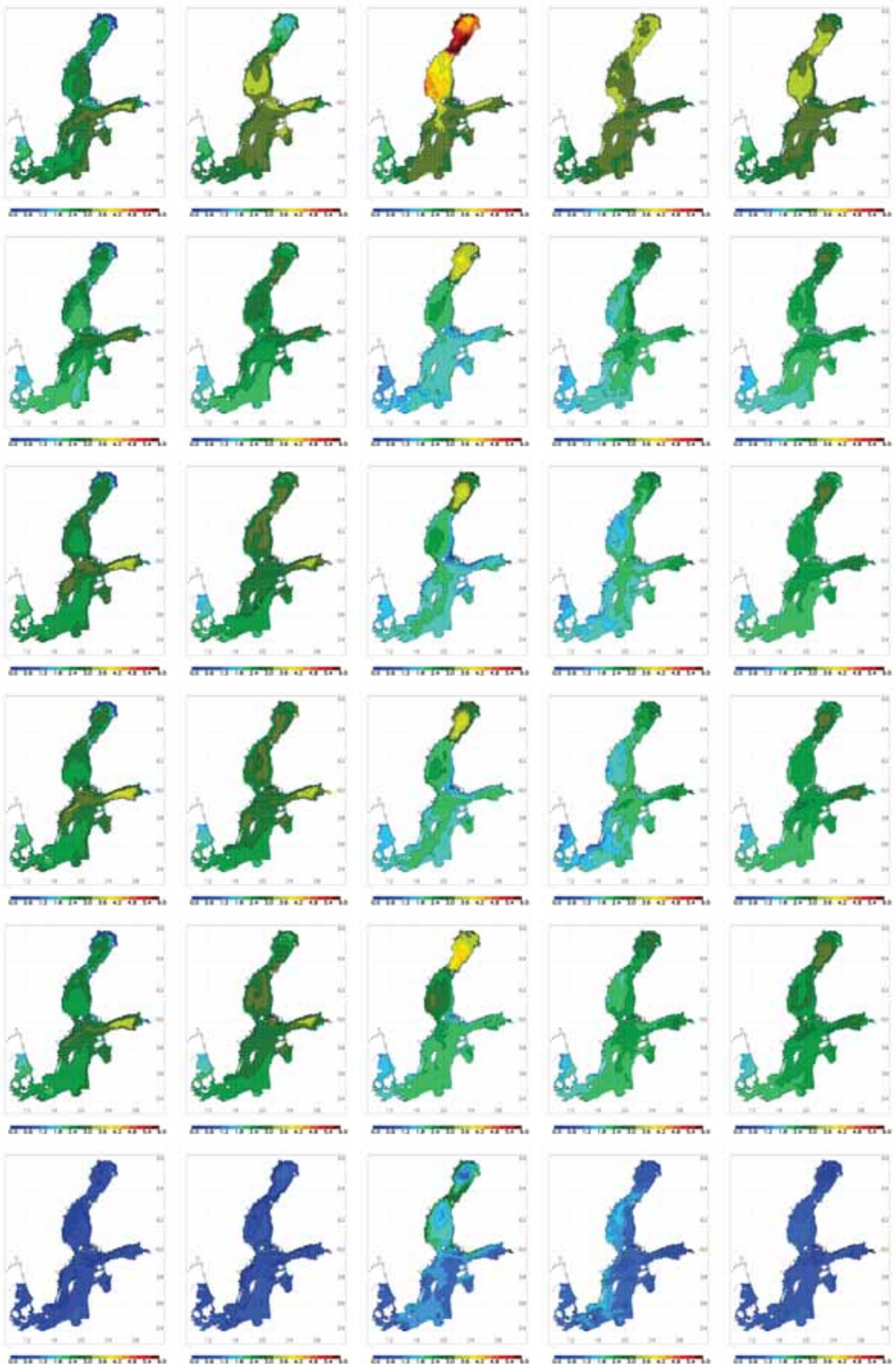

Figure 34. Continued.

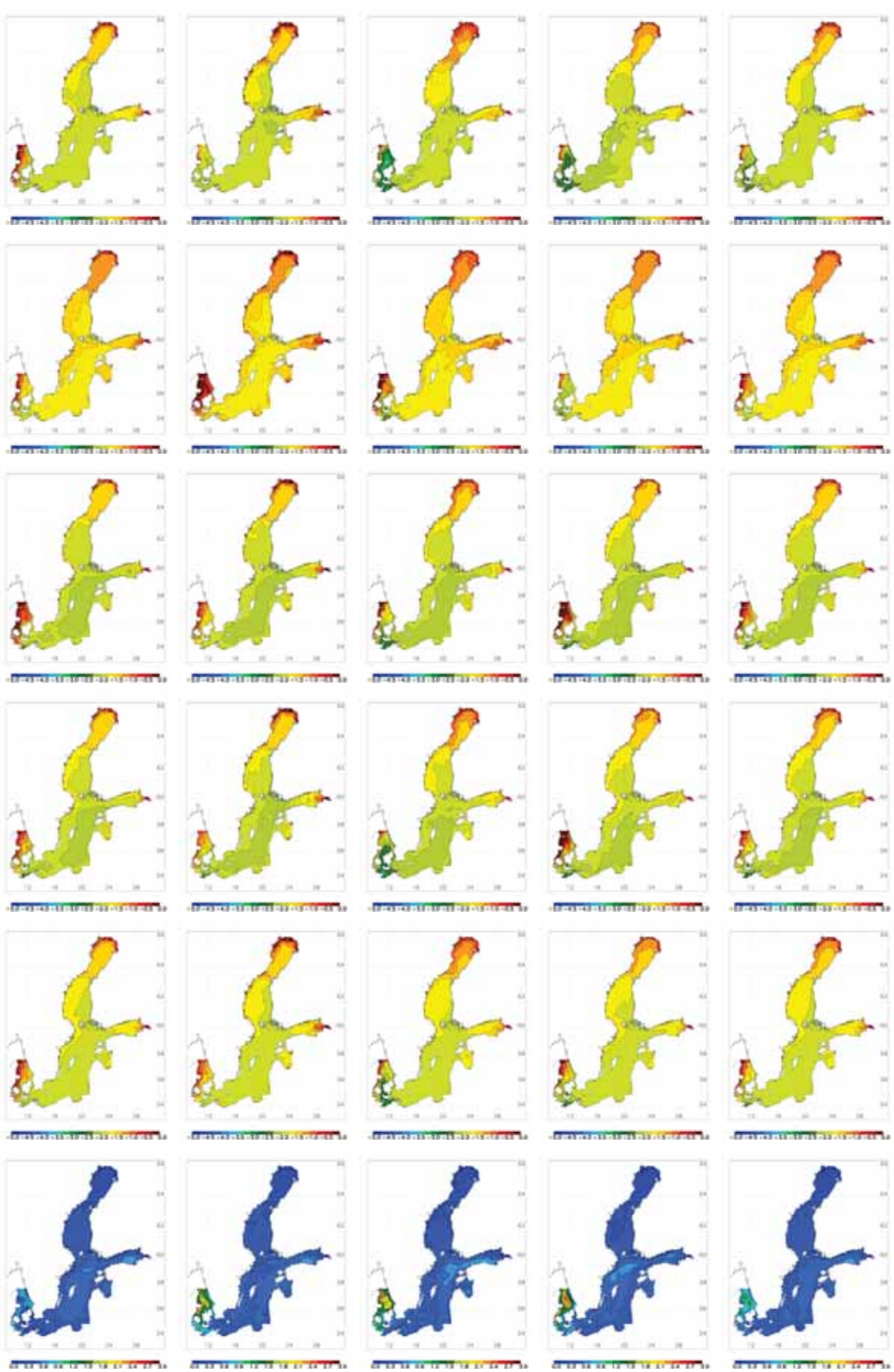

Figure 35. As Fig. 34 but for sea surface salinity (SSS) changes (in g kg^{-1}).

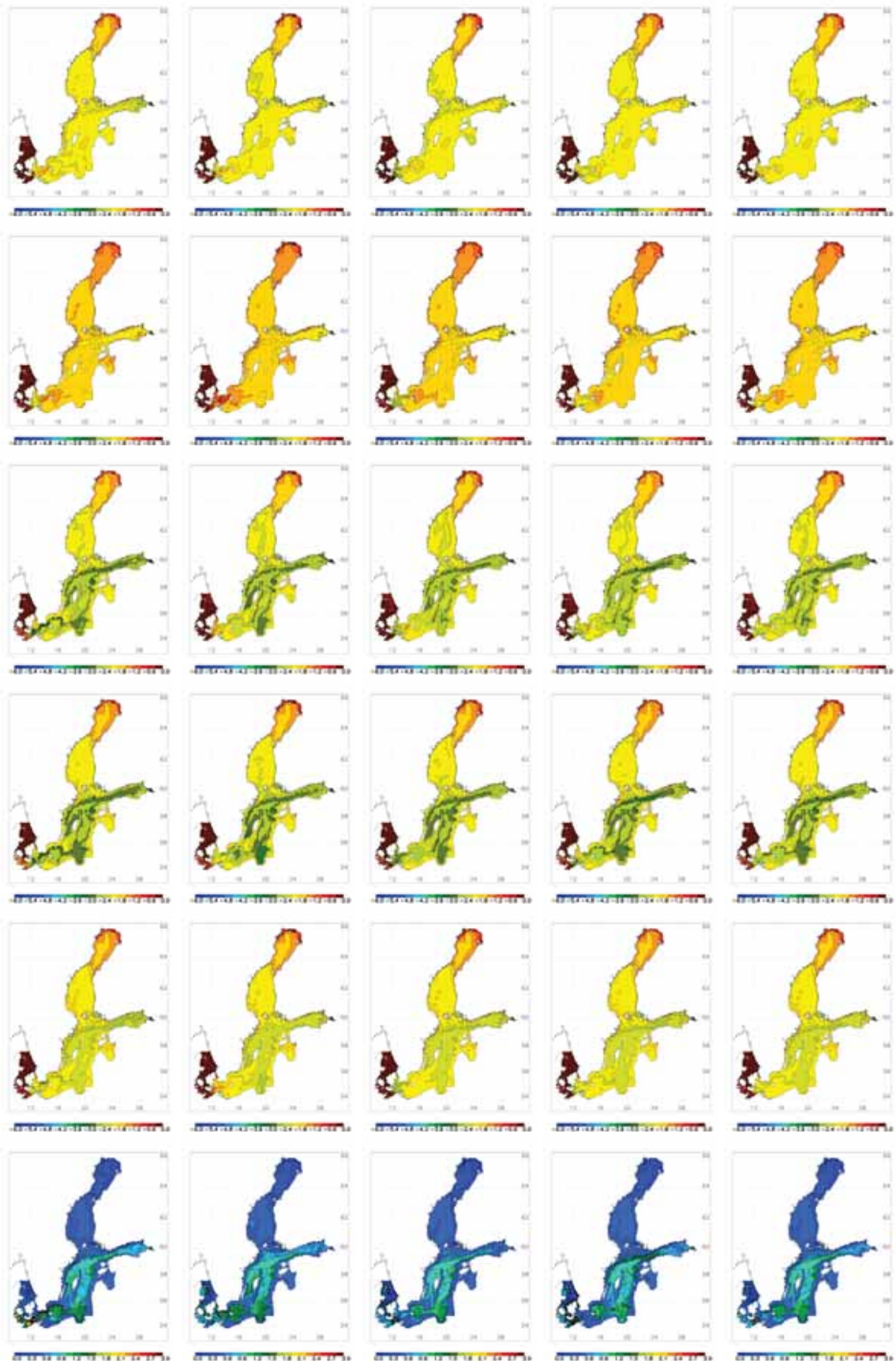

Figure 36. As Fig. 34 but for bottom salinity changes (in g kg^{-1}).

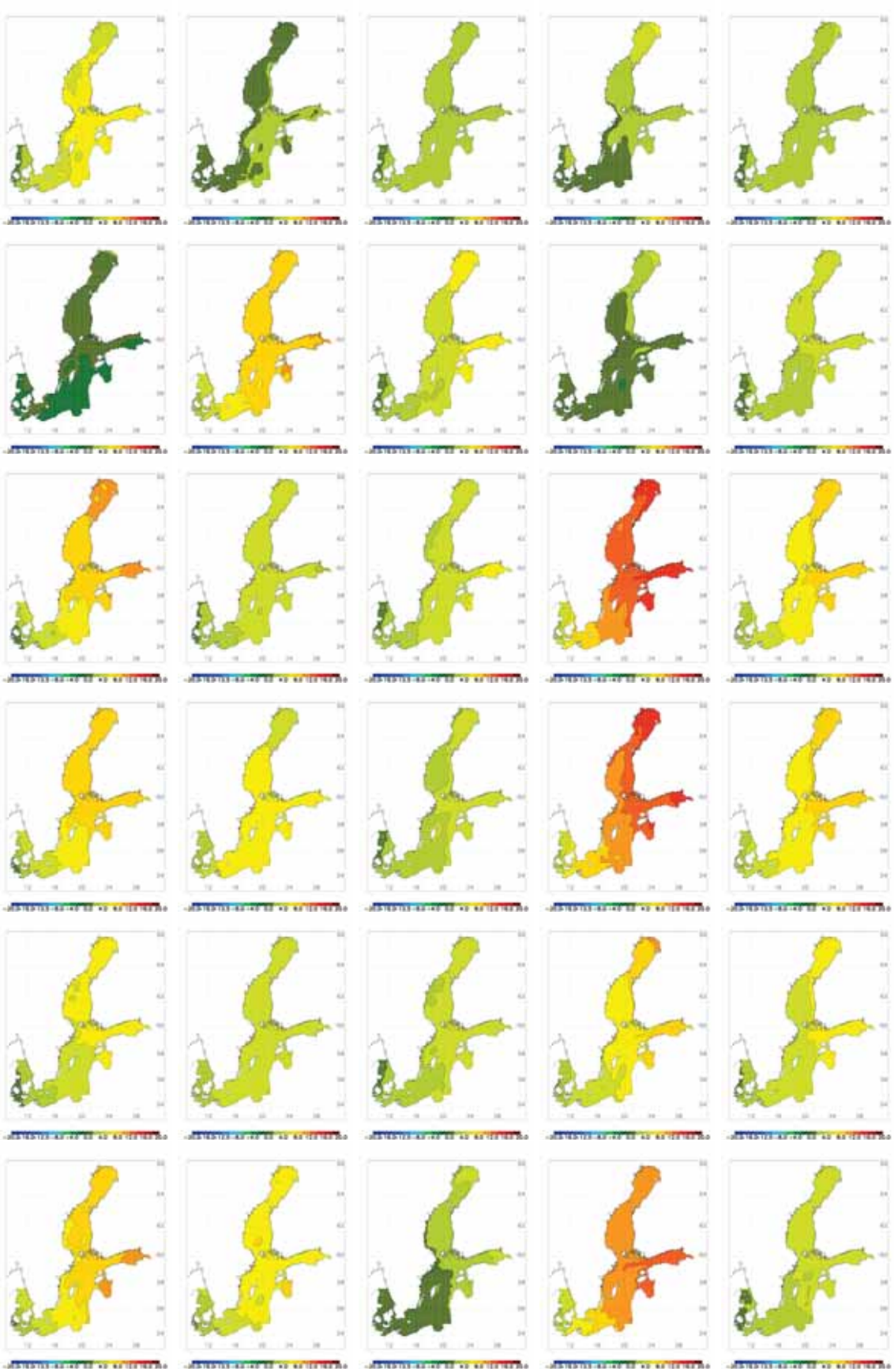

Figure 37. As Fig. 34 but for sea surface height (SSH) changes (cm).

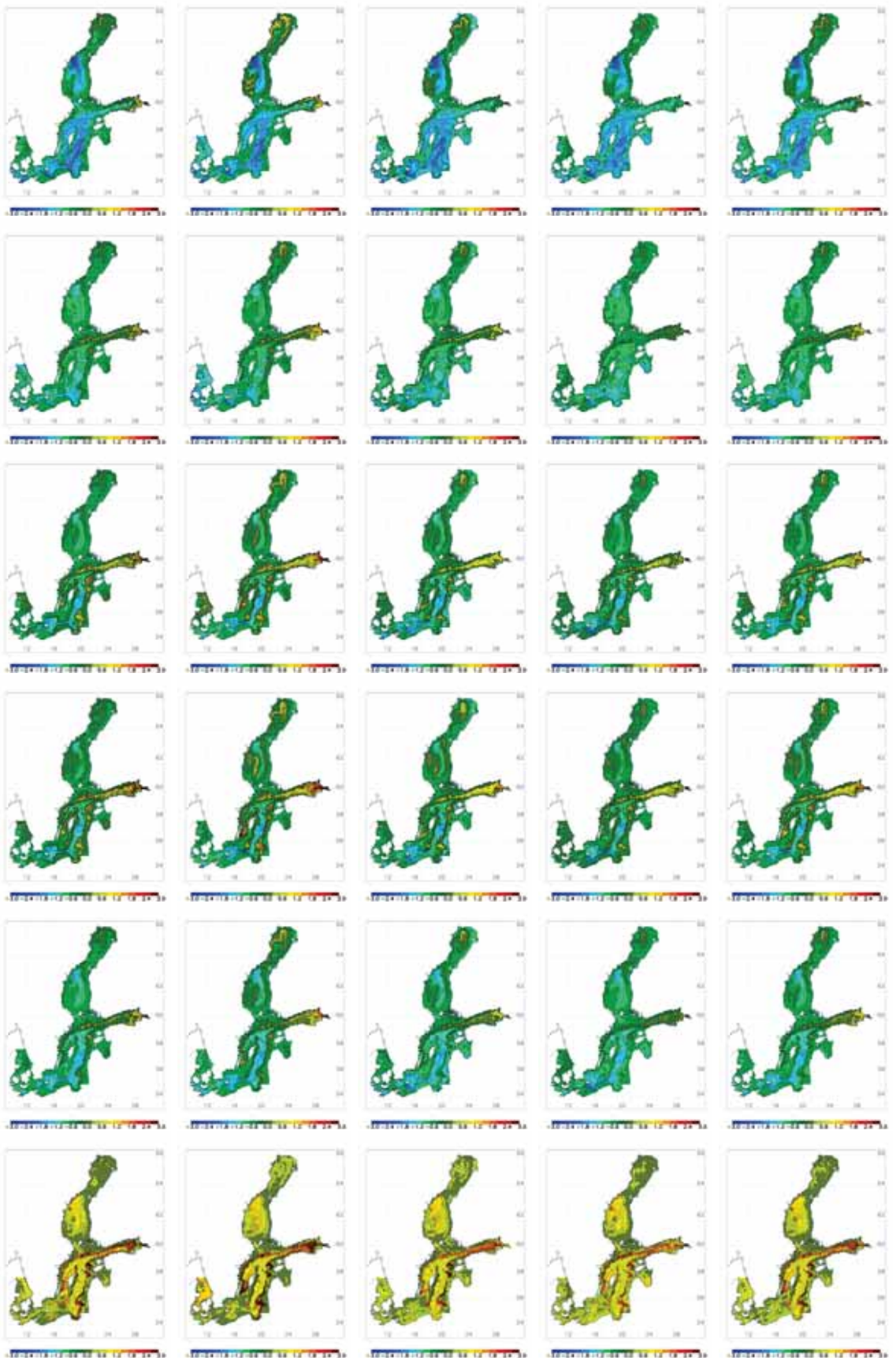

Figure 38. As Fig. 34 but for bottom oxygen concentration changes (ml l^{-1}).

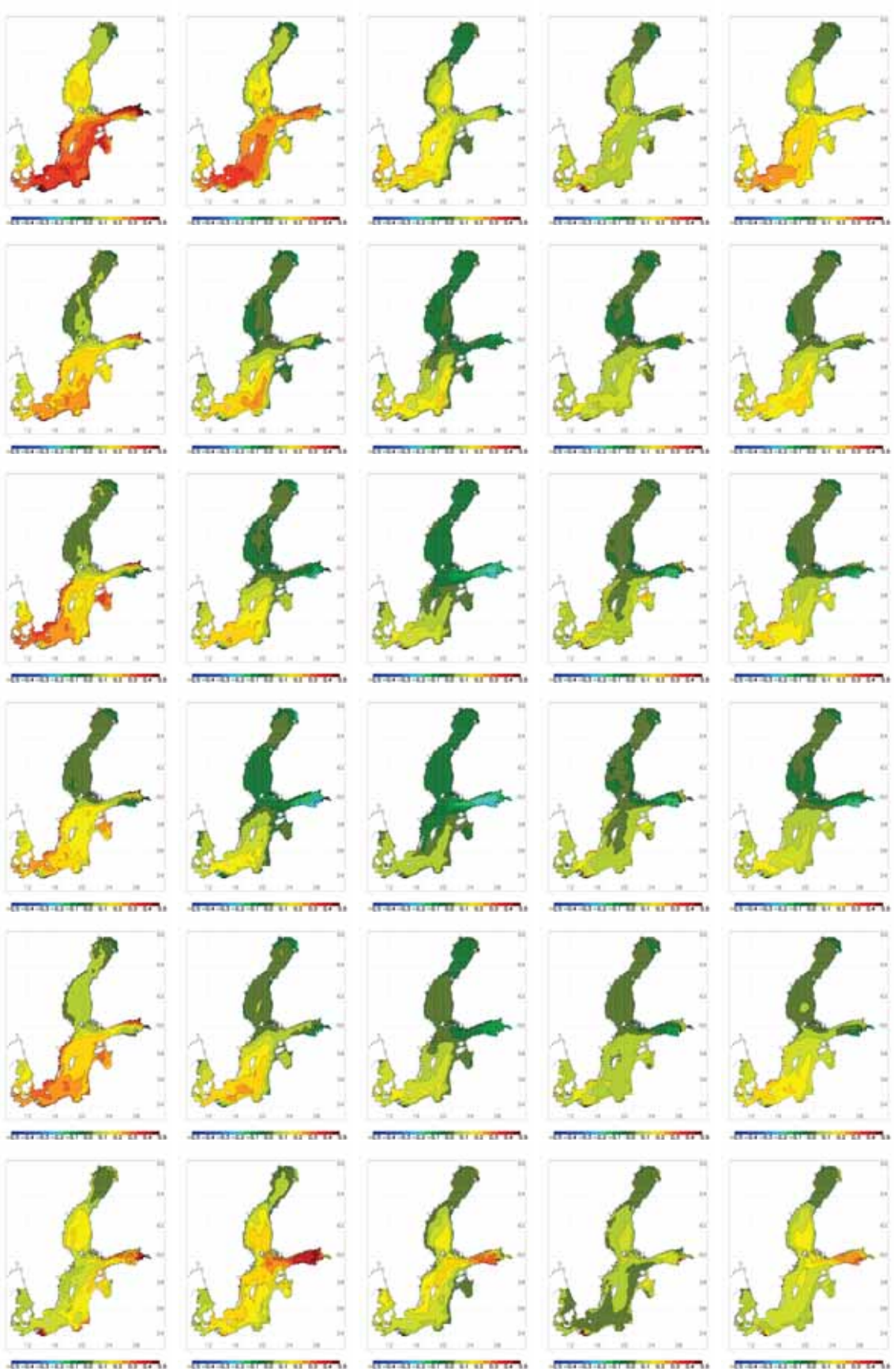

Figure 39. As Fig. 34 but for phosphate concentration changes (mmolP m^{-3}).

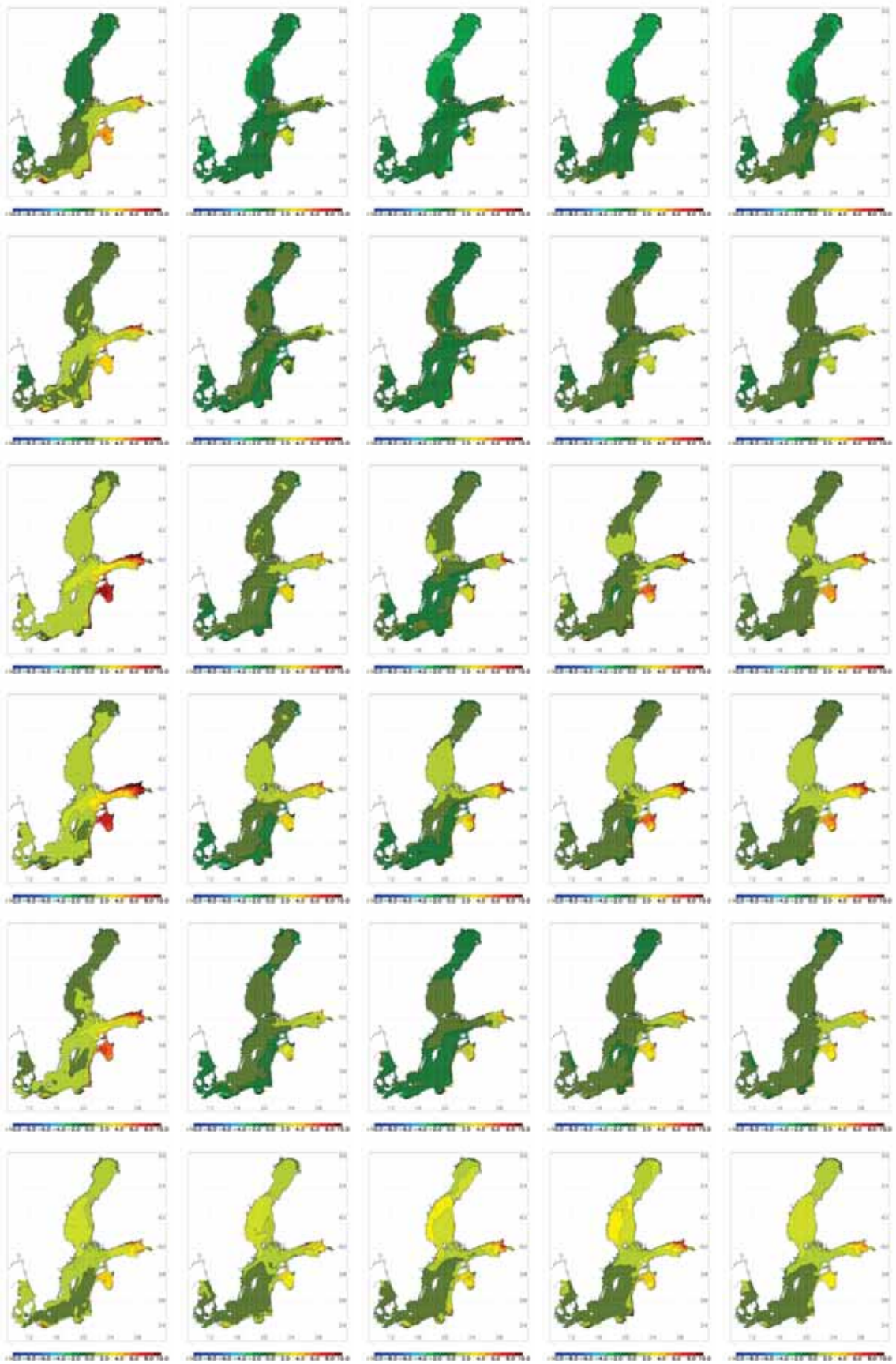

Figure 40. As Fig. 34 but for nitrate concentration changes (mmolN m^{-3}).

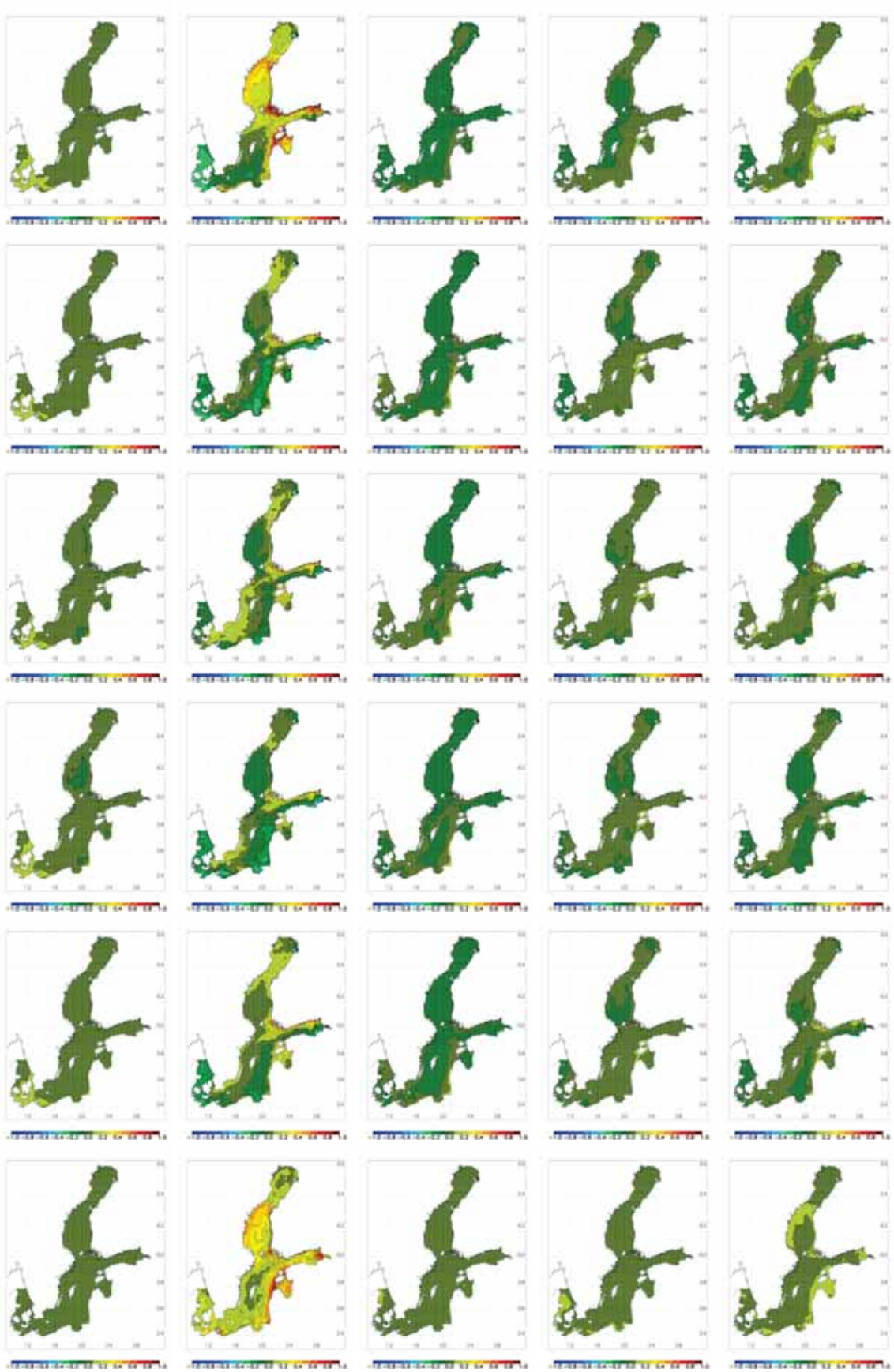

Figure 41. As Fig. 34 but for diatom concentration changes (mgChl m^{-3}).

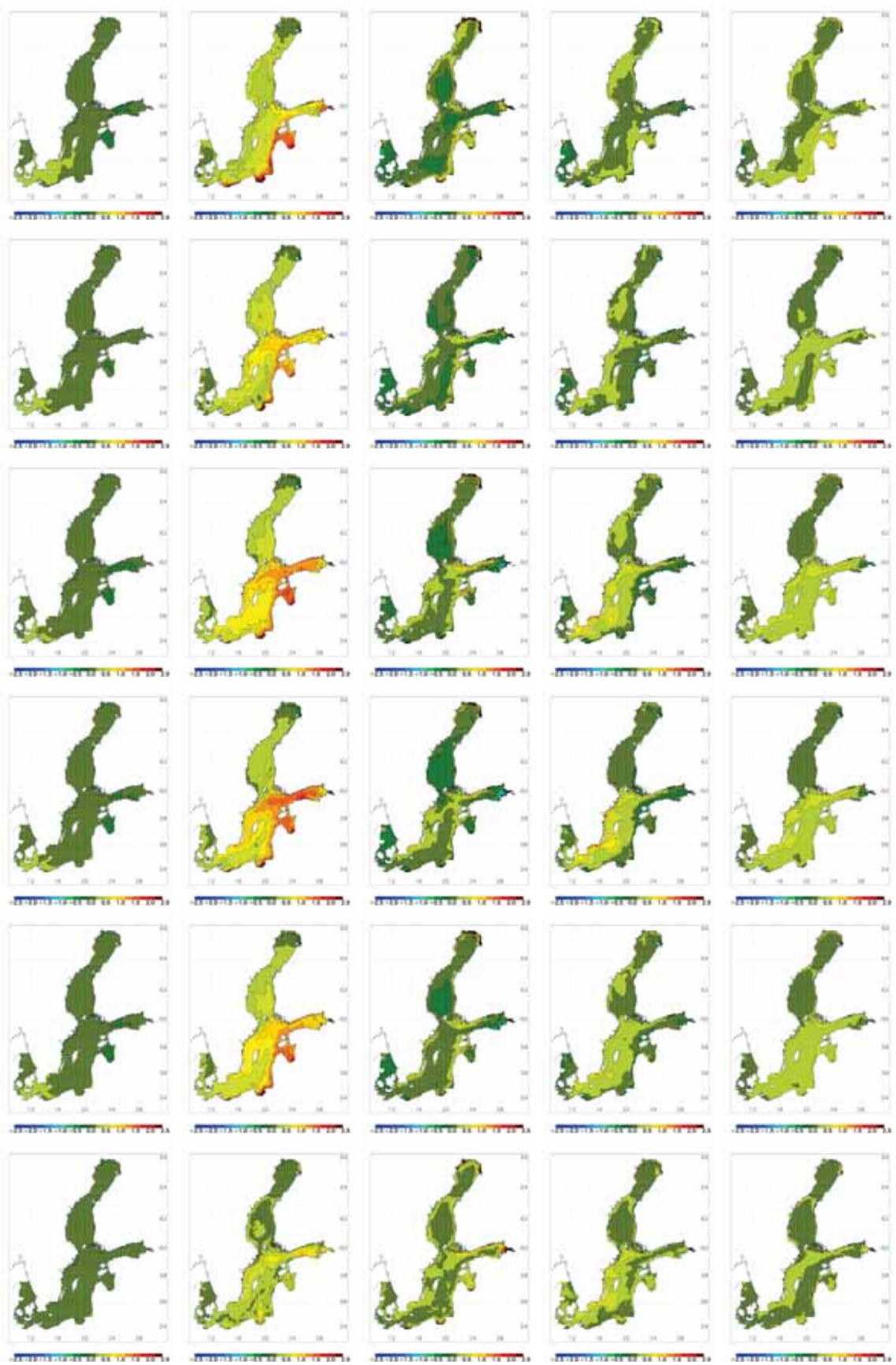

Figure 42. As Fig. 34 but for concentration changes of flagellates and others (mgChl m^{-3}).

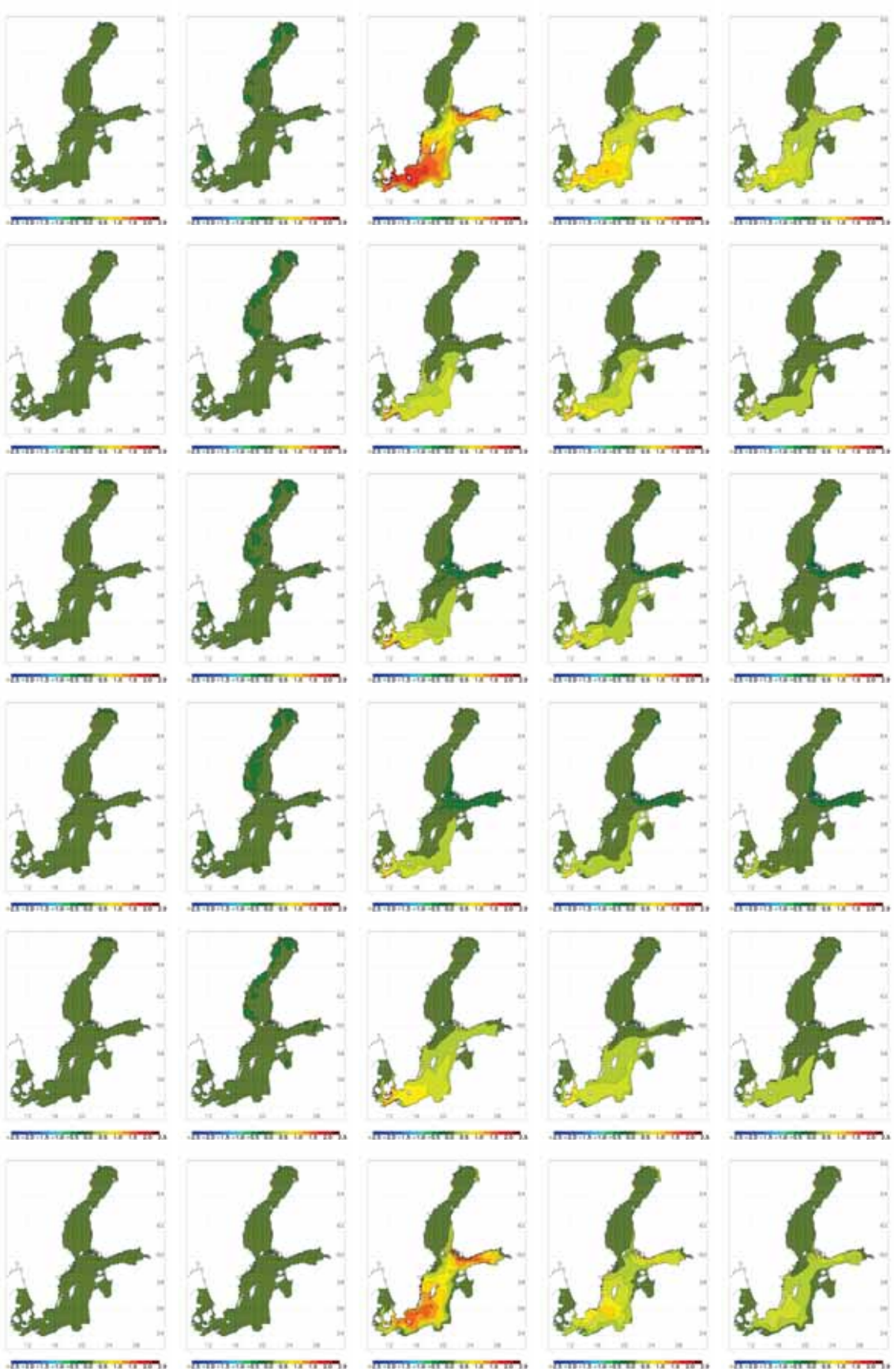

Figure 43. As Fig. 34 but for cyanobacteria concentration changes (mgChl m^{-3}).

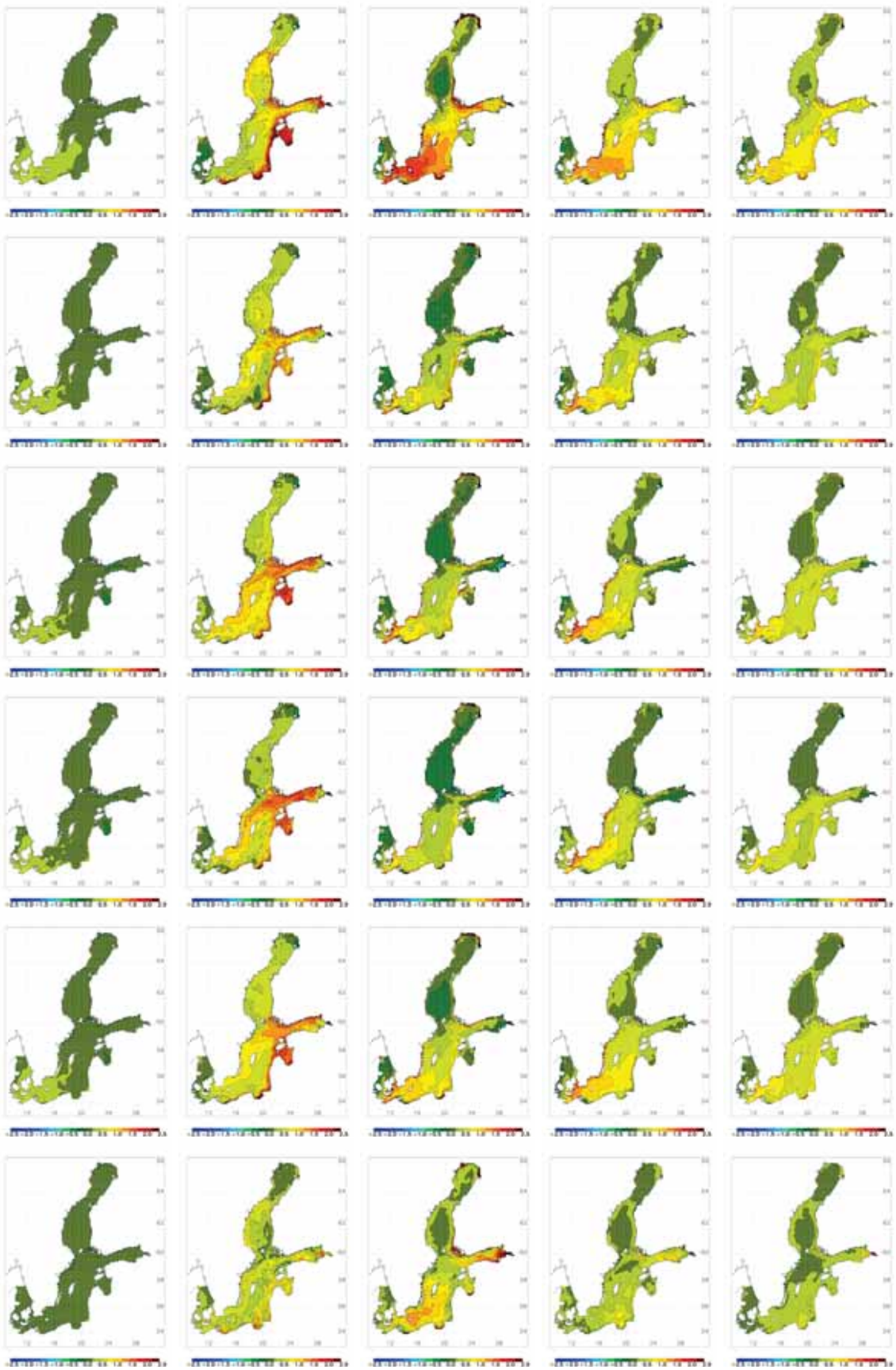

Figure 44. As Fig. 34 but for phytoplankton concentration changes (mgChl m^{-3}).

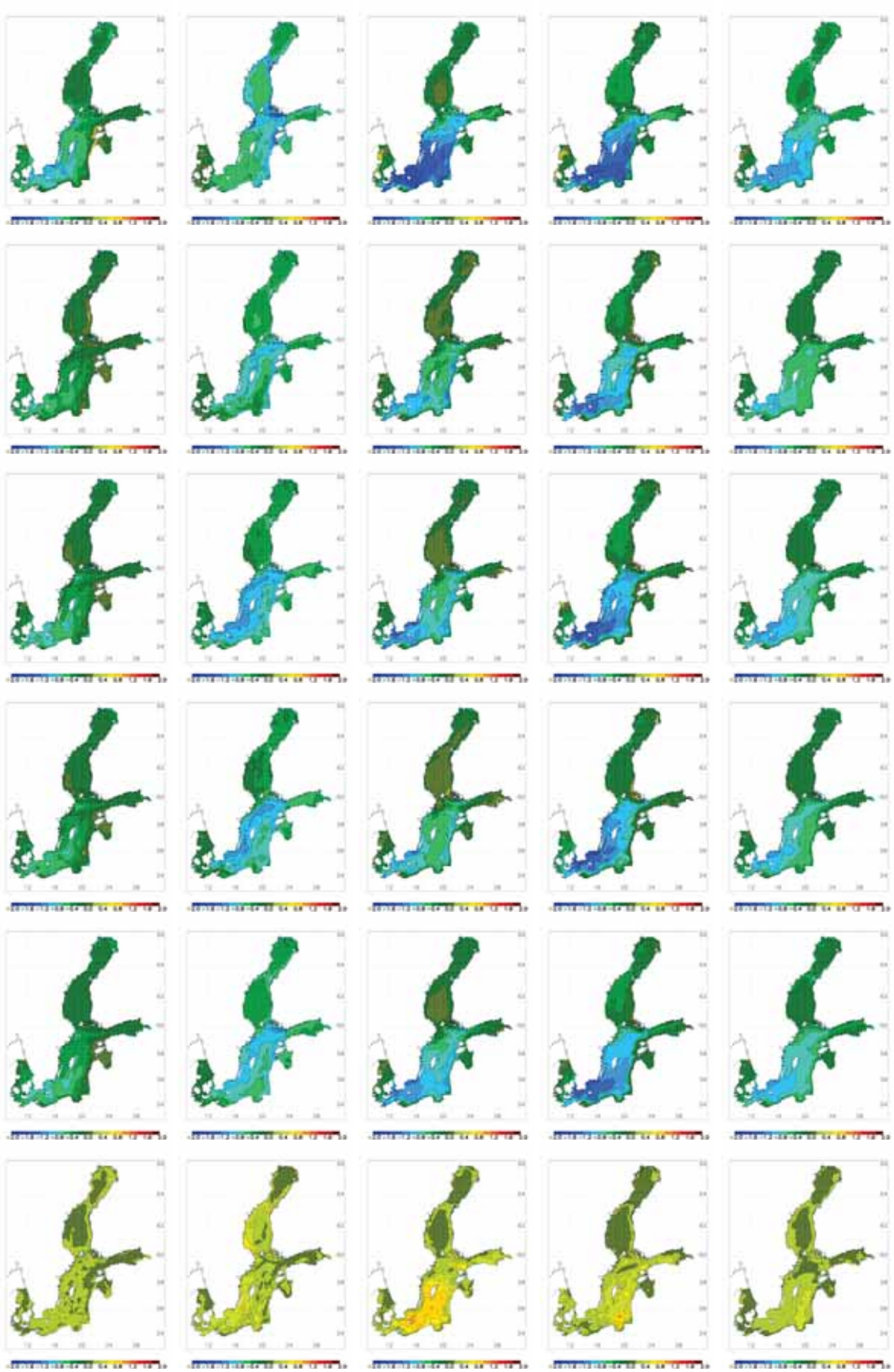

Figure 45. As Fig. 34 but for Secchi depth changes (m).

Figure 46. Annual and seasonal mean bottom oxygen concentration changes (ml l^{-1}) between 2070-2099 and 1969-1998 in RCO-SCOBI simulations driven by regionalized GCM results. From left to right results for winter (December through February), spring (March through May), summer (June through August), autumn (September through November) and the annual mean are shown. From top to bottom the results of the following scenario simulations and analysis results are shown: RCAO-HadCM3-A1B-BSAP, RCAO-ECHAM5-A1B-3-BSAP, RCAO-ECHAM5-A1B-1-BSAP, RCAO-ECHAM5-A2-1-BSAP, ensemble mean, and range.

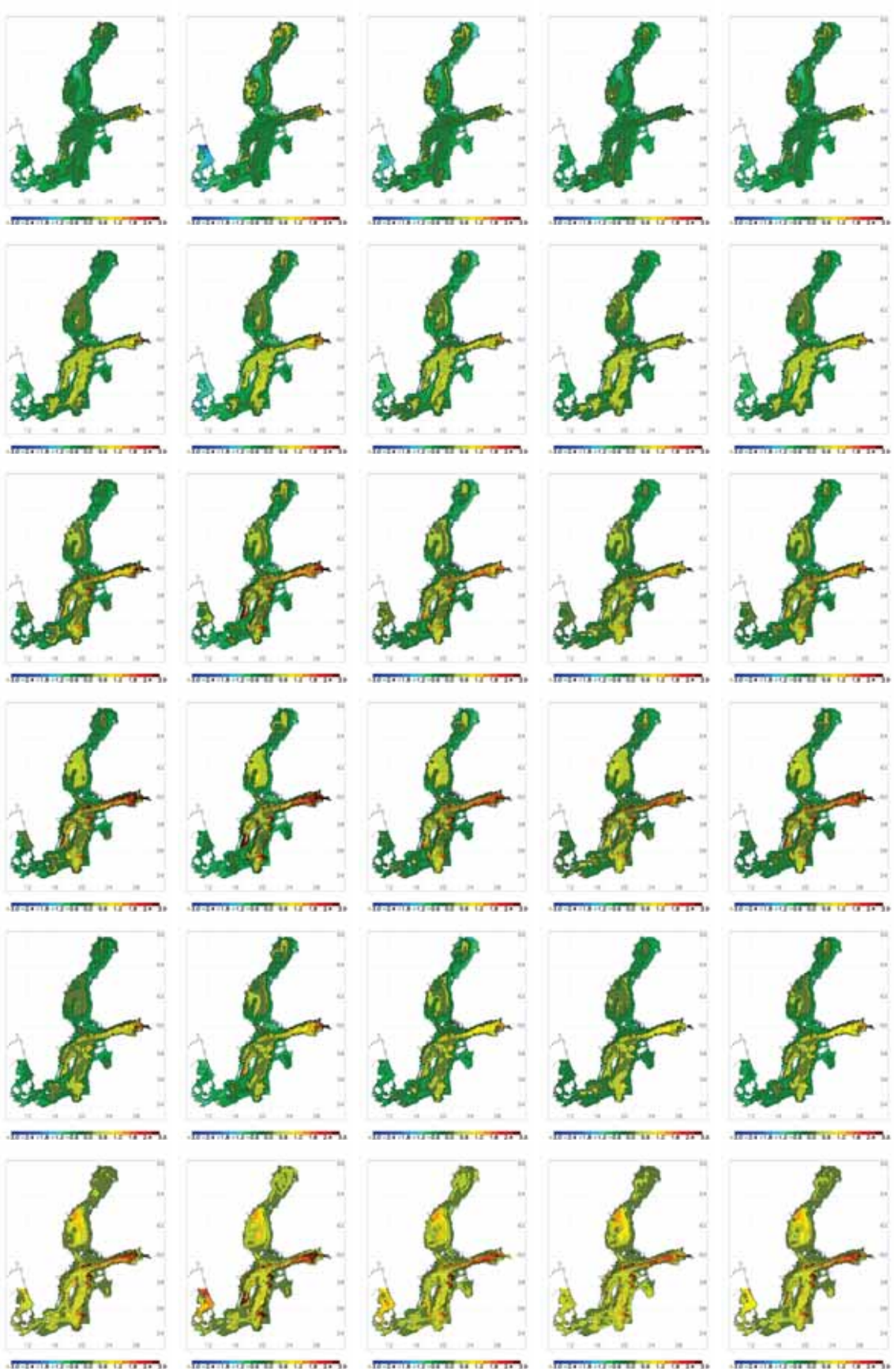

Figure 46. Continued.

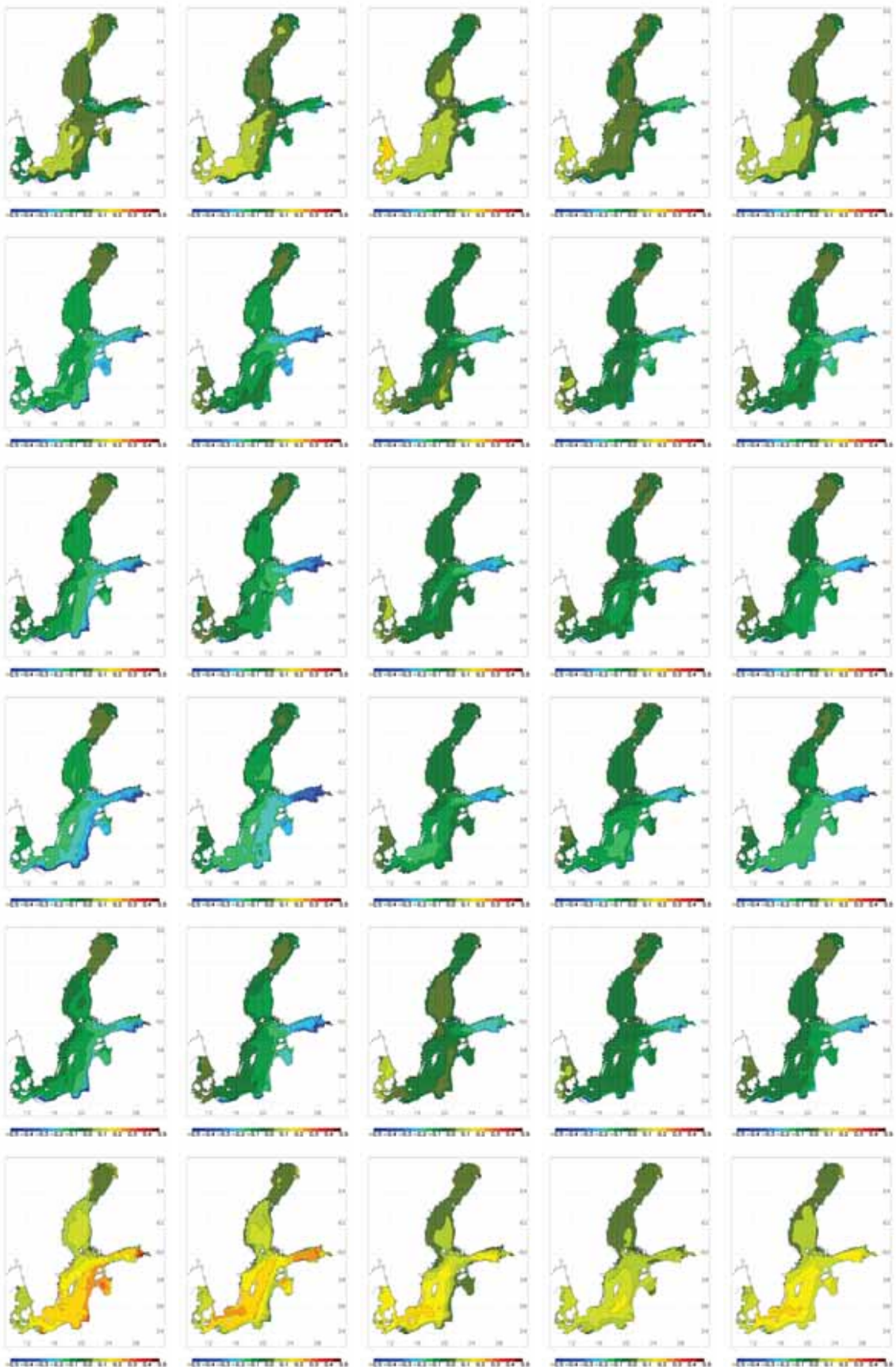

Figure 47. As Fig. 46 but for phosphate concentration changes (mmolP m^{-3}).

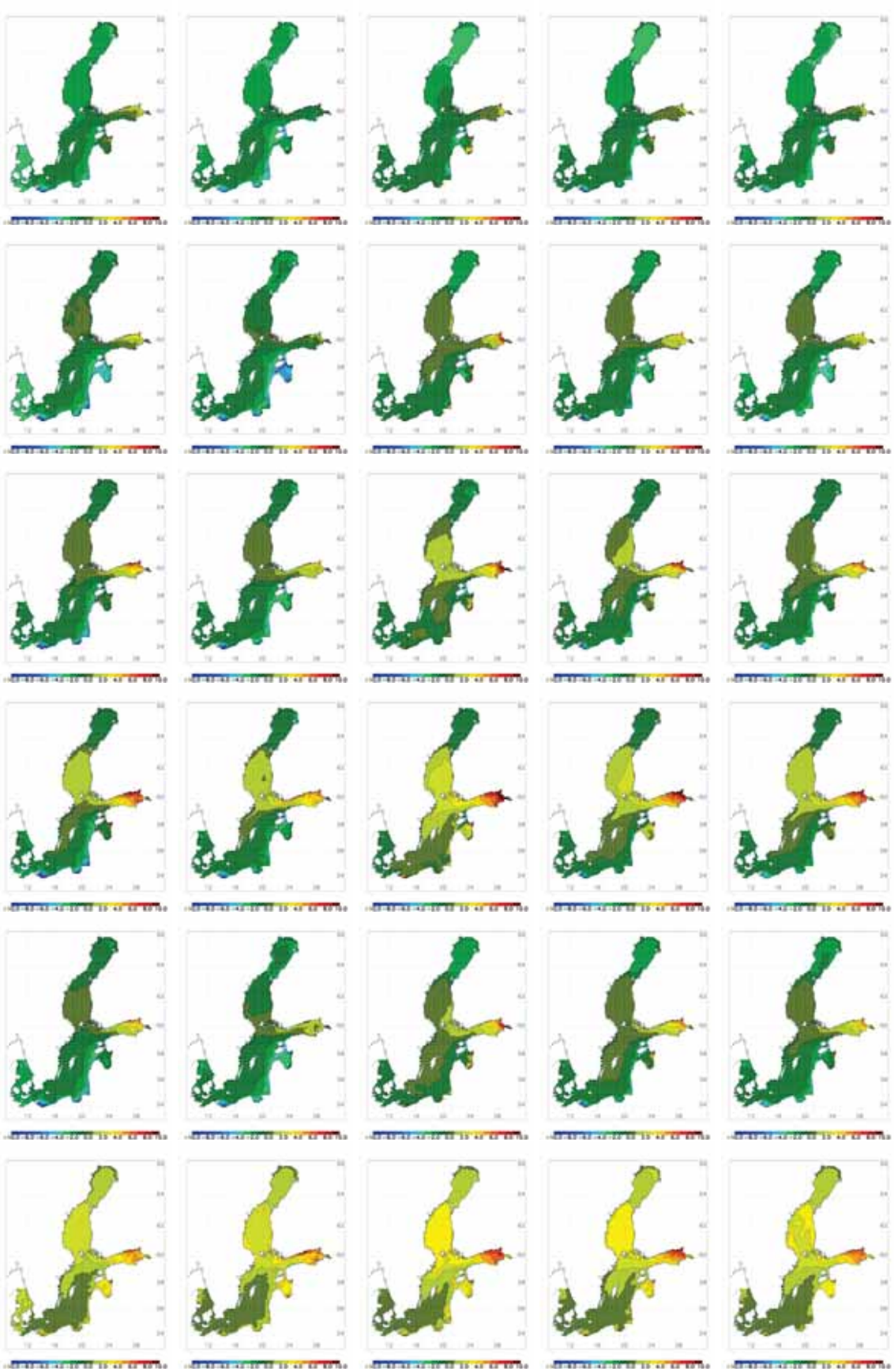

Figure 48. As Fig. 46 but for nitrate concentration changes (mmolN m^{-3}).

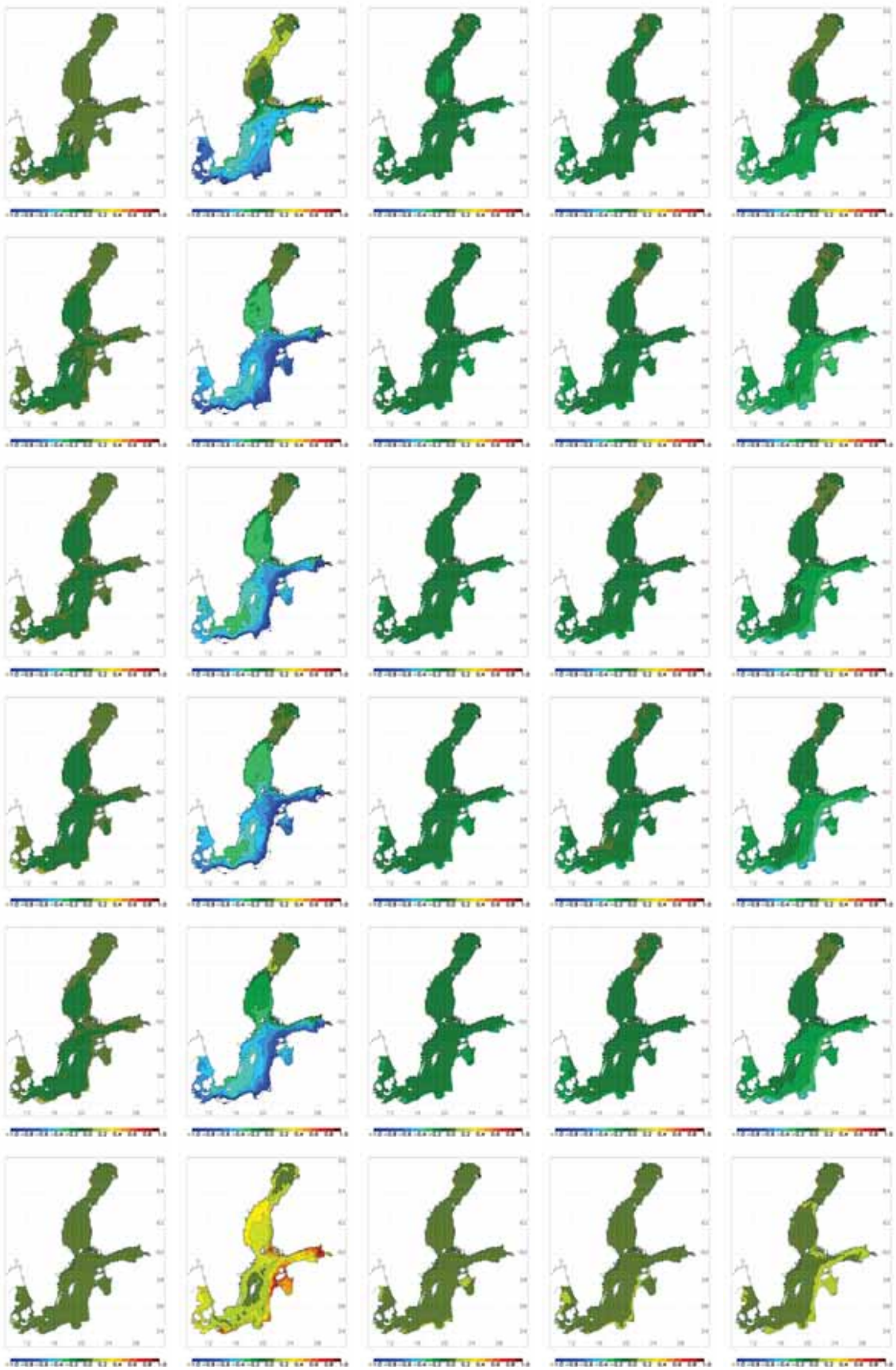

Figure 49. As Fig. 46 but for diatom concentration changes (mgChl m^{-3}).

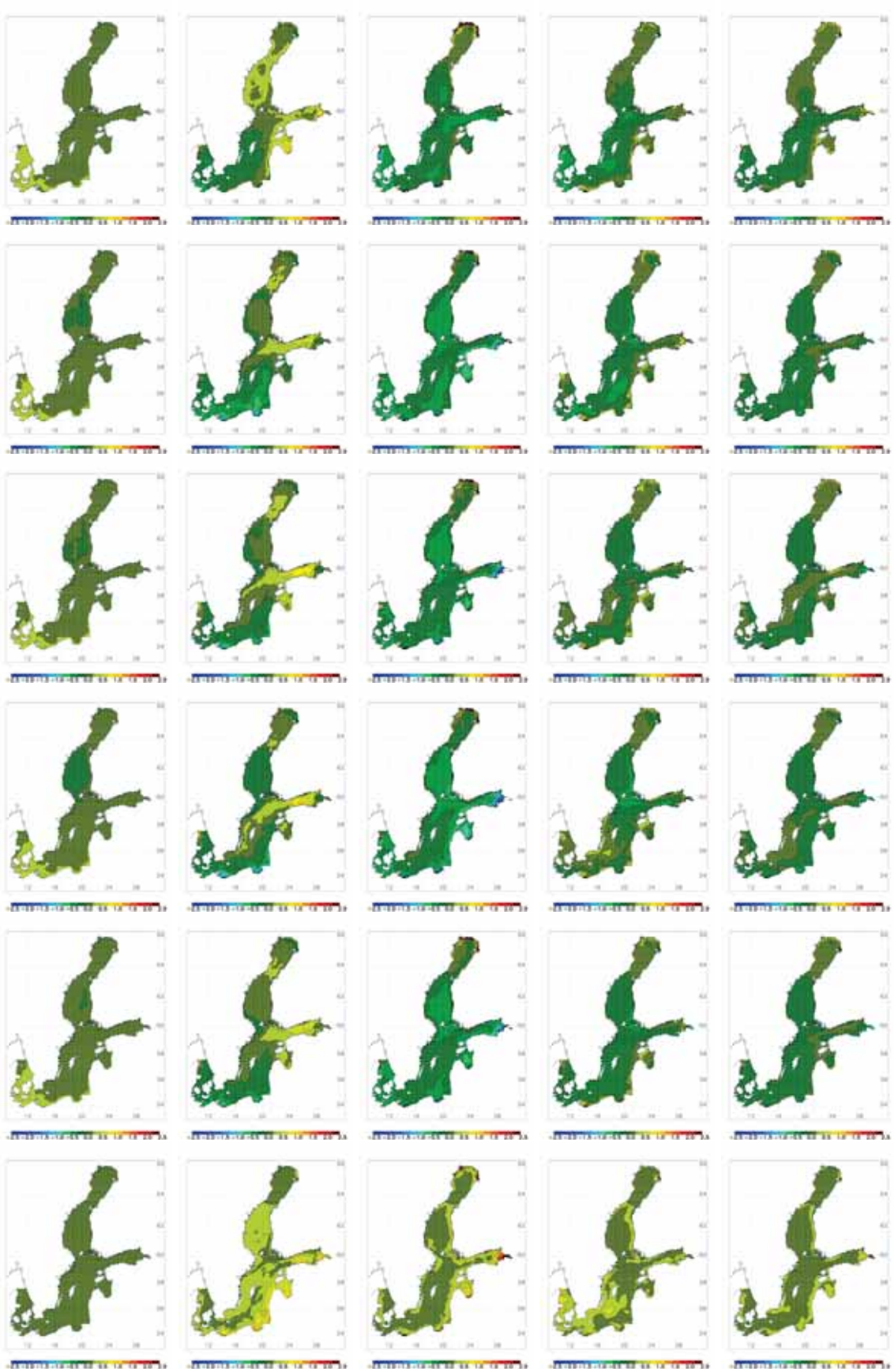

Figure 50. As Fig. 46 but for concentration changes of flagellates and others (mgChl m^{-3}).

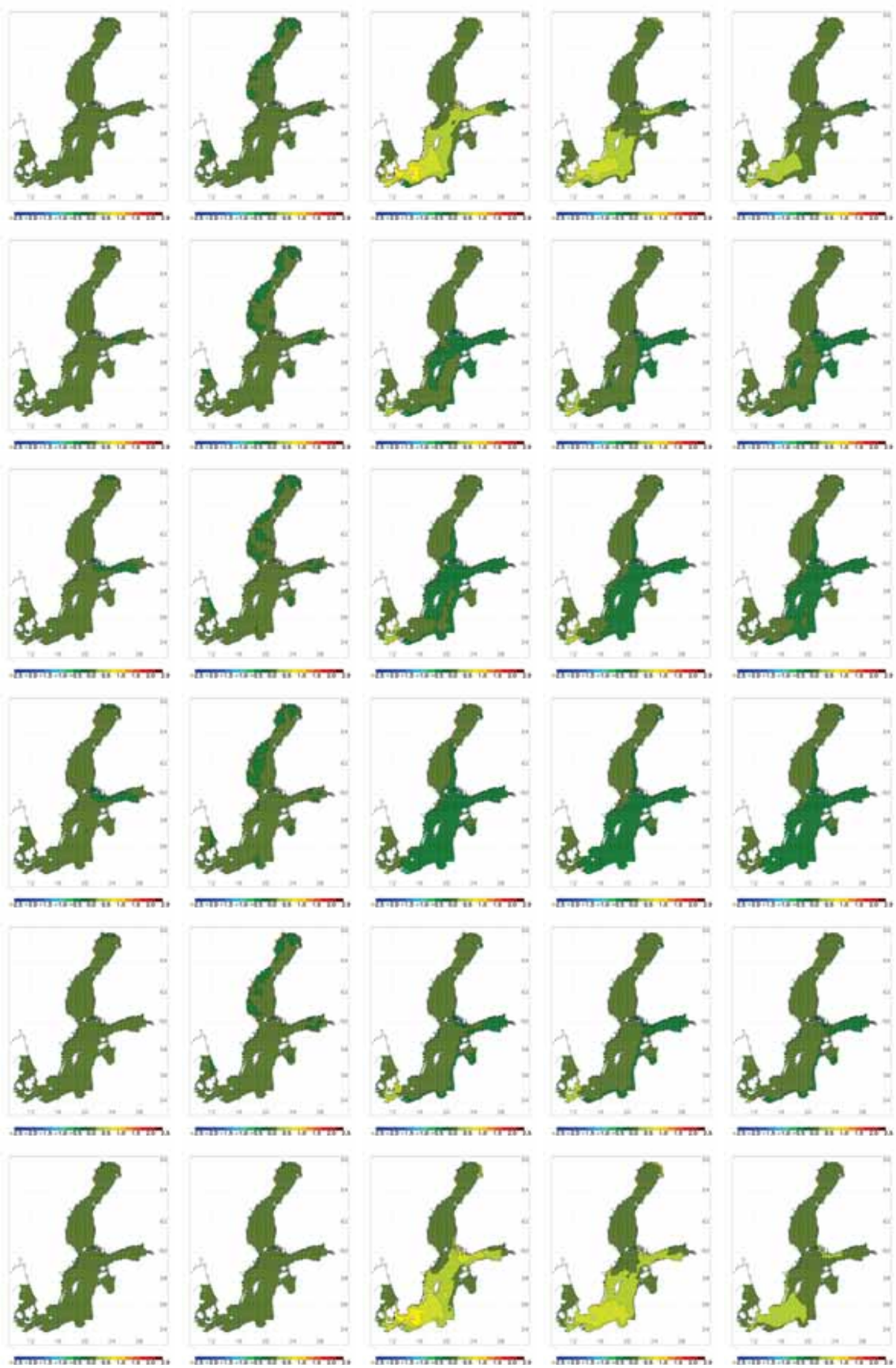

Figure 51. As Fig. 46 but for cyanobacteria concentration changes (mgChl m^{-3}).

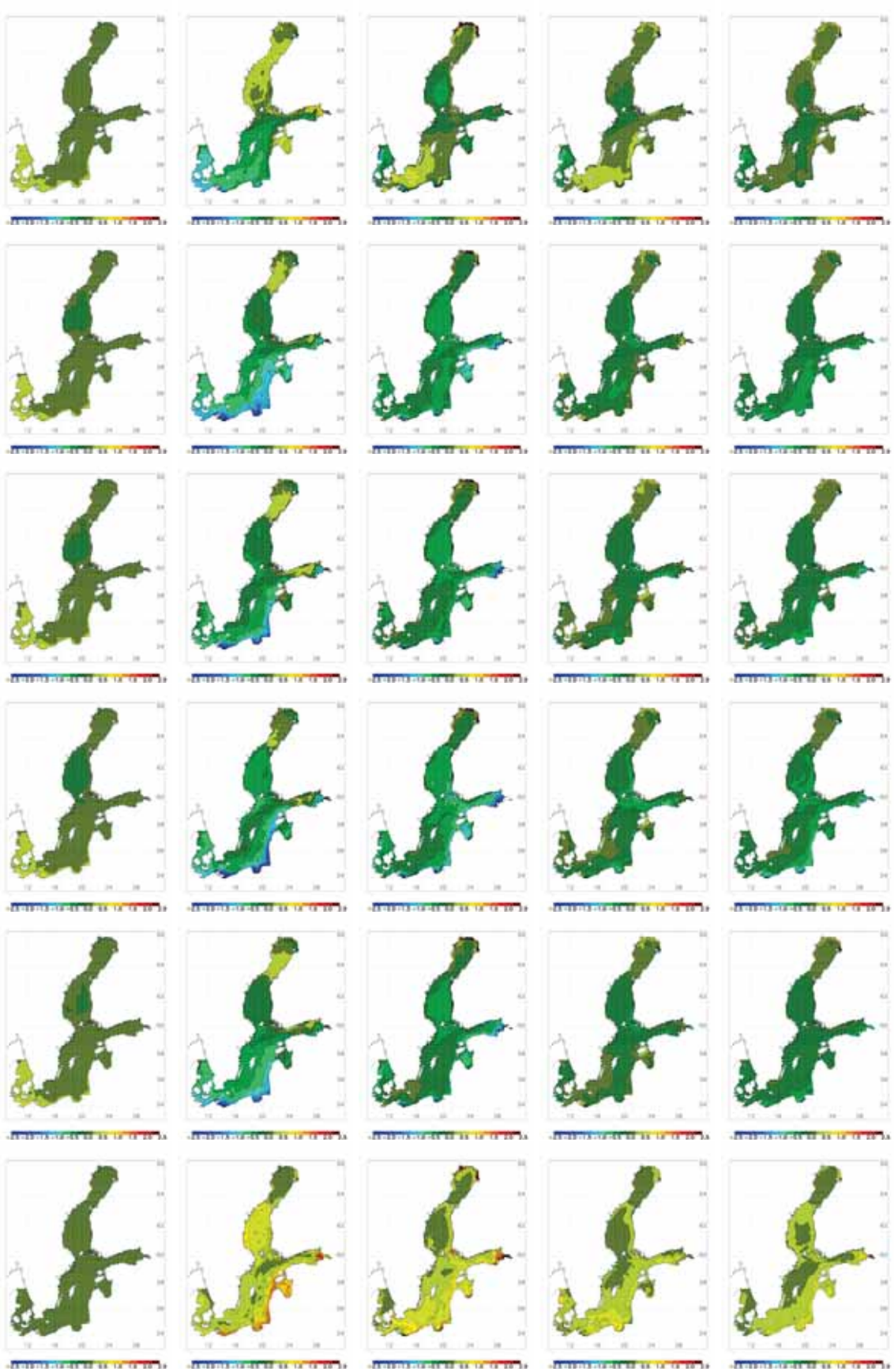

Figure 52. As Fig. 46 but for phytoplankton concentration changes (mgChl m^{-3}).

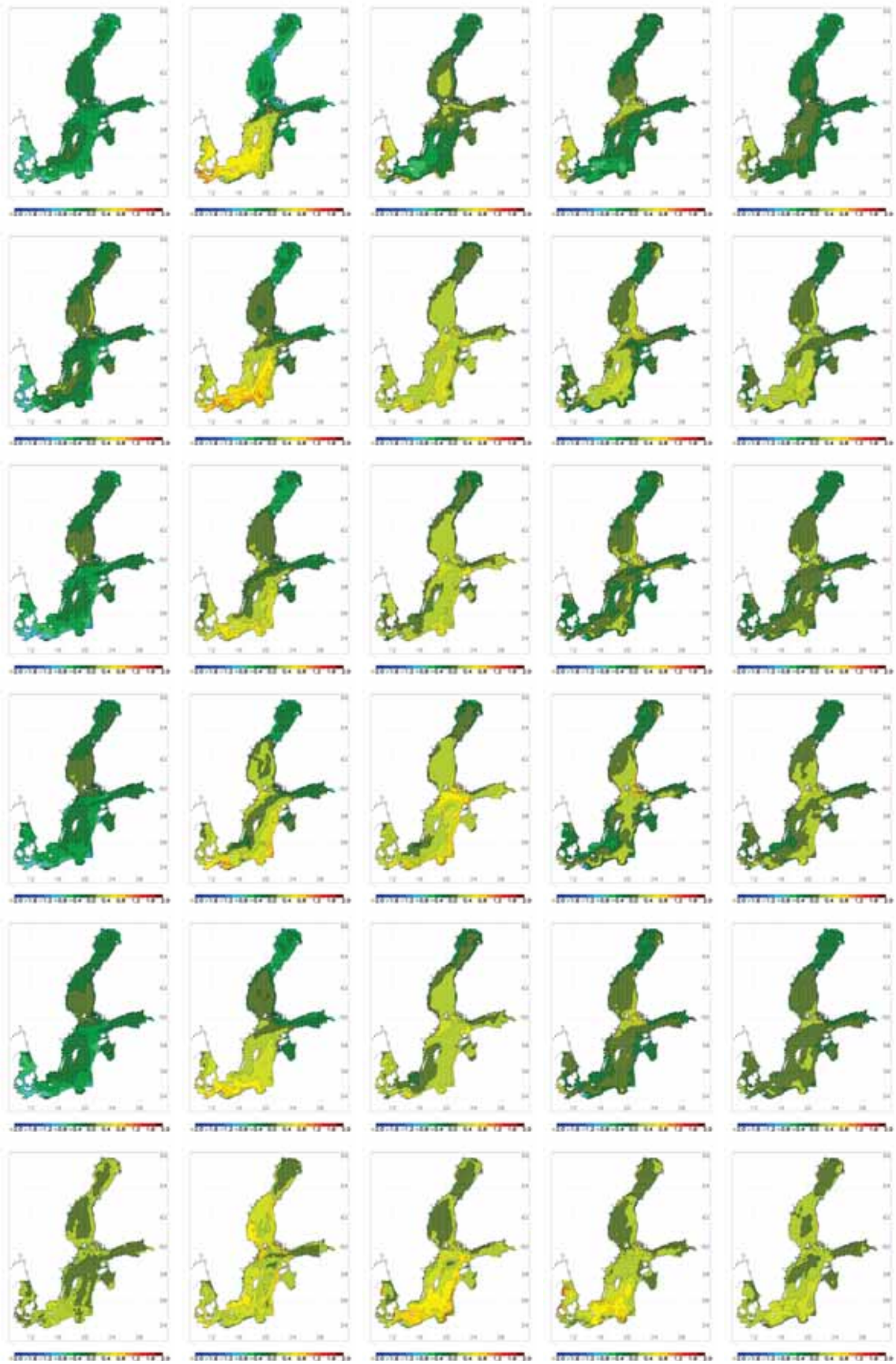

Figure 53. As Fig. 46 but for Secchi depth changes (m).

Figure 54. Annual and seasonal mean bottom oxygen concentration changes (ml l^{-1}) between 2070-2099 and 1969-1998 in RCO-SCOBI simulations driven by regionalized GCM results. From left to right results for winter (December through February), spring (March through May), summer (June through August), autumn (September through November) and the annual mean are shown. From top to bottom the results of the following scenario simulations and analysis results are shown: RCAO-HadCM3-A1B-CLEG, RCAO-ECHAM5-A1B-3-CLEG, RCAO-ECHAM5-A1B-1-CLEG, RCAO-ECHAM5-A2-1-CLEG, ensemble mean, and range.

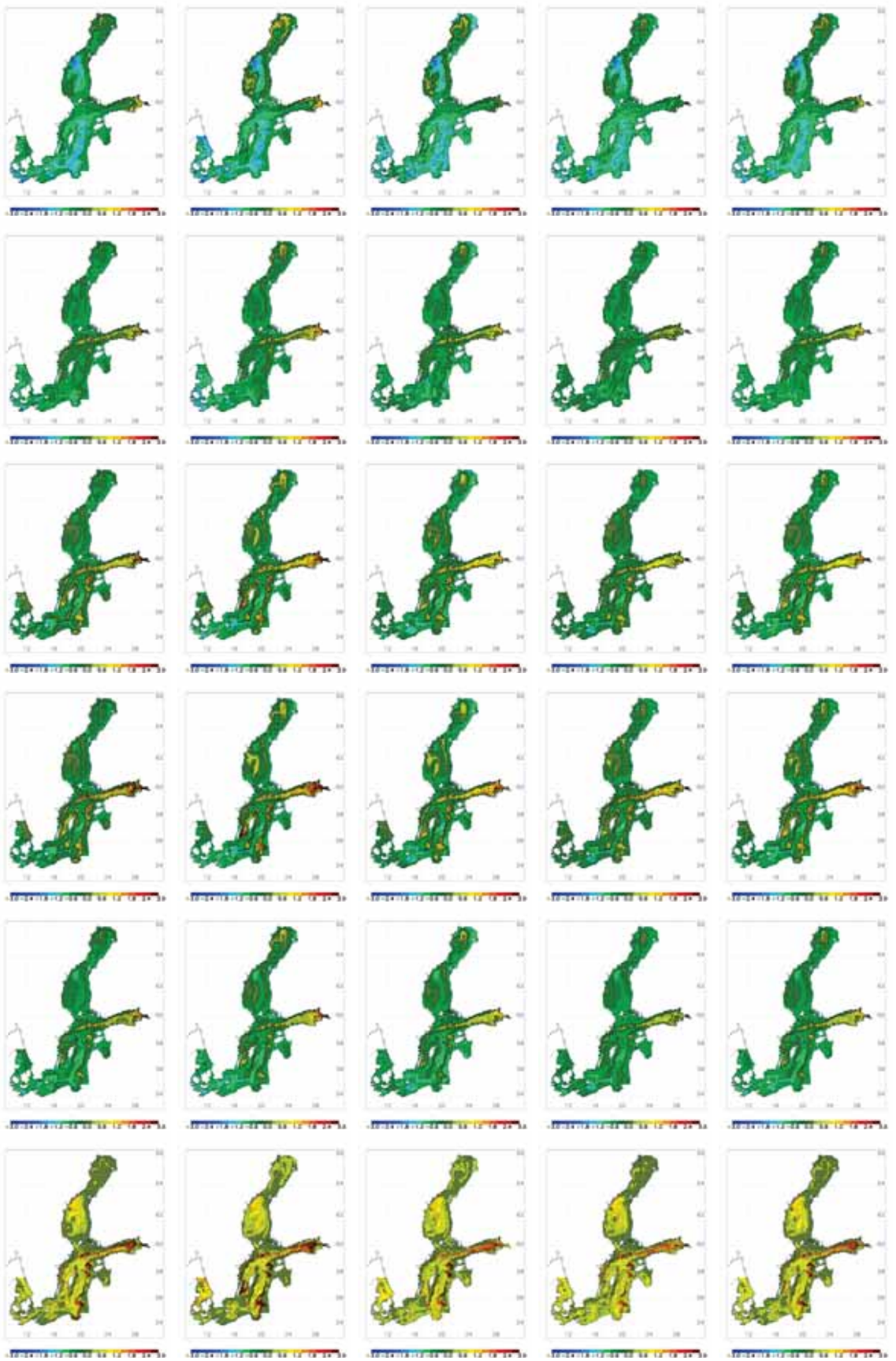

Figure 54. Continued.

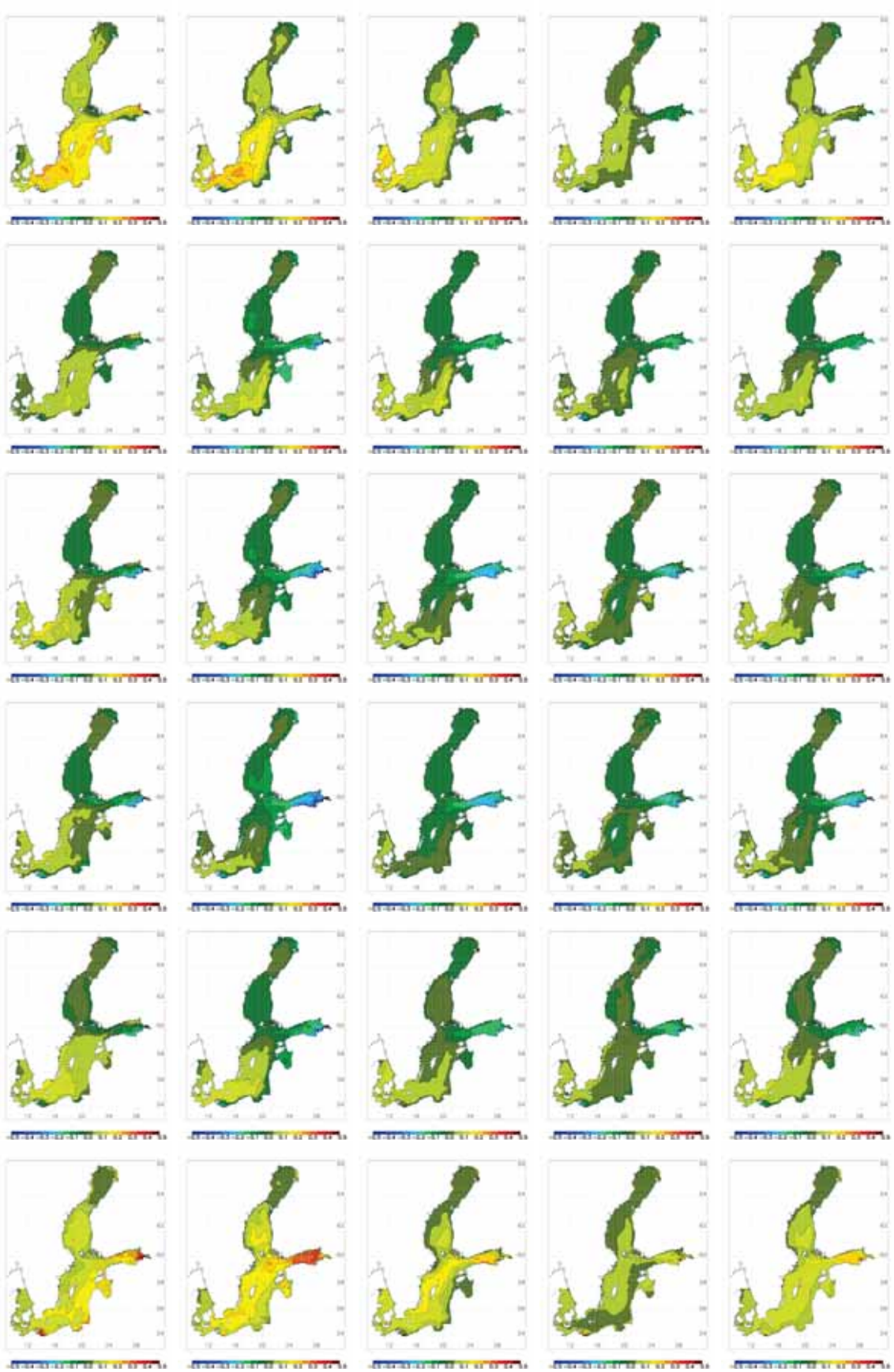

Figure 55. As Fig. 54 but for phosphate concentration changes (mmolP m^{-3}).

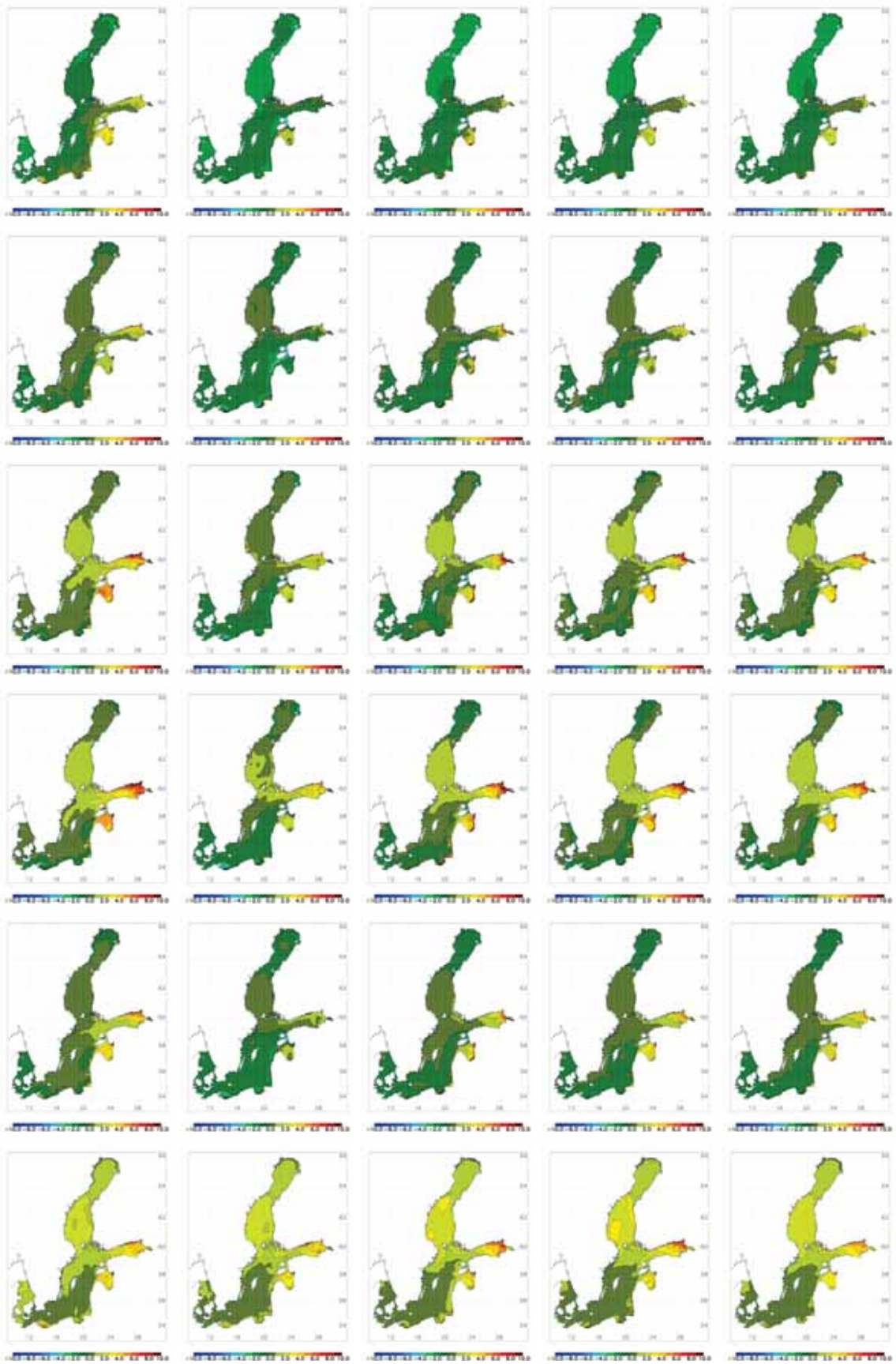

Figure 56. As Fig. 54 but for nitrate concentration changes (mmolN m^{-3}).

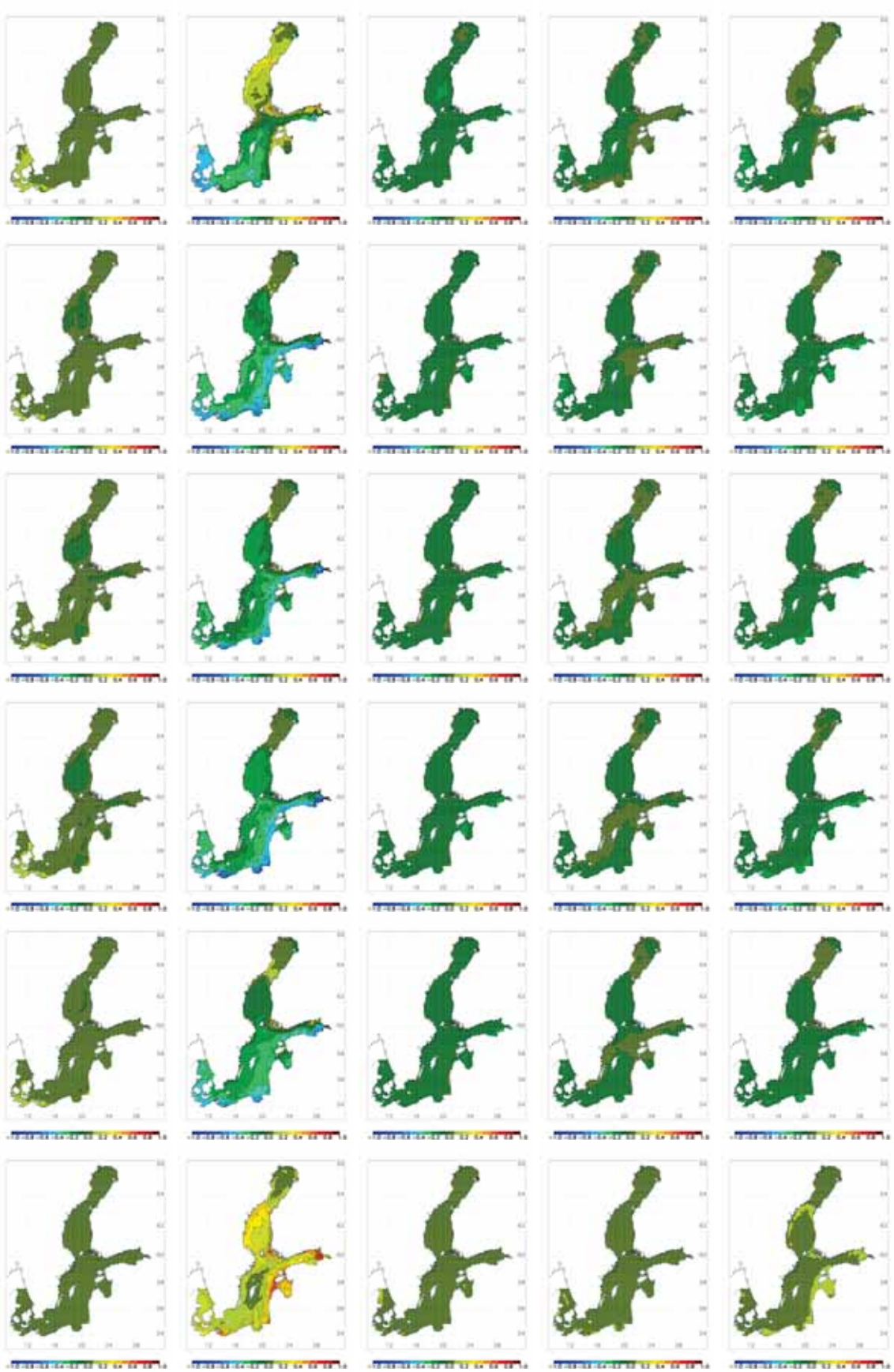

Figure 57. As Fig. 54 but for diatom concentration changes (mgChl m^{-3}).

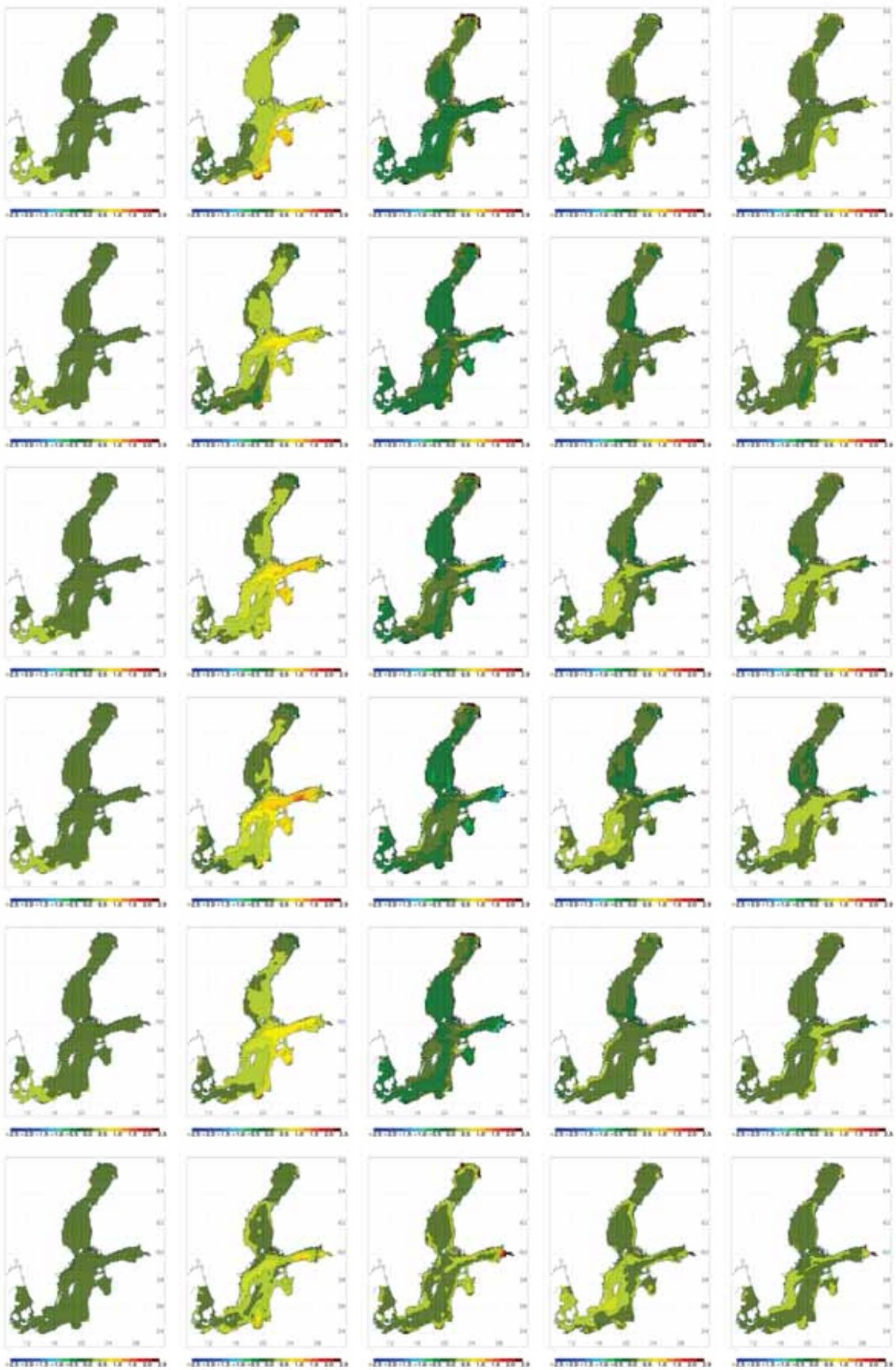

Figure 58. As Fig. 54 but for concentration changes of flagellates and others (mgChl m^{-3}).

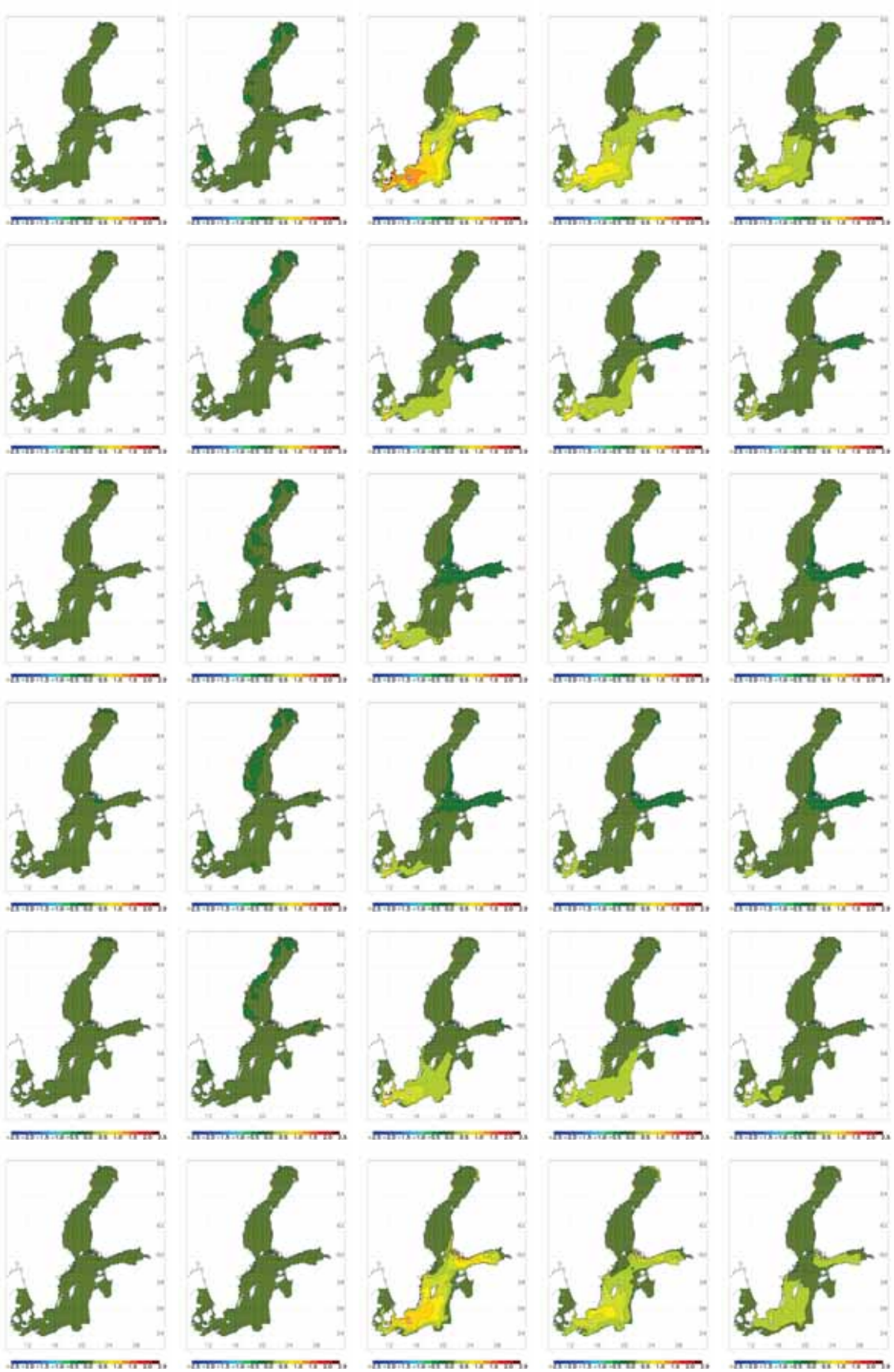

Figure 59. As Fig. 54 but for cyanobacteria concentration changes (mgChl m^{-3}).

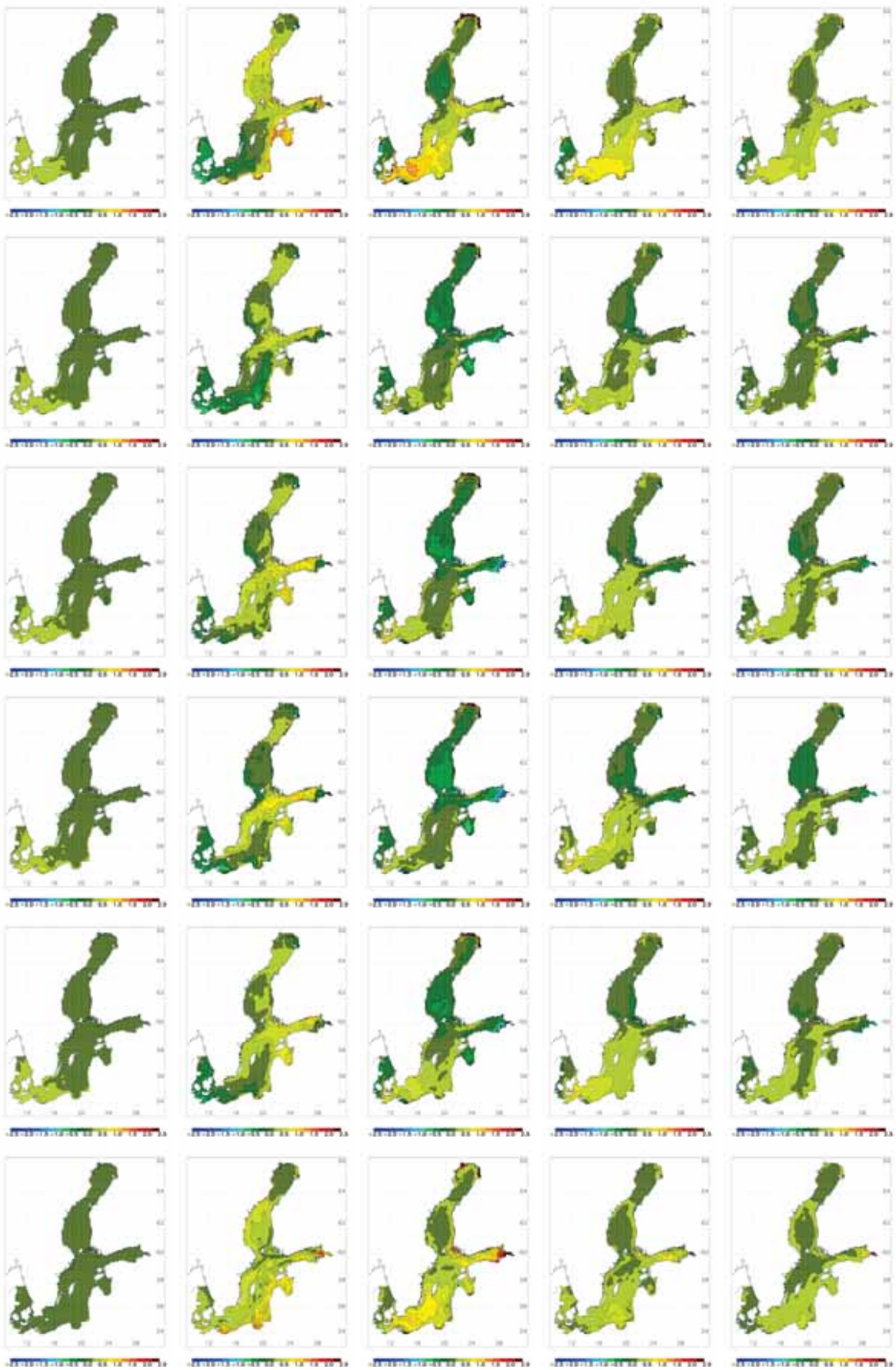

Figure 60. As Fig. 54 but for phytoplankton concentration changes (mgChl m^{-3}).

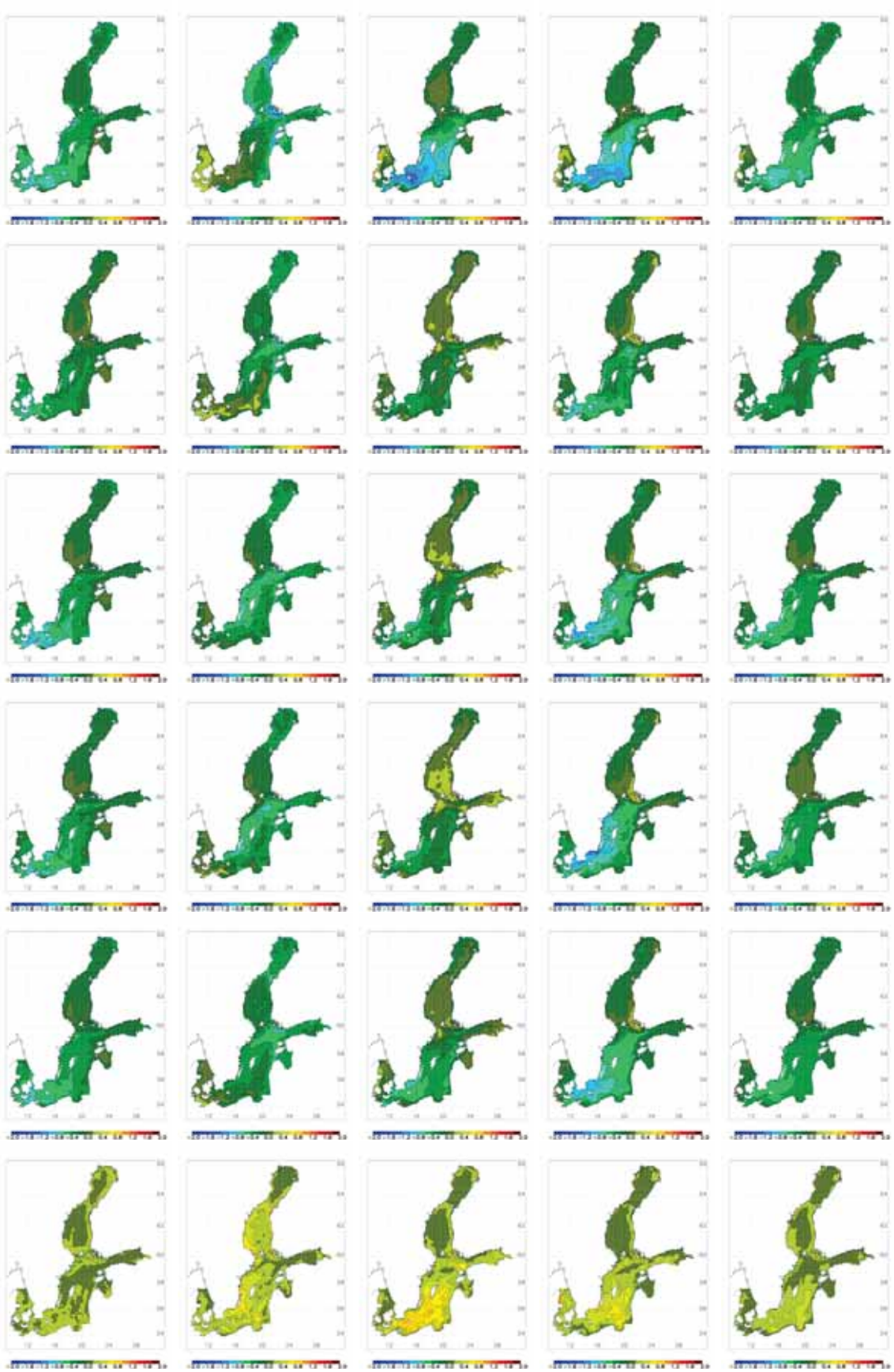

Figure 61. As Fig. 54 but for Secchi depth changes (m).

Figure 62. Annual and seasonal mean bottom oxygen concentration changes (ml l^{-1}) between 2070-2099 and 1969-1998 in RCO-SCOBI simulations driven by regionalized GCM results. From left to right results for winter (December through February), spring (March through May), summer (June through August), autumn (September through November) and the annual mean are shown. From top to bottom the results of the following scenario simulations and analysis results are shown: RCAO-HadCM3-A1B-BAU, RCAO-ECHAM5-A1B-3-BAU, RCAO-ECHAM5-A1B-1-BAU, RCAO-ECHAM5-A2-1-BAU, ensemble mean, and range.

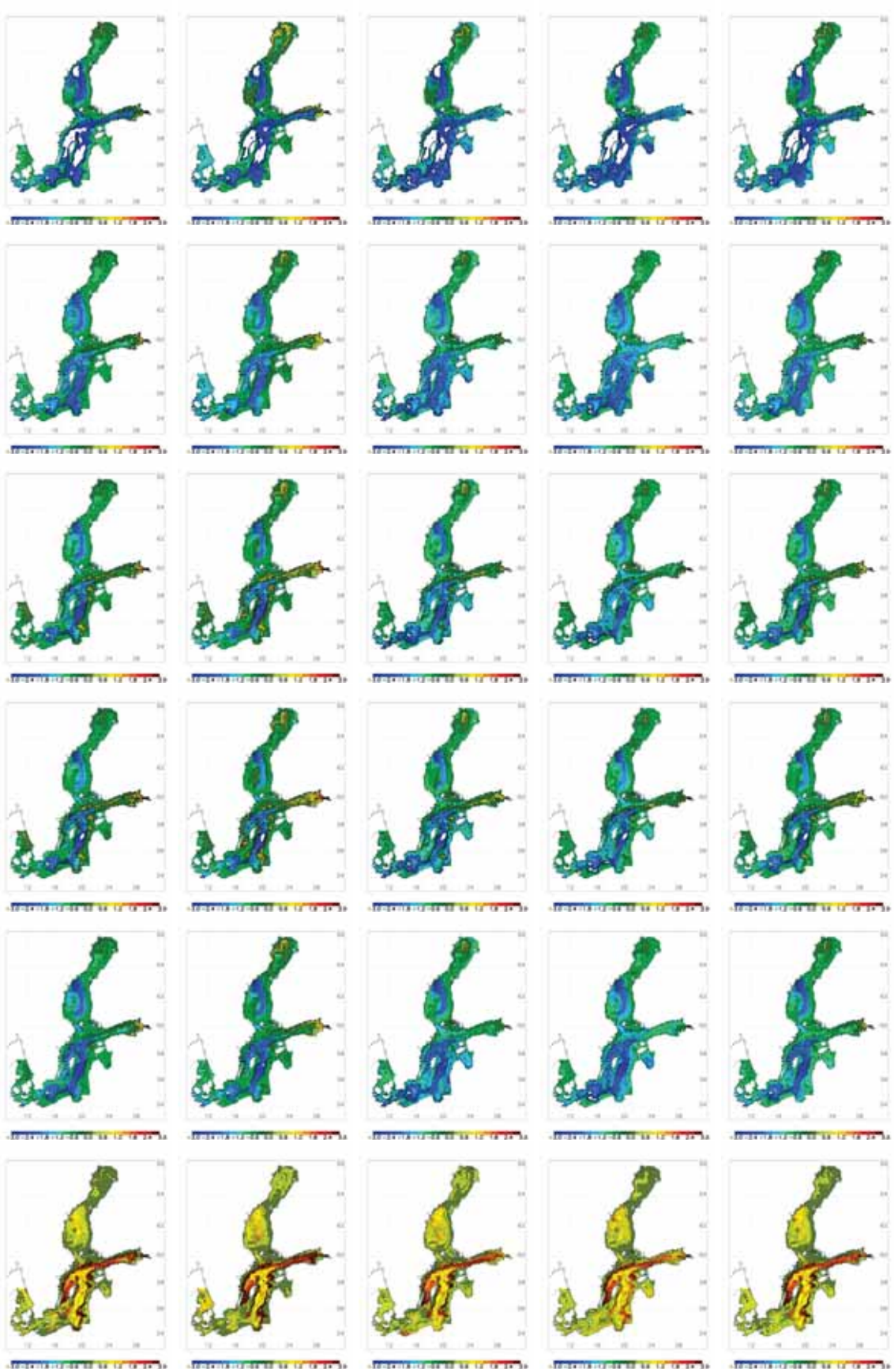

Figure 62. Continued.

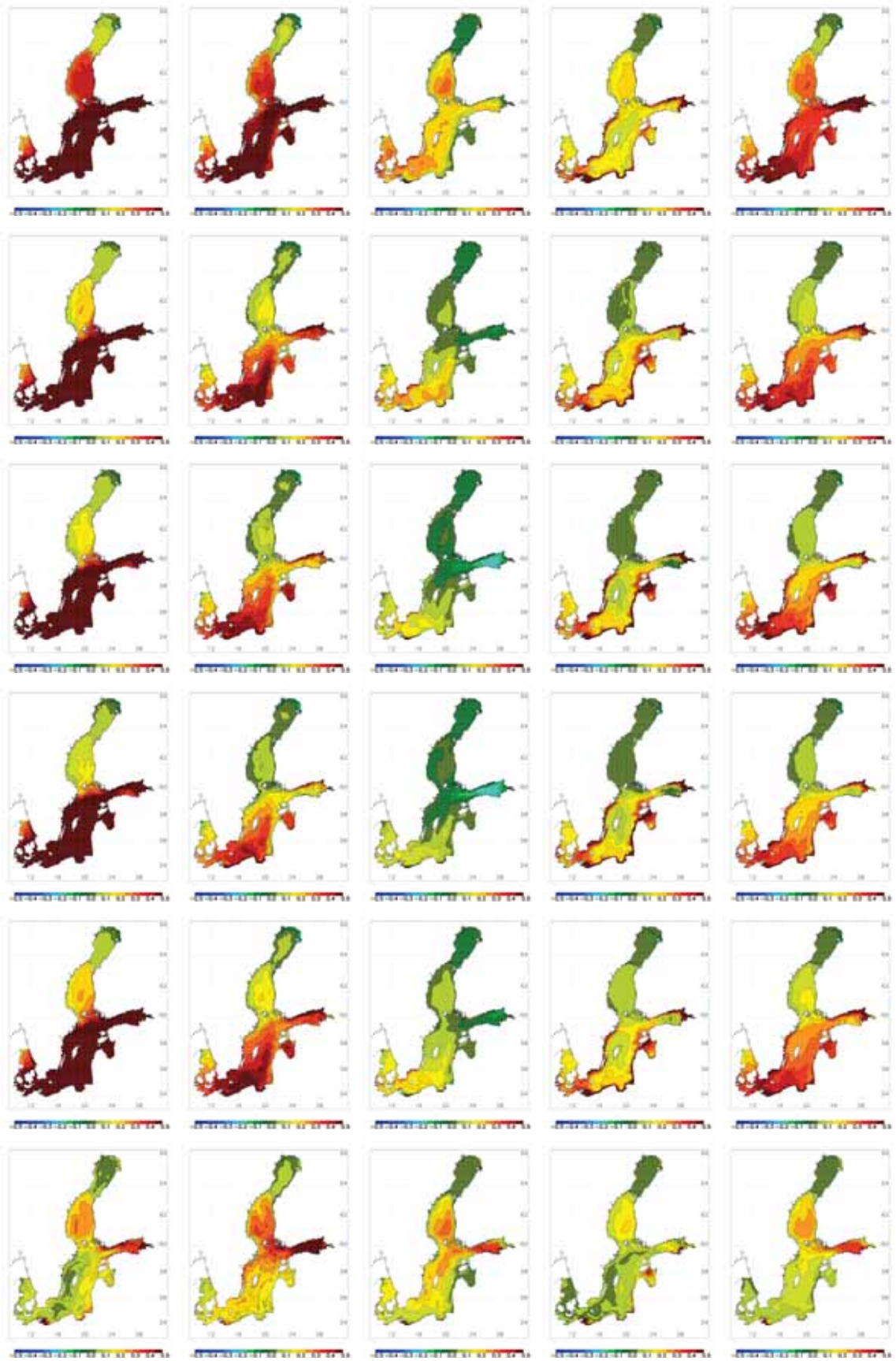

Figure 63. As Fig. 62 but for phosphate concentration changes (mmolP m^{-3}).

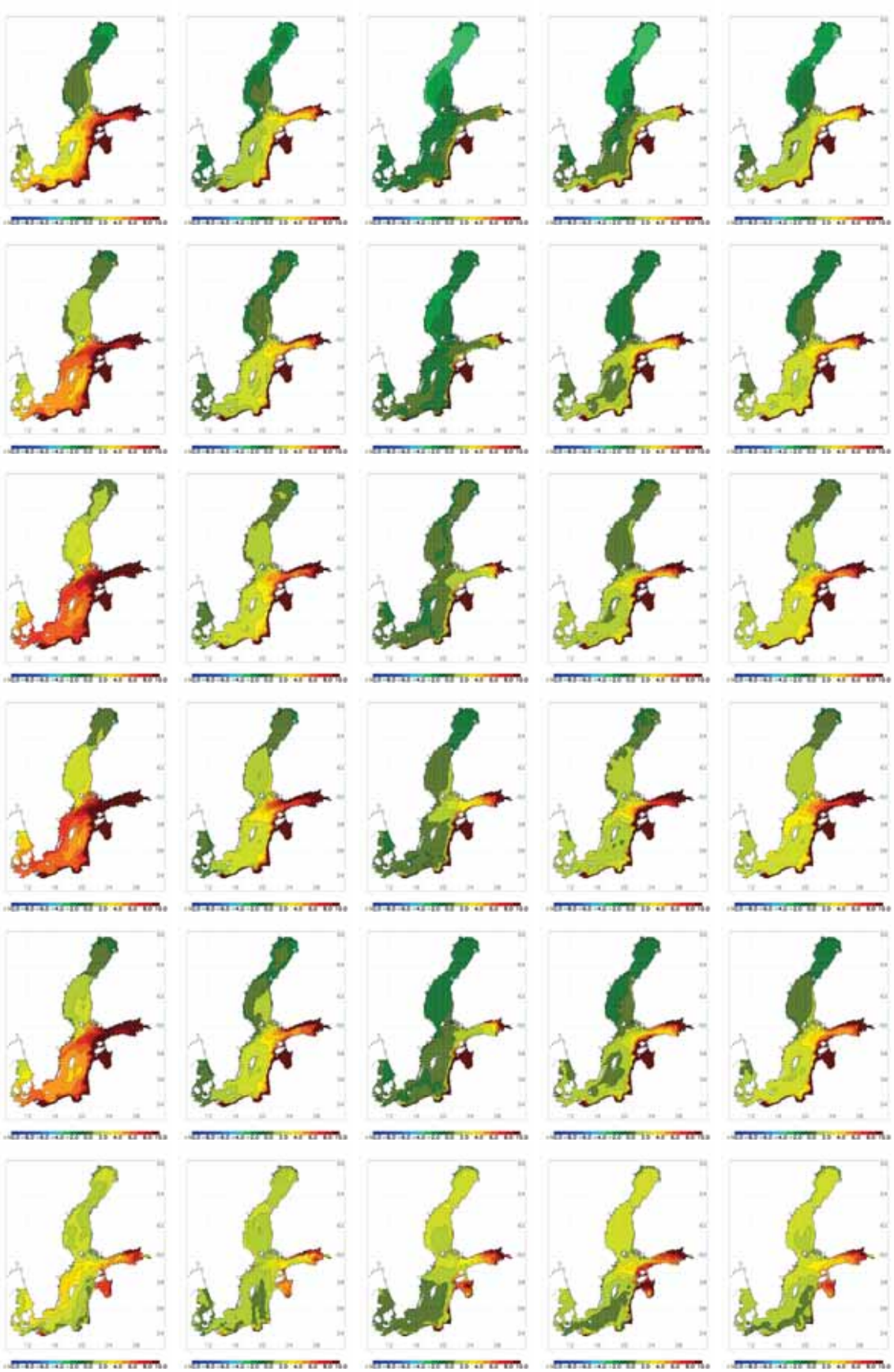

Figure 64. As Fig. 62 but for nitrate concentration changes (mmolN m^{-3}).

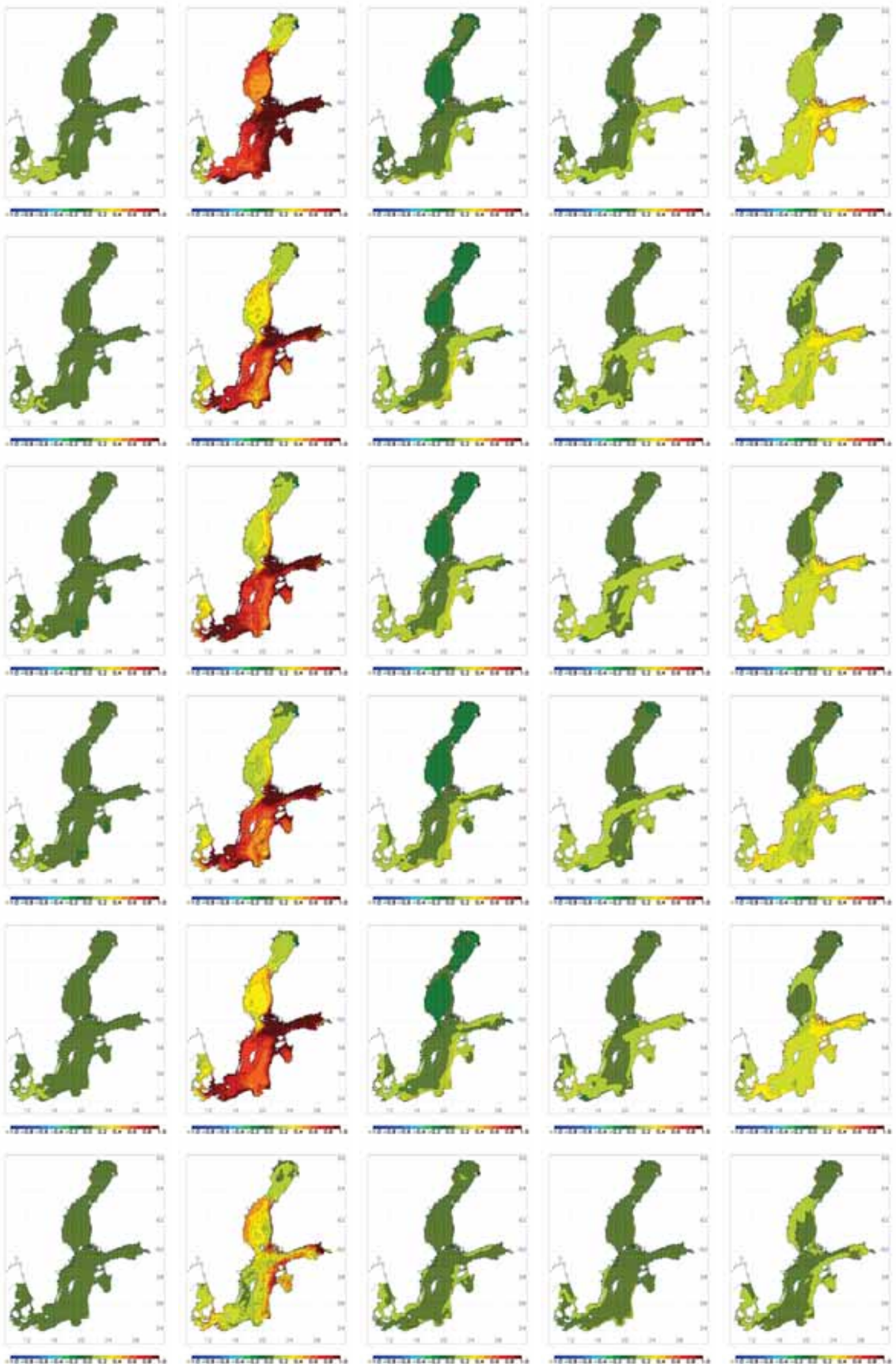

Figure 65. As Fig. 62 but for diatom concentration changes (mgChl m^{-3}).

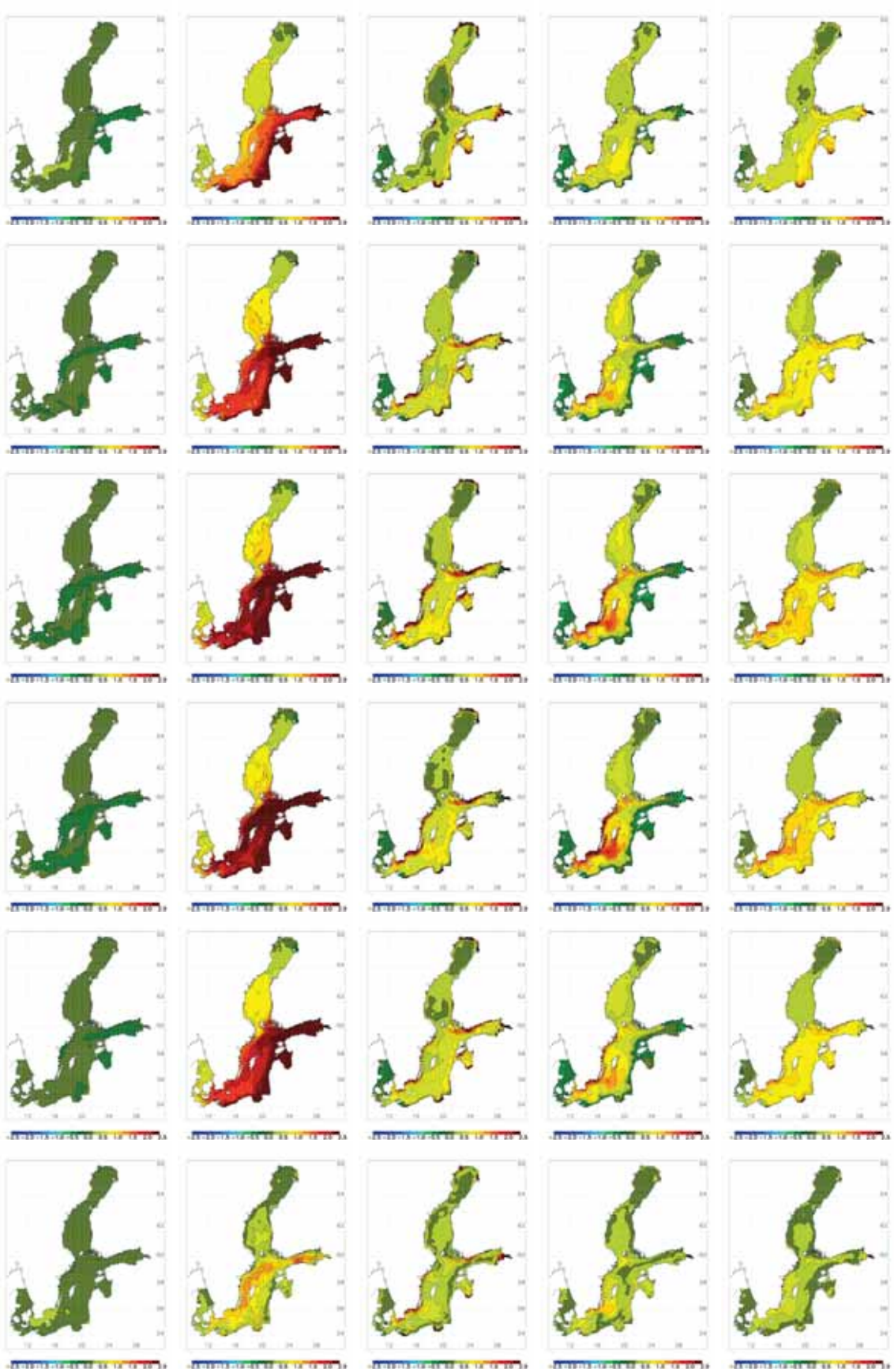

Figure 66. As Fig. 62 but for concentration changes of flagellates and others (mgChl m^{-3}).

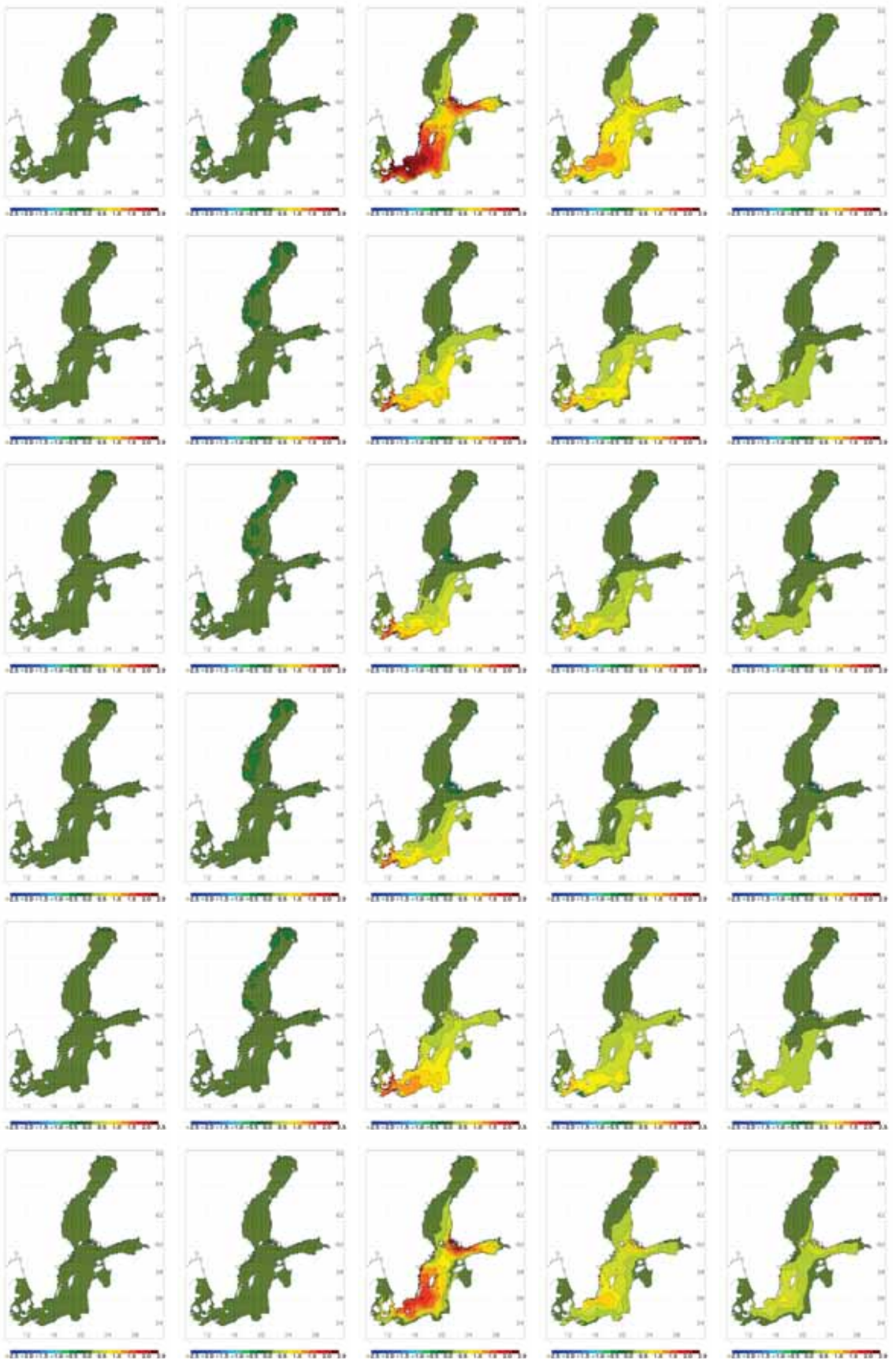

Figure 67. As Fig. 62 but for cyanobacteria concentration changes (mgChl m^{-3}).

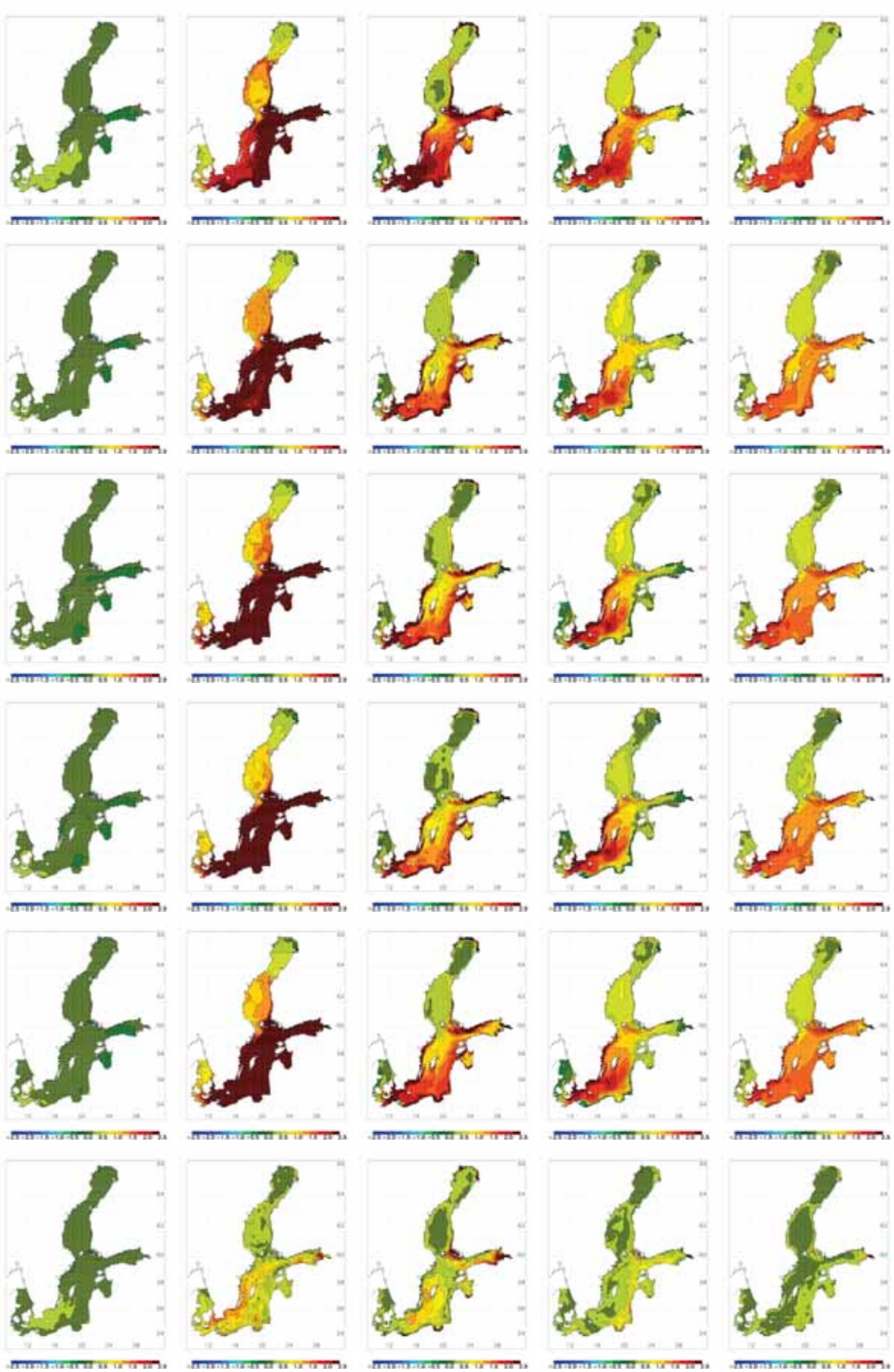

Figure 68. As Fig. 62 but for phytoplankton concentration changes (mgChl m^{-3}).

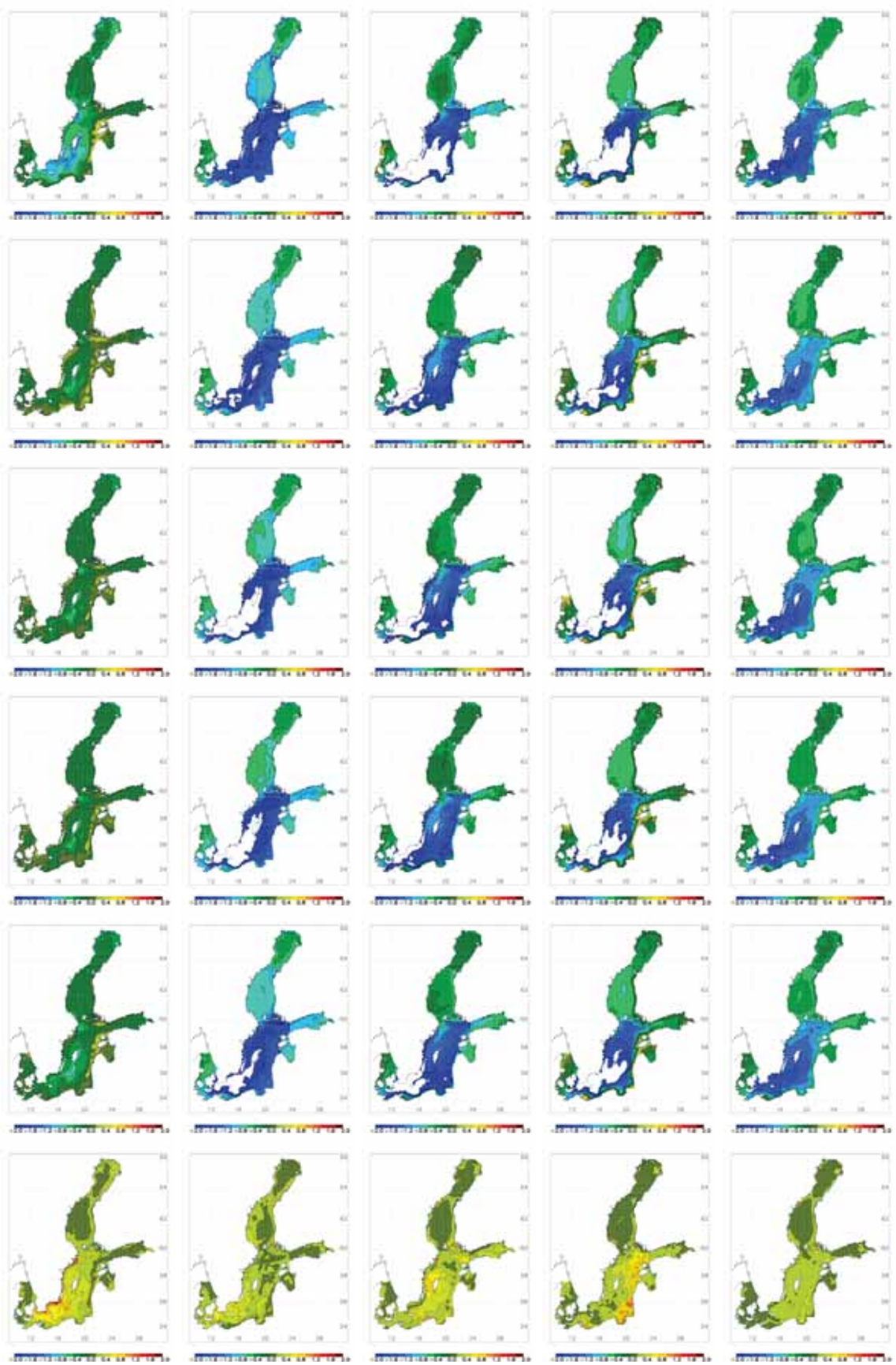

Figure 69. As Fig. 62 but for Secchi depth changes (m).

I serien OCEANOGRAFI har tidigare utgivits:

1 Lennart Funkquist (1985)
En hydrodynamisk modell för spridnings- och cirkulationsberäkningar i Östersjön Slutrapport.

2 Barry Broman och Carsten Pettersson. (1985)
Spridningsundersökningar i yttre fjärden Piteå.

3 Cecilia Ambjörn (1986).
Utbyggnad vid Malmö hamn; effekter för Lommabuktens vattenutbyte.

4 Jan Andersson och Robert Hillgren (1986).
SMHIs undersökningar i Öregrundsgrepen perioden 84/85.

5 Bo Juhlin (1986)
Oceanografiska observationer utmed svenska kusten med kustbevakningens fartyg 1985.

6 Barry Broman (1986)
Uppföljning av sjövärmepump i Lilla Värtan.

7 Bo Juhlin (1986)
15 års mätningar längs svenska kusten med kustbevakningen (1970 - 1985).

8 Jonny Svensson (1986)
Vågdata från svenska kustvatten 1985.

9 Barry Broman (1986)
Oceanografiska stationsnät - Svenskt Vattenarkiv.

10 -

11 Cecilia Ambjörn (1987)
Spridning av kylvatten från Öresundsverket

12 Bo Juhlin (1987)
Oceanografiska observationer utmed svenska kusten med kustbevakningens fartyg 1986.

13 Jan Andersson och Robert Hillgren (1987)
SMHIs undersökningar i Öregrundsgrepen 1986.

14 Jan-Erik Lundqvist (1987)
Impact of ice on Swedish offshore lighthouses. Ice drift conditions in the area at Sydostbrotten - ice season 1986/87.

15 SMHI/SNV (1987)
Fasta förbindelser över Öresund - utredning av effekter på vattenmiljön i Östersjön.

16 Cecilia Ambjörn och Kjell Wickström (1987)
Undersökning av vattenmiljön vid utfyllnaden av Kockums varvsbassäng. Slutrapport för perioden 18 juni - 21 augusti 1987.

17 Erland Bergstrand (1987)
Östergötlands skärgård - Vattenmiljön.

18 Stig H. Fonselius (1987)
Kattegatt - havet i väster.

19 Erland Bergstrand (1987)
Recipientkontroll vid Breviksnäs fiskodling 1986.

20 Kjell Wickström (1987)
Bedömning av kylvattenrecipienten för ett kolkraftverk vid Oskarshamnsverket.

21 Cecilia Ambjörn (1987)
Förstudie av ett nordiskt modellsystem för kemikaliespridning i vatten.

22 Kjell Wickström (1988)
Vågdata från svenska kustvatten 1986.

23 Jonny Svensson, SMHI/National Swedish Environmental Protection Board (SNV) (1988)
A permanent traffic link across the Öresund channel - A study of the hydro-environmental effects in the Baltic Sea.

24 Jan Andersson och Robert Hillgren (1988)
SMHIs undersökningar utanför Forsmark 1987.

25 Carsten Peterson och Per-Olof Skoglund (1988)
Kylvattnet från Ringhals 1974-86.

26 Bo Juhlin (1988)
Oceanografiska observationer runt svenska kusten med kustbevakningens fartyg 1987.

27 Bo Juhlin och Stefan Tobiasson (1988)
Recipientkontroll vid Breviksnäs fiskodling 1987.

28 Cecilia Ambjörn (1989)
Spridning och sedimentation av tippat lermaterial utanför Helsingborgs hamnområde.

29 Robert Hillgren (1989)
SMHIs undersökningar utanför Forsmark 1988.

30 Bo Juhlin (1989)
Oceanografiska observationer runt svenska kusten med kustbevakningens fartyg 1988.

31 Erland Bergstrand och Stefan Tobiasson (1989)
Samordnade kustvattenkontrollen i Östergötland 1988.

32 Cecilia Ambjörn (1989)
Oceanografiska förhållanden i Brofjorden i samband med kylvattenutsläpp i Trommekilen.

33a Cecilia Ambjörn (1990)
Oceanografiska förhållanden utanför Vendelsöfjorden i samband med kylvatten-utsläpp.

33b Eleonor Marmefelt och Jonny Svensson (1990)
Numerical circulation models for the Skagerrak - Kattegat. Preparatory study.

34 Kjell Wickström (1990)
Oskarshamnsverket - kylvattenutsläpp i havet - slutrapport.

35 Bo Juhlin (1990)
Oceanografiska observationer runt svenska kusten med kustbevakningens fartyg 1989.

36 Bertil Håkansson och Mats Moberg (1990)
Glommaälvens spridningsområde i nord-östra Skagerrak

37 Robert Hillgren (1990)
SMHIs undersökningar utanför Forsmark 1989.

38 Stig Fonselius (1990)
Skagerrak - the gateway to the North Sea.

39 Stig Fonselius (1990)
Skagerrak - porten mot Nordsjön.

40 Cecilia Ambjörn och Kjell Wickström (1990)
Spridningsundersökningar i norra Kalmarsund för Mönsterås bruk.

41 Cecilia Ambjörn (1990)
Strömningsteknisk utredning avseende utbyggnad av gipsdeponi i Landskrona.

42 Cecilia Ambjörn, Torbjörn Grafström och Jan Andersson (1990)
Spridningsberäkningar - Klints Bank.

43 Kjell Wickström och Robert Hillgren (1990)
Spridningsberäkningar för EKA-NOBELs fabrik i Stockviksverken.

44 Jan Andersson (1990)
Brofjordens kraftstation - Kylvattenspridning i Hanneviken.

45 Gustaf Westring och Kjell Wickström (1990)
Spridningsberäkningar för Höganäs kommun.

46 Robert Hillgren och Jan Andersson (1991)
SMHIs undersökningar utanför Forsmark 1990.

47 Gustaf Westring (1991)
Brofjordens kraftstation - Kompletterande simulering och analys av kylvattenspridning i Trommekilen.

48 Gustaf Westring (1991)
Vågmätningar utanför Kristianopel - Slutrapport.

49 Bo Juhlin (1991)
Oceanografiska observationer runt svenska kusten med kustbevakningens fartyg 1990.

50A Robert Hillgren och Jan Andersson (1992)
SMHIs undersökningar utanför Forsmark 1991.

50B Thomas Thompson, Lars Ulander, Bertil Håkansson, Bertil Brusmark, Anders Carlström, Anders Gustavsson, Eva Cronström och Olov Fäst (1992).
BEERS -92. Final edition.

51 Bo Juhlin (1992)
Oceanografiska observationer runt svenska kusten med kustbevakningens fartyg 1991.

52 Jonny Svensson och Sture Lindahl (1992)
Numerical circulation model for the Skagerrak - Kattegat.

53 Cecilia Ambjörn (1992)
Isproppsförebyggande muddring och dess inverkan på strömmarna i Torneälven.

54 Bo Juhlin (1992)
20 års mätningar längs svenska kusten med kustbevakningens fartyg (1970 - 1990).

55 Jan Andersson, Robert Hillgren och Gustaf Westring (1992)
Förstudie av strömmar, tidvatten och vattenstånd mellan Cebu och Leyte, Filippinerna.

56 Gustaf Westring, Jan Andersson, Henrik Lindh och Robert Axelsson (1993)
Forsmark - en temperaturstudie.
Slutrapport.

57 Robert Hillgren och Jan Andersson (1993)
SMHIs undersökningar utanför Forsmark 1992.

58 Bo Juhlin (1993)
Oceanografiska observationer runt svenska kusten med kustbevakningens fartyg 1992.

59 Gustaf Westring (1993)
Isförhållandena i svenska farvatten under normalperioden 1961-90.

60 Torbjörn Lindkvist (1994)
Havsområdesregister 1993.

61 Jan Andersson och Robert Hillgren (1994)
SMHIs undersökningar utanför Forsmark 1993.

62 Bo Juhlin (1994)
Oceanografiska observationer runt svenska kusten med kustbevakningens fartyg 1993.

63 Gustaf Westring (1995)
Isförhållanden utmed Sveriges kust - isstatistik från svenska farleder och farvatten under normalperioderna 1931-60 och 1961-90.

64 Jan Andersson och Robert Hillgren (1995)
SMHIs undersökningar utanför Forsmark 1994.

65 Bo Juhlin (1995)
Oceanografiska observationer runt svenska kusten med kustbevakningens fartyg 1994.

66 Jan Andersson och Robert Hillgren (1996)
SMHIs undersökningar utanför Forsmark 1995.

67 Lennart Funkquist och Patrik Ljungemyr (1997)
Validation of HIROMB during 1995-96.

68 Maja Brandt, Lars Edler och Lars Andersson (1998)
Översvämningar längs Oder och Wisla sommaren 1997 samt effekterna i Östersjön.

69 Jörgen Sahlberg SMHI och Håkan Olsson, Länsstyrelsen, Östergötland (2000).
Kustzonsmodell för norra Östergötlands skärgård.

70 Barry Broman (2001)
En vågatlas för svenska farvatten.
Ej publicerad

71 ***Vakant – kommer ej att utnyttjas!***

72 Fourth Workshop on Baltic Sea Ice Climate
Norrköping, Sweden 22-24 May, 2002
Conference Proceedings
Editors: Anders Omstedt and Lars Axell

73 Torbjörn Lindkvist, Daniel Björkert, Jenny Andersson, Anders Gyllander (2003)
Djupdata för havsområden 2003

74 Håkan Olsson, SMHI (2003)
Erik Årnefelt, Länsstyrelsen Östergötland
Kustzonssystemet i regional miljöanalys

75 Jonny Svensson och Eleonor Marmefelt (2003)
Utvärdering av kustzonsmodellen för norra Östergötlands och norra Bohusläns skärgårdar

76 Eleonor Marmefelt, Håkan Olsson, Helma Lindow och Jonny Svensson, Thalassos Computations (2004)
Integrerat kustzonssystem för Bohusläns skärgård

77 Philip Axe, Martin Hansson och Bertil Håkansson (2004)
The national monitoring programme in the Kattegat and Skagerrak

78 Lars Andersson, Nils Kajrup och Björn Sjöberg (2004)
Dimensionering av det nationella marina pelagialprogrammet

79 Jörgen Sahlberg (2005)
Randdata från öppet hav till kustzons-modellerna (Exemplet södra Östergötland)

80 Eleonor Marmefelt, Håkan Olsson (2005)
Integrerat Kustzonssystem för Hallandskusten

81 Tobias Strömgren (2005)
Implementation of a Flux Corrected Transport scheme in the Rossby Centre Ocean model

82 Martin Hansson (2006)
Cyanobakterieblomningar i Östersjön, resultat från satellitövervakning 1997-2005

83 Kari Eilola, Jörgen Sahlberg (2006)
Model assessment of the predicted environmental consequences for OSPAR problem areas following nutrient reductions

84 Torbjörn Lindkvist, Helma Lindow (2006)
Fyrskeppsdata. Resultat och bearbetnings-metoder med exempel från Svenska Björn 1883 – 1892

85 Pia Andersson (2007)
Ballast Water Exchange areas – Prospect of designating BWE areas in the Baltic Proper

86 Elin Almroth, Kari Eilola, M. Skogen, H. Søiland and Ian Sehested Hansen (2007)
The year 2005. An environmental status report of the Skagerrak, Kattegat and North Sea

87 Eleonor Marmefelt, Jörgen Sahlberg och Marie Bergstrand (2007)
HOME Vatten i södra Östersjöns vattendistrikt. Integrerat modellsystem för vattenkvalitetsberäkningar

88 Pia Andersson (2007)
Ballast Water Exchange areas – Prospect of designating BWE areas in the Skagerrak and the Norwegian Trench

89 Anna Edman, Jörgen Sahlberg, Niclas Hjerdt, Eleonor Marmefelt och Karen Lundholm (2007)
HOME Vatten i Bottenvikens vatten-distrikt. Integrerat modellsystem för vattenkvalitetsberäkningar

90 Niclas Hjerdt, Jörgen Sahlberg, Eleonor Marmefelt och Karen Lundholm (2007)
HOME Vatten i Bottenhavets vattendistrikt. Integrerat modellsystem för vattenkvalitets-beräkningar

91 Elin Almroth, Morten Skogen, Ian Sehsted Hansen, Tapani Stipa, Susa Niiranen (2008)
The year 2006
An Eutrophication Status Report of the North Sea, Skagerrak, Kattegat and the Baltic Sea
A demonstration Project

92 Pia Andersson, editor and co-authors Bertil Håkansson*, Johan Håkansson*, Elisabeth Sahlsten*, Jonathan Havenhand**, Mike Thorndyke**, Sam Dupont** * Swedish Meteorological and Hydrological Institute ** Sven Lovén, Centre of Marine Sciences (2008)
Marine Acidification – On effects and monitoring of marine acidification in the seas surrounding Sweden

93 Jörgen Sahlberg, Eleonor Marmefelt, Maja Brandt, Niclas Hjerdt och Karen Lundholm (2008)
HOME Vatten i norra Östersjöns vatten-distrikt. Integrerat modellsystem för vattenkvalitetsberäkningar.

94 David Lindstedt (2008)
Effekter av djupvattenomblandning i Östersjön – en modellstudie

95 Ingemar Cato*, Bertil Håkansson**, Ola Hallberg*, Bernt Kjellin*, Pia Andersson**, Cecilia Erlandsson*, Johan Nyberg*, Philip Axe** (2008)
*Geological Survey of Sweden (SGU)
**The Swedish Meteorological and Hydrological Institute (SMHI)
A new approach to state the areas of oxygen deficits in the Baltic Sea

96 Kari Eilola, H.E. Markus Meier, Elin Almroth, Anders Höglund (2008)
Transports and budgets of oxygen and phosphorus in the Baltic Sea

97 Anders Höglund, H.E. Markus Meier, Barry Broman och Ekaterini Kriezi (2009)
Validation and correction of regionalised ERA-40 wind fields over the Baltic Sea using the Rossby Centre Atmosphere model RCA3.0

98 Jörgen Sahlberg (2009)
The Coastal Zone Model

99 Kari Eilola (2009)
On the dynamics of organic nutrients, nitrogen and phosphorus in the Baltic Sea

100 Kristin I. M. Andreasson (SMHI), Johan Wikner (UMSC), Berndt Abrahamsson (SMF), Chris Melrose (NOAA), Svante Nyberg (SMF) (2009)
Primary production measurements – an intercalibration during a cruise in the Kattegat and the Baltic Sea

101 K. Eilola, B. G. Gustafson, R. Hordoir, A. Höglund, I. Kuznetsov, H.E.M. Meier T. Neumann, O. P. Savchuk (2010)
Quality assessment of state-of-the-art coupled physical-biogeochemical models in hind cast simulations 1970-2005

102 Pia Andersson (2010)
Drivers of Marine Acidification in the Seas Surrounding Sweden

103 Jörgen Sahlberg, Hanna Gustavsson (2010)
HOME Vatten i Mälaren

104 K.V Karmanov., B.V Chubarenko, D. Domnin, A. Hansson (2010)
Attitude to climate changes in everyday management practice at the level of Kaliningrad region municipalities

105 Helén C. Andersson., Patrik Wallman, Chantal Donnelly (2010)
Visualization of hydrological, physical and biogeochemical modelling of the Baltic Sea using a GeoDome™

106 Maria Bergelo (2011)
Havsvattenståndets påverkan längs Sveriges kust – enkätsvar från kommuner, räddningstjänst, länsstyrelser och hamnar

107 H.E. Markus Meier, Kari Eilola (2011)
Future projections of ecological patterns in the Baltic Sea

SMHI

Sveriges meteorologiska och hydrologiska institut
601 76 Norrköping
Tel 011-495 80 00 Fax 011-495 80 01

ISSN 0283-7714